SPECTROSCOPY, ELECTROCHEMISTRY, AND PHOTOCHEMISTRY OF POLYNUCLEAR METAL-METAL BONDED COMPLEXES

Thesis by

Daniel George Nocera

In Partial Fulfillment of the Requirements

for the Degree of

Doctor of Philosophy

California Institute of Technology

Pasadena, California

1984

(Submitted 16 August 1983)

to my wife,

Karen

ACKNOWLEDGEMENTS

I express my deepest gratitude to past and present Gray group members for creating a scientifically stimulating and challenging environment in which to pursue my scientific goals. I thank Harry Gray for his friendship, encouragement, and scientific insight during my tenure at Caltech. Harry's capacity to linger in the delta-star excited state for *exceedingly* long periods of time has resulted in many of my chemical endeavors. Many colleagues have contributed to my research effort: John Buhr, Andrew Maverick, Steven Rice, and Terry Smith deserve special credit for their guidance during my initial scientific ventures; Mike Hopkins, Vinnie Miskowski, and Tom Zietlow (Zeitlow ?) for their solicited (and more frequent, unsolicited) critiques of my work; and Vince Cammarata and Doug MacKenzie for sacrificing their undergraduate research careers at my hands. I also thank Jay Winkler for his friendship and for accompanying me during my sojourn in bioinorganic chemistry.

I am indebted to many people outside the Gray group. For their many helpful discussions, I thank Professors Fred Anson, John Bercaw, Terry Collins, Rudy Marcus, and Bill Schaefer. Special thanks goes to: Fred Anson for permitting the use of his electrochemical equipment; Bill Schaefer who performed the entire crystal analysis of $NBu_4Re_2Br_9$; and Professor Oliver Wulf for many enlightening discussions on the electronic spectroscopy of diatomic

molecules. I also thank Dan Buttry and Mark Paffett for their electrochemical expertise and Don Berry and Eric Moore for their synthetic prowess.

Certainly, one of the many pleasant aspects of the Gray group is the establishment of scientific collaborations with visiting research scholars. In conjunction with my work in bioinorganic chemistry, thanks go to Professors Emilio Bordignon, John Chesick, George "Gold Shooter" McLendon, and Israel Pecht; and I am further indebted to Professor Woody Woodruff for sharing with me his knowledge of Raman spectroscopy and for beginning the TR^3 studies on the $M_6X_{14}^{2-}$ clusters.

I acknowledge the financial support from a Sun Company graduate fellowship during the 1982-83 academic year and summer recess.

I was fortunate to establish friendships with many people outside of Caltech. Among them are those with Roy Harrison, Melissa Patton, and Betsa and Vincent Richards (and their families). I especially thank Noah, who should be taller than I any day now, for his special friendship and many wonderful experiences.

The love and support which I have received from my parents and sisters have been guiding lights throughout my formal educational years.

And finally, the radiant love, steadfast loyalty, and tireless patience of my wife, Karen, have been the sources of my strength and inspiration.

ABSTRACT

The spectroscopic, electrochemical, and photochemical properties of two d^4 metal polynuclear complex systems were investigated: the quadruple bond complex, $Re_2Cl_8^{2-}$, and the $M_6X_{14}^{2-}$ halide cluster ions of molybdenum(II) and tungsten(II).

The vibrationally structured luminescence spectrum of $Re_2Cl_8^{2-}$ at 5 K has confirmed that emission arises from the $\delta\delta^*$ singlet state. Both $Re_2Cl_8^{2-}$ and electronically excited $Re_2Cl_8^{2-}$ ($Re_2Cl_8^{2-*}$) undergo facile one-electron oxidation and reduction reactions. Aromatic amines quench $Re_2Cl_8^{2-*}$ luminescence and a Marcus analysis of the steady-state quenching rate constants suggest that $Re_2Cl_8^{3-}|D^+$ is formed in the quenching reaction and that the ion-pair decays rapidly by back electron transfer. The luminescence of $Re_2Cl_8^{2-*}$ is also quenched by electron acceptors (TCNE and chloranil) in nonaqueous solutions, forming $Re_2Cl_8^{-}$ and reduced acceptor. The back electron transfer reactions are near the diffusion controlled limit. Electrochemical measurements suggested that photogenerated $Re_2Cl_8^{-}$ anion could be trapped by Cl^- to produce $Re_2Cl_9^{2-}$, thereby circumventing the efficient back reaction. Irradiation (λ>660 nm) of nonaqueous solutions of $Re_2Cl_8^{2-}$ and chloranil or TCNE in the presence of excess Cl^- does, indeed, produce $Re_2Cl_9^{2-}$ in quantitative yield. Photolysis reactions employing a quencher (e.g. 2,3-dichloro-5,6-dicyano-

benzoquinone) possessing a redox couple with a potential greater than that of $Re_2Cl_9^{-/2-}$ (0.53 V *vs.* SCE) yielded $Re_2Cl_9^-$ as a final product. Thus, a single low energy photon facilitates a two-electron oxidation of $Re_2Cl_8^{2-}$. Direct two-electron oxidation of $Re_2Cl_8^{2-*}$ by chlorine atom transfer reagents such as $PtCl_6^{2-}$ to produce $Re_2Cl_9^-$ was also attempted. Irradiation (λ>590 nm) of dichloromethane solutions containing $Re_2Cl_8^{2-}$ and $PtCl_6^{2-}$ quantitatively yield $Re_2Cl_9^-$. Qualitative kinetic experiments measuring the wavelength dependence of the reaction rate suggest that the photochemical reaction proceeds by a free radical pathway involving the $^3A_{2u}$ ligand field excited state of $PtCl_6^{2-}$ and does not involve an atom transfer reaction mechanism. These experiments are not without their ambiguities, however, and further areas of research are discussed. The crystal structure analysis of $NBu_4Re_2Br_9$ is also presented.

The $M_6X_{14}^{2-}$ (M=Mo,W; X=Cl,Br,I) ions are intensely luminescent in the solid state and solution and the photophysical properties of the six cluster ions are documented. These results in conjunction with those of the EPR spectra of the electrochemically generated $M_6X_{14}^-$ anions are discussed in terms of recent theoretical models for the electronic structure of the cluster ions. Electrochemical experiments were also conducted and showed the $M_6X_{14}^{2-}$ cluster ions to undergo reversible single-electron oxidation reactions. For $Mo_6Cl_{14}^{2-}$, a quasi-reversible one-electron

reduction wave was observed in addition to its oxidation wave. The electrochemical and photophysical properties of $Mo_6Cl_{14}^{2-}$ suggested electrogenerated chemiluminescent behavior of the cluster ion. Emission, characteristic of $Mo_6Cl_{14}^{2-*}$, is observed upon electrochemical generation of $Mo_6Cl_{14}^{-}$ and $Mo_6Cl_{14}^{3-}$.

TABLE OF CONTENTS

LIST OF FIGURES

LIST OF TABLES

CHAPTER I

INTRODUCTION

A central theme of inorganic photochemistry during the past two decades is the activation of small molecules by transition metal complexes. A major difficulty of this activation chemistry lies in the kinetic and/or thermodynamic barriers which typically confront these small molecule reactions. Inorganic photochemistry is an extremely important area of chemistry, because the energy of the electronically excited transition metal complex may be utilized to surmount these reaction barriers. The long excited state lifetimes exhibited by many transition metal complexes entitles them to be viewed as authentic chemical reagents with their own reaction chemistry. Indeed, a major development in inorganic chemistry has been the incorporation of electronically excited molecules in bimolecular processes.[1] Prominent among these are electron transfer reactions.[2] Many small molecule activation reactions involve multielectron transfer processes, and it would therefore be desirable to involve the excited state directly in these multielectron transfer reactions. Unfortunately, inorganic photochemistry, to date, has ignored excited state multielectron transfer chemistry. The shortcoming of employing single-electron transfer reactions of photoreagents to drive multielectron transfer processes arises from large kinetic barriers which are built into such reaction pathways. Nowhere is this problem better illustrated than in solar energy conversion chemistry.

The storage of solar energy in chemical species has been a topic for intensive photochemical investigation, due principally to the ramifications of such reactions for alternate fuel sources.[3] The photochemical energy storage reaction which has challenged the imaginations of most photochemists is the splitting of water by a transition metal catalyst, M, to produce hydrogen and oxygen

$$H_2O \xrightarrow[M]{\text{solar energy}} H_2 + \frac{1}{2} O_2,$$

a reaction which stores 2.46 eV of chemical energy. Present solar energy conversion schemes emphasize one-photon/one-electron/catalyst cycles; the most popular of which employ $Ru(bpy)_3^{2+}$ (bpy = bipyridine) as a photosensitizer.[4] In all systems, a heterogeneous catalyst or relay catalyst is required to couple the one-electron chemistry of the photosensitizer to the multielectron transfer chemistry of the water splitting reaction. The design of such energy conversion schemes imposes severe limitations on the overall efficiency of the reaction.

Owing to our interest in small molecule activation chemistry, we have concentrated on effecting multielectron transfer reactions with polynuclear metal complexes. These compounds are well-suited for multielectron photochemistry with their coordinative unsaturation and juxtaposed redox centers in a single molecule (which can be electronically

excited with a single photon of light). It should be possible to facilitate multielectron reactions at the available coordination sites of the cluster species.

The photochemistry of polynuclear metal complexes in recent years has primarily involved cluster compounds which are comprised of two and three metal centers. From these investigations, homolytic cleavage of the metal-metal bond has emerged as a general reaction pathway for polynuclear complexes in their excited state.[5] Dimanganese decacarbonyl is the cornerstone example of this photochemistry,[6] which may easily be understood in terms of the metal σ and π molecular orbital interactions schematically represented in Figure 1. The lowest energy transitions in $Mn_2(CO)_{10}$ arise from the promotion of an electron from a σ or π molecular orbital to σ^*. Of course, both transitions significantly weaken the metal bond, thereby inducing metal-metal bond cleavage. The photofragmentation chemistry of $Ru_3(CO)_{12}$[7] may be similarly explained by excitation of the analogous metal localized $\sigma \rightarrow \sigma^*$ transition in the trinuclear cluster.[8] In order to preserve the excited state polynuclear complex for bimolecular reaction chemistry, it is obvious that metal-metal bond cleavage chemistry must be circumvented. Two primary classes of compounds have developed along these lines. One class of compounds is comprised of binuclear d^8-d^8 complexes in which the structural integrity of the polynuclear complex is maintained by ancillary ligands which bridge the two

Figure 1. Qualitative σ and π interactions of metal d orbitals in $Mn_2(CO)_{10}$.

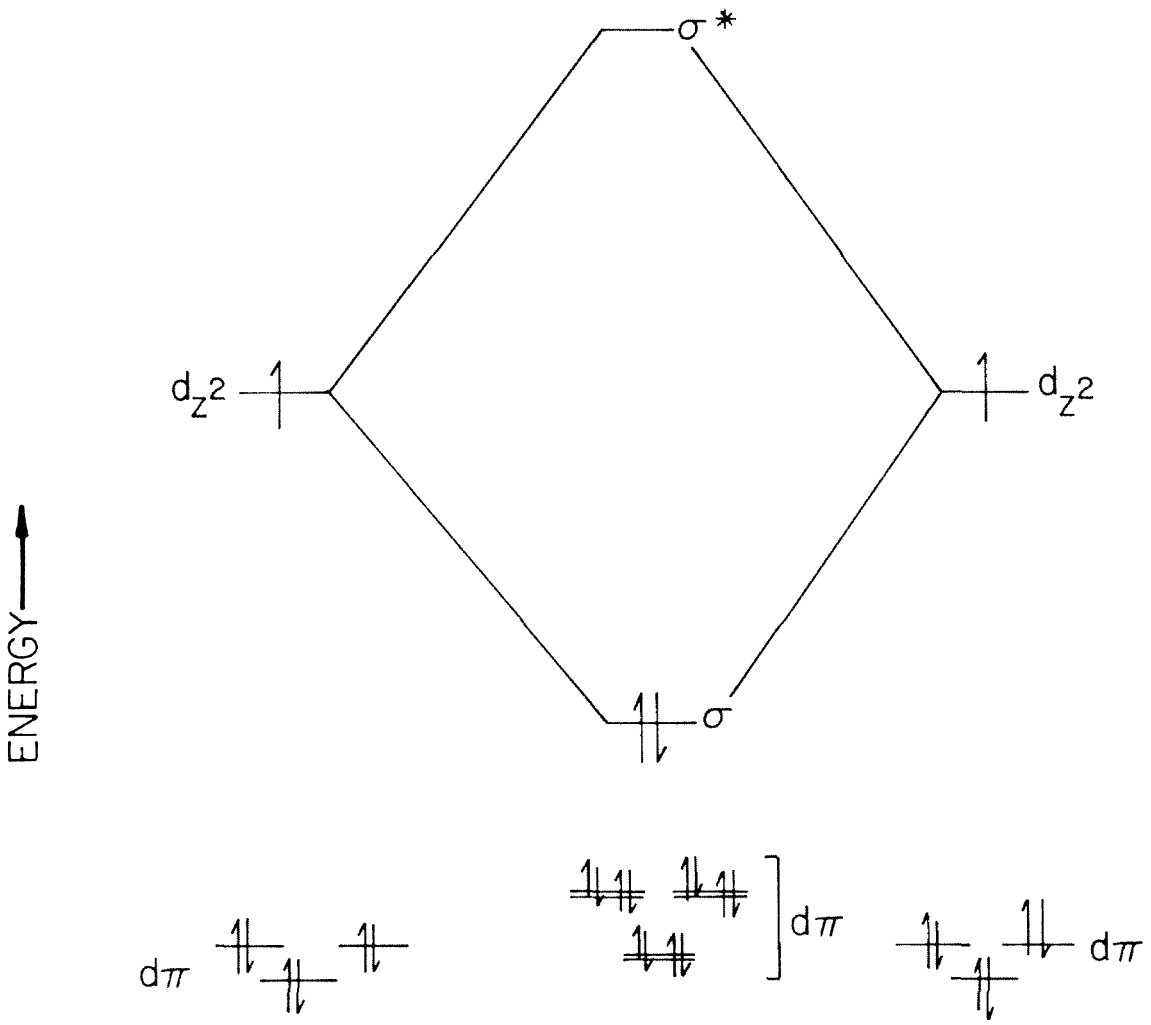

$(CO)_5Mn\bullet$ $(CO)_5Mn-Mn(CO)_5$ $\bullet Mn(CO)_5$

metal centers.[9] Simple molecular orbital theory suggests that the excited state metal interaction is much stronger than in the ground state! Electronic absorption and emission spectra[10] and resonance Raman spectroscopy of the ground and excited states of these dimers[11] substantiate the predictions of theory. The excited states of these complexes readily undergo bimolecular oxidative and reductive electron transfer reactions.[12] The second class of compounds consists of clusters with cores of multiply bonded metal centers. In these systems, occupation of metal-metal antibonding molecular orbitals by a single electron promotion only slightly weakens the extensive metal-metal bonding framework.

Herein are described our experiments on compounds of this second class of polynuclear complexes, cluster compounds of d^4 metals at two bonding extremes: single multiple and multiple single metal-metal bonding. In the former system, the four d electrons of one metal are utilized to form one quadruple bond to another metal. Chapter II describes our investigations of the spectroscopy, electrochemistry and photochemistry of octachlorodirhenate dianion, $Re_2Cl_8^{2-}$, the prototypal quadruple metal bonded system. At the other bonding extreme, the four d electrons of each metal center are used to make four single bonds to four other metal centers in the octahedral metal core of the $M_6X_{14}^{2-}$ (M=Mo,W; X=Cl,Br,I) cluster compounds. To emphasize the similarity between these two seemingly diverse

polynuclear complexes, the $M_6X_{14}^{2-}$ cluster may be viewed as the condensation product of three quadruple bond systems.[13] Experiments aimed at the elucidation of the electronic structure and redox chemistry of $M_6X_{14}^{2-}$ clusters are documented in Chapter III.

REFERENCES

1. (a) Balzani, V.; Bolletta, F.; Gandolfi, M. T.; Maestri, M. Topics Curr. Chem. **1978**, 75, 1. (b) Balzani, V.; Moggi, L.; Manfrin, M. F.; Bolletta, F.; Laurence, G. S. Coord. Chem. Rev. **1975**, 15, 321.

2. (a) Meyer, T. J. Prog. Inorg. Chem. **1983**, 30, 389 and references therein. (b) Meyer, T. J. Acc. Chem. Res. **1978**, 11, 94.

3. (a) Gray, H. B.; Maverick, A. W. Science **1981**, 214, 1201. (b) Maverick, A. W.; Gray, H. B. Pure. Appl. Chem. **1980**, 52, 2339. (c) Sutin, N.; Creutz, C. Pure Appl. Chem. **1980**, 52, 2717. (d) Sutin, N. J. Photochem. **1979**, 10, 19.

4. (a) Brugger, P.-A.; Grätzel, M. J. Am. Chem. Soc. **1980**, 102, 2461. (b) Lehn, J.-M.; Sauvage, J. P.; Ziessel, R. Nouv. J. Chim. **1981**, 5, 291. (c) Brugger, P.-A.; Cuendet, P.; Grätzel, M. J. Am. Chem. Soc. **1981**, 103, 2923. (d) Kalyanasundaram, K.; Grätzel, M. Angew. Chem., Int. Ed. Engl. **1980**, 19, 646. (e) Borgarello, E.; Kiwi, J.; Pelizzetti, E.; Visca, M.; Grätzel, M. J. Am. Chem. Soc. **1981**, 103, 6324. (f) Chan, S.-F.; Chou, M.; Creutz, C., Matsubara, T.; Sutin, N. J. Am. Chem. Soc. **1981**, 103, 369. (g) Nijs, H.; Cruz, M. I.; Fripiat, J. J.; Van Damme, H. Nouv. J. Chim. **1982**, 6, 551. (h) Grätzel, M.

Acc. Chem. Res. 1981, 14, 376. (i) Shafirovich, V.; Khannanov, N. K.; Strelets, V. V. Nouv. J. Chim. 1981, 4, 81. (j) Collin, J. P.; Lehn, J.-M.; Ziessel, R. Nouv. J. Chim. 1982, 6, 405. (k) Krishnan, C. V.; Sutin, N. J. Am. Chem. Soc. 1981, 103, 2141. (l) Humphry-Baker, R.; Lilie, J.; Grätzel, M. J. Am. Chem. Soc. 1982, 104, 422. (m) Brown, G. M.; Brunschwig, B. S.; Creutz, C.; Endicott, J. F.; Sutin N. J. Am. Chem. Soc. 1979, 101, 1298.

5. (a) Geoffroy, G. L.; Wrighton, M. S. "Organometallic Chemistry"; Academic Press: New York, 1979. (b) Wrighton, M. S.; Graff, J. L.; Luong, J. C.; Reichel, C. L.; Robbins, J. L. in "Reactivity of Metal-Metal Bonds"; Chisholm, M. H., ed.; American Chemical Society: Washington, D. C., 1981; ACS Symposium Ser. No. 155.

6. (a) Wrighton, M. S.; Ginley, D. S. J. Am. Chem. Soc. 1975, 97, 2065. (b) Wrighton, M. S. Topics Curr. Chem. 1976, 65, 37. (c) Fox, A.; Poë, A.; Ruminski, R. J. Am. Chem. Soc. 1982, 104, 7327. (d) Karny, Z.; Naaman, R.; Zare, R. N. Chem. Phys. Lett. 1978, 59, 33

7. Johnson, B. F. G.; Lewis, J.; Twigg, M. V. J. Organomet. Chem. 1974, 67, C75.

8. Tyler, D. R.; Levenson, R. A.; Gray, H. B. J. Am. Chem. Soc. 1978, 100, 7888.

9. (a) Lewis, N. S.; Mann, K. R.; Gordon, J. G. II; Gray, H. B. J. Am. Chem. Soc. 1976, 98, 7461. (b) Mann, K. R.; Thich, J. A.; Bell, R. A.; Coyle, C. L.; Gray, H. B. Inorg. Chem. 1980, 19, 2462. (c) Mann, K. R.; Gray, H. B. Adv. Chem. Ser. 1979, 173, 225. (d) Gray, H. B.; Miskowski, V. M.; Milder, S. J.; Smith, T. P.; Maverick, A. W.; Buhr, J. D.; Gladfelter, W. L.; Sigal, I. S.; Mann, K. R. Fundam. Res. Homogeneous Catal. 1979, 3, 819. (e) Che, C.-M.; Butler, L. G.; Gray, H. B. J. Am. Chem. Soc. 1981, 103, 7796. (f) Che, C.-M.; Schaefer, W. P.; Gray, H. B.; Dickson, M. K.; Stein, P. B.; Roundhill, D. M. J. Am. Chem. Soc. 1982, 104, 4253.

10. (a) Rice, S. F.; Gray, H. B. J. Am. Chem. Soc. 1981, 103, 1593. (b) Rice, S. F.; Milder, S. J.; Gray, H. B.; Goldbeck, R. A.; Kliger, D. A. Coord. Chem. Rev. 1982, 43, 349. (c) Rice, S. F. Ph.D. Dissertation, California Institute of Technology, 1982.

11. Dallinger, R. F.; Miskowski, V. M.; Gray, H. B.; Woodruff, W. H. J. Am. Chem. Soc. 1981, 103, 1595.

12. Milder, S. J.; Goldbeck, R. A.; Kliger, D. S.; Gray, H. B. J. Am. Chem. Soc. 1980, 102, 6761.

13. Indeed, $Mo_6Cl_{14}^{2-}$ may be prepared simply by heating the quadruple bond complex, $Mo_2Cl_8^{4-}$, to 300°C. (Jödden, Von K.; Schäfer, H. Z. Anorg. Allg. Chem. 1977, 430, 5).

CHAPTER II

THE OCTACHLORODIRHENATE(III) ANION

A. INTRODUCTION

The chemistry of multiple metal-metal bonded dimers has been an area of active research during the past two decades.[1] The trinuclear rhenium halide cluster, $Re_3Cl_{12}^{3-}$, was the first inorganic molecule in which multiple metal-metal bonding was predicted.[2] On the basis of a simple molecular orbital analysis, a metal core of doubly bonded rhenium atoms was formulated. Interestingly, since the discovery of $Re_3Cl_{12}^{3-}$ in 1963, few other doubly bonded metal-metal complexes have been realized, and it was the synthesis and characterization of triply and quadruply bonded metal-metal dimers which spurred the development of multiple bonded metal complex chemistry. Indeed, it was the identification of the octachlorodirhenate dianion, $Re_2Cl_8^{2-}$, to possess a quadruple metal-metal bond[3] which kindled the search for other such multiply bonded species. A plethora of quadruply bonded metal-metal complexes are now known, comprised primarily of molybdenum, tungsten and rhenium metal cores, with a variegated array of ligating systems.

The prevalence of quadruply bonded metal complexes has engendered numerous theoretical and experimental investigations directed toward elucidating their electronic structures.[4] The general molecular orbital diagram depicted in Figure 1 has evolved from these studies. The metal-metal bonding in L_4MML_4 quadruply bonded dimers is most easily derived from a MM core ($D_{\infty h}$ symmetry) in which the z axis

Figure 1. Qualitative σ, π, and δ interactions of metal d orbitals in a MM ($\mathcal{D}_{\infty h}$) core and L_4MML_4 ($\mathcal{D}_{4h}$) complex. A ground state $\sigma^2\pi^4\delta^2$ electronic configuration is generated in d^4-d^4 L_4MML_4 complexes, corresponding to quadruple bond formation. (Ref. 4b).

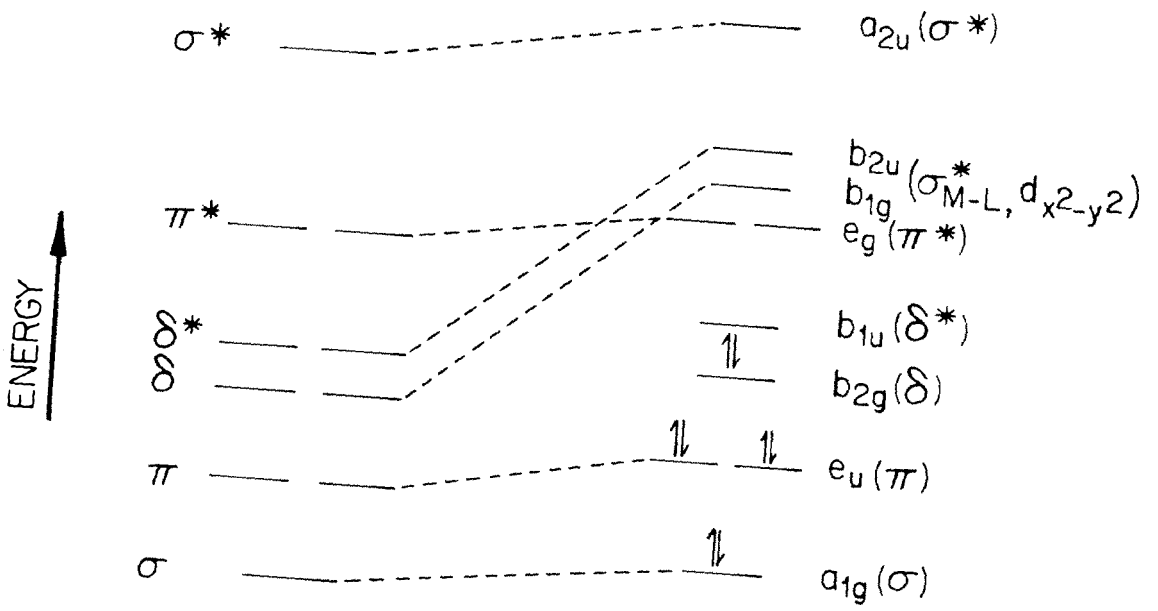
σ*
a2u(σ*)
π*
b2u (σ*M-L, dx2-y2)
b1g
eg(π*)
ENERGY
δ*
δ
b1u(δ*)
b2g(δ)
π
eu(π)
σ
a1g(σ)

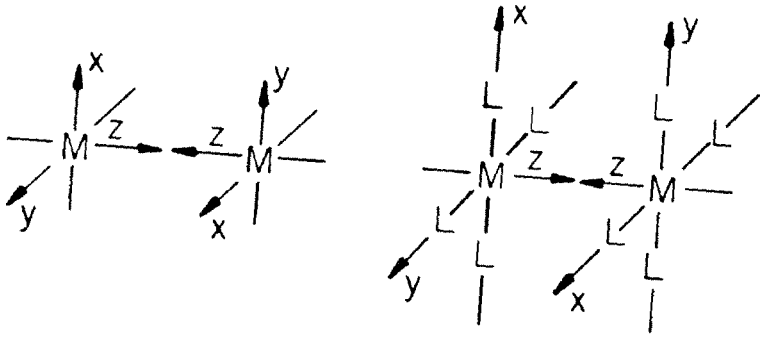
x
y
z
z
M
M
y
x
L

of a right-handed Cartesian coordinate system is chosen to lie along the metal-metal axis. Linear combinations of the d_{z^2}, (d_{xz}, d_{yz}) and ($d_{x^2-y^2}$, d_{xy}) atomic orbitals on each metal produce bonding and antibonding molecular orbitals of σ, π, and δ symmetries, respectively. The π and δ molecular orbitals are each doubly degenerate in a $D_{\infty h}$ point group. From the nodal theorem and atomic orbital overlap considerations, the molecular orbital energy ordering of an MM diatomic core shown in Figure 1 is obtained. The equidistant positioning of eight ligands in a L_4MML_4 complex perturbs the bonding of the diatomic metal core by lowering the symmetry of the system to D_{4h}, thereby splitting the δ orbital degeneracy. By definition of the coordinate system in Figure 1, the ligands will lie along the x and y axes and their orbitals will overlap with the $d_{x^2-y^2}$ derived δ and δ^* orbitals. The linear combination of these ligand and metal orbitals causes the δ (b_{1g}) and δ^* (b_{2u}) orbitals to increase dramatically in energy. As designated in Figure 1, the b_{1g} and b_{2u} orbitals are essentially σ metal-ligand antibonding in character. The energies of the σ, π, and δ (d_{xy}) molecular orbitals, for the most part, are unperturbed as the ligands approach the metal core and the L_4MML_4 molecular orbital diagram shown in Figure 1 is obtained. Occupation of the σ, π, and δ molecular orbitals with eight electrons gives a quadruple bond. The characteristic properties of a diamagnetic ground state, eclipsed ligand geometry, and *exceedingly* short metal-metal bond

exhibited by quadruple bond complexes are clearly explained by this bonding scheme.

According to the simple molecular orbital diagram in Figure 1, the lowest energy transition arises from the promotion of an electron from the δ to the δ^* molecular orbital. Polarized electronic absorption spectroscopic investigations of numerous quadruply bonded metal complexes[4b,5] verify that their lowest energy absorption band corresponds to the $\delta \rightarrow \delta^*$ transition. Excitation of the $\delta \rightarrow \delta^*$ transition frequently leads to luminescent excited states with lifetimes greater than 50 ns. As we shall discuss later, the luminescence, when observed, typically originates from the $\delta\delta^*$ singlet state.

Quadruply bonded metal-metal dimers possess many properties of an ideal polynuclear photoredox reagent. First, the longevity of the $\delta\delta^*$ excited state should permit the electronically excited metal complex to participate in bimolecular reactions, in addition to any unimolecular photoprocesses available to higher energy excited states. Second, the all inorganic quadruple bond metal complexes should be robust photoreagents, capable of maintaining their structural integrity upon irradiation. Bimolecular photochemical reactions will, of course, proceed through the $\delta\delta^*$ excited state. Theoretical estimates predict the overall energetic contribution of the δ bond to the total quadruple bond energy to be less than 10%.[6] Irradiation of the $\delta \rightarrow \delta^*$ transition will, therefore, only nominally

weaken the metal-metal bond and photoinduced metal-metal bond cleavage reactions will be circumvented in these complexes. Third, the multiple metal-metal bond may act as an electron source or sink in multielectron transfer reactions while maintaining a strong metal-metal interaction. Walton and coworkers have prepared a series of L_4MML_4 triply bonded metal complexes with $\sigma^2\pi^4\delta^2\delta^{*2}$ ground state electronic configurations.[7] In all cases investigated, these complexes demonstrated facile electron transfer reactions at electrode surfaces.[8] The absence of the δ bond does not greatly perturb the L_4MML_4 structural unit as evidenced by the crystal structures of $Re_2Cl_6(PEt_3)_2$[9] and triply bonded ($\sigma^2\pi^4\delta^2\delta^{*2}$) $Re_2Cl_4(PEt_3)_4$[10] complexes, which show ReRe bond distances of 2.222(3)Å and 2.232(5)Å, respectively. The ability of the multiple metal-metal bond to undergo only minor structural reorganization upon changes in the δ and δ^* orbital electronic configurations may greatly facilitate the photoredox chemistry of quadruple bond metal complexes.

In view of the attractive photochemical properties of quadruple bond metal complexes along with their extensive reaction chemistry, it is rather surprising that the photochemistry of these systems has virtually been ignored. The $Re_2Cl_8^{2-}$ dianion undergoes a metal-metal bond cleavage reaction when irradiated with ultraviolet light.[11] The mononuclear photoproducts, $ReCl_4(CH_3CN)_2^-$ and $ReCl_3(CH_3CN)_3$, were demonstrated to arise from high energy excited states

of $Re_2Cl_8^{2-}$. Further work indicated a solvent assisted metal bond cleavage reaction.[12] The only other reported photochemistry of quadruple bond metal complexes deals with the photo-oxidation chemistry of molybdenum dimers. Ultraviolet irradiation of aqueous acidic solutions of $Mo_2(SO_4)_4^{4-}$ and $Mo_2(aq)^{4+}$ yields the oxidized products, $Mo_2(SO_4)_4^{3-}$ and $Mo_2(aq)(\mu\text{-}OH)_2^{4+}$, respectively, and hydrogen as the reduction product.[13] Similarly, irradiation of $Mo_2X_8^{4-}$ (X=Cl,Br) dimers in hydrohalic acid solutions gives the hydrido bridged oxidation product, $Cl_3Mo(\mu\text{-}H)(\mu\text{-}Cl)_2MoCl_3^{3-}$, which thermally reacts with another mole of HX to produce hydrogen.[14] Similar reactivity was observed for solutions of $Mo_2Cl_4(PR_3)_4$ (R=alkyl) dimers.[15] The photo-oxidation chemistry of the above systems was demonstrated to arise from high energy excited states (probably ligand-to-metal charge transfer states). In no case has bimolecular photochemistry of quadruple bond complexes yet been described in which one reactant is not a solvent molecule.[16]

In light of the potential importance of polynuclear metal complexes in photochemical energy storage reactions in homogeneous solution,[17] we turned our attention toward the systematic development of the $\delta\delta^*$ excited state chemistry of quadruply bonded metal-metal complexes. The thrust of our work has been directed toward the photochemistry of the octachlorodirhenate dianion, $Re_2Cl_8^{2-}$. The motivation for investigating $Re_2Cl_8^{2-}$ is two-fold: (i) its chemical

reactivity and physical properties are the best defined of any quadruple bond metal complex and (ii) the long-lived luminescence of $Re_2Cl_8^{2-}$ in fluid solutions[12] (0.14 μs in CH_3CN; 0.08 μs in CH_2Cl_2) permits bimolecular reactivity of the electronically excited molecule. The following sections describe our investigations of the spectroscopy and the thermal and photochemical redox chemistry of the $Re_2Cl_8^{2-}$ anion. Since the electronically excited molecule is a reactant in a photochemical process, elucidation of the properties of the excited state is imperative to a comprehensive understanding of the photochemistry of the system. New luminescence properties of the $\delta\delta^*$ excited state are presented in Section C. Section D documents the electrochemical reactions of $Re_2Cl_8^{2-}$ and structurally related binuclear rhenium halides. As we shall see, these electrochemical studies were a beacon to the ensuing photochemical investigations of $Re_2Cl_8^{2-}$ which are discussed in Section E of this chapter.

B. EXPERIMENTAL

Binuclear Rhenium Halide Compounds. The tetrabutylammonium salt of $Re_2Cl_8^{2-}$ was prepared by either of two procedures: (i) hypophosphorus acid reduction of potassium perrhenate[18] or (ii) reductive coupling of NBu_4ReO_4 with benzoyl chloride (PhCOCl).[19] Reagent grade solvents and acids were thoroughly deoxygenated prior to use, otherwise they were used as received. The necessary solvent transfers associated with the above synthetic routes were carried out under high purity argon. Tetrabutylammonium perrhenate was prepared by addition of a hot aqueous solution of NBu_4Br (Eastman) to one of $KReO_4$ (Alfa Ventron). The white flocculent precipitate was thoroughly washed with diethyl ether and dried under vacuum for 24 hr . The crude blue powder of $(Bu_4N)_2Re_2Cl_8$, obtained from either of the above synthetic routes, was purified as a microcrystalline solid upon cooling hot acidified methanol solutions which were saturated with the compound. Large, rectangular prismatic crystals of $(Bu_4N)_2Re_2Cl_8$ were grown from acetonitrile solutions which had been layered with diethyl ether. The cesium salt of $Re_2Cl_8^{2-}$ was prepared by the slow addition of a hot CsCl (Aldrich Chemical Co.) saturated ethanol solution to a boiling, acidified ethanol solution of $(Bu_4N)_2Re_2Cl_8$ with constant stirring. After a few minutes, $Cs_2Re_2Cl_8$ precipitated as a bluish-green powder. Constant boiling HCl solutions of $Cs_2Re_2Cl_8$, upon cooling in

an air-tight dewar, produced crystals which were large enough for electronic spectroscopy. The tetrabutylammonium salt of $Re_2Br_8^{2-}$ was prepared and recrystallized according to published procedures.[20]

The quadruple bond complex, $Re_2Cl_6(PEt_3)_2$, prepared by its reported synthetic route[21] and recrystallized from a dichloromethane solution layered with light petroleum ether, was obtained from Jay R. Winkler. The hexafluorophosphate salt of $Re_2Cl_4(PMe_2Ph)_4^{2+}$ cation was generously supplied from the laboratories of Dr. R. A. Walton at Purdue University. Due to the instability of this compound with respect to reduction, a small quantity of $Re_2Cl_5(PMe_2Ph)_3$ was also present.

The confacial bioctahedral monoanions, $Re_2X_9^-$ (X=Cl,Br) were prepared from their quadruply bonded rhenium halide analogues.[22] The conversion of the quadruply bonded dimer to product was monitored by the disappearance of the $\delta \rightarrow \delta^*$ absorption band. Small, wafer-thin, green platelets of $NBu_4Re_2Cl_9$ were recrystallized from chloroform. Crude $NBu_4Re_2Br_9$ was dissolved in dichloromethane, and enough chloroform was added to produce a solution saturated in confacial bioctahedra. Upon standing in a beaker overnight, large, highly reflective, prismatic crystals of $NBu_4Re_2Br_9$ were deposited on the beaker wall.

The preparation of $Re_2Cl_9^{2-}$ by the reduction of $Re_2Cl_9^-$ with various metals (Cu, Zn and Hg) gave violet oils which seldom crystallized. A better synthetic method

involved dissolution of $NBu_4Re_2Cl_9$ in a CH_2Cl_2/ethanol solution to saturation, followed by the addition of a molar excess (to that of $NBu_4Re_2Cl_9$) of NBu_4Cl. A stream of hydrogen was passed over a platinum gauze which was immersed in solution, causing the green solution to turn violet within minutes. As CH_2Cl_2 evaporated with continued bubbling, purple microcrystalline $(Bu_4N)_2Re_2Cl_9$ precipitated from the ethanol enriched solution. The purity of the product was confirmed by its electronic absorption spectrum.

Quenchers. All aromatic amines were obtained from Aldrich Chemical Co., with the exception of 10-methylphenothiazine (10-MPTH), which was purchased from Pfaltz and Bauer. *N*,*N*-dimethylaniline (DMA), *N*,*N*-diethylaniline (DEA), and *N*,*N*-dimethyl-p-toluidine (DMT) were distilled onto activated Linde 4A Molecular Sieve (*vide supra*) and stored under argon, which had been passed through a MnO scrubbing tower. Phenothiazine (PTH) and *N*,*N*,*N*',*N*'-tetramethyl-p-phenylenediamine (TMPD) were vacuum sublimed twice before use. Diphenylamine (DPA), 4,4'-dimethoxydiphenylamine (DMDPA) and 10-MPTH were recrystallized three times from benzene/petroleum ether solutions. After purification, liquid quenchers were colorless and solid quenchers were white with melting points within 2°C of their reported values.

Tetracyanoethylene (TCNE; Aldrich Chemical Co.) was recrystallized from chlorobenzene and vacuum sublimed twice before use. Chloranil (2,3,5,6-tetrachloro-1,4-benzoquinone;

Aldrich) was recrystallized three times from toluene to give yellow rectangular platelets. Sodium 12-tungstophosphate, $Na_3PW_{12}O_{40} \cdot 10\ H_2O$, prepared by the method of Wu[23] with minor modification[24] and recrystallized three times from 1 M H_2SO_4 and once from 1 M HCl, was supplied by Andrew W. Maverick. Orange-red 2,3-dichloro-5,6-dicyano-benzoquinone (DDQ) was purchased from Aldrich and used as received. The potassium and sodium salts of TCNE and chloranil radical anions, respectively, were prepared according to published procedures.[25]

The tetrabutylammonium salts of $PtCl_6^{2-}$ and $PtCl_4^{2-}$ are obtained by the addition of aqueous solutions of NBu_4Cl to 1 M HCl solutions of $(H_3O)_2PtCl_6$ (Aldrich) and K_2PtCl_4 (Alfa Ventron), respectively. Dichloromethane solution of $(Bu_4N)_2PtCl_6$ which was treated with petroleum ether, yielded orange crystals when stored at -40°C. Attempts at growing $(Bu_4N)_2PtCl_4$ crystals by the same procedure produced red-brown oily residues, which persisted after solvent evaporation under a dynamic vacuum. The oil solidified only after violent agitation with pre-cooled (-40°C) petroleum ether. A crystalline $PtCl_4^{2-}$ salt which is soluble in nonaqueous solvents is found with tetraphenyl-arsonium (Ph_4As^+) cation. Large, red-brown bricks of the Ph_4As^+ salt are deposited from dichloromethane solutions layered with hexane.

Other Reagents. Tetrabutylammonium perchlorate (TBAP), obtained from Southwestern Analytical Chemicals, Inc. as a

white damp powder, was dissolved in ethyl acetate, dried over $MgSO_4$, and filtered. The filtrate was heated to boiling and hexane was added until a saturated solution of TBAP was achieved. Slow cooling produced colorless rectangular crystals which were collected, washed with ice-cooled ethyl acetate/hexane solution and dried for 48 hr. at 60°C under vacuum. Tetrabutylammonium chloride was purchased from Southwestern Analytical Chemicals and used without further purification. Tetrabutylammonium trifluoromethanesulfonate, NBu_4TFMS, prepared by Brändström's procedure,[26] was donated by Andrew W. Maverick and was recrystallized from *very cold* 2-propanol/diethyl ether solution.

Poly(methyl methacrylate) (PMMA) and methyl methacrylate (MMA) were purchased from Aldrich Chemical Co. and used without further purification.

Solvents. Electrochemical, spectroscopic (electronic absorption, electronic emission, time-resolved laser, laser transient and flash photolysis), and photochemical experiments employed solvents which were purified by the following procedures. All solvents were stored in glass containers which consisted of a one liter flask equipped with a high vacuum valve. Linde 3A and 4A Molecular Sieve and Woelm Grade I alumina (Nutritional Biochemicals) were activated by baking at 500°C for 24 hr. under a dynamic vacuum (<1 micron). Acetonitrile (UV), dichloromethane, tetrahydrofuran, chloroform, and acetone were obtained from

Burdick and Jackson Laboratories. Chloroform, acetone, and dichloromethane were degassed by seven freeze-pump-thaw cycles and then vacuum distilled onto activated Linde 4A Molecular Sieve. Tetrahydrofuran was degassed, also by seven freeze-pump-thaw cycles, and vacuum distilled into a flask containing benzophenone and sodium metal. Upon warming, the blue benzophenone radical anion immediately formed and after one day the violet dianion was produced, indicating an extremely dry, deoxygenated solvent. Acetonitrile was degassed by seven freeze-pump-thaw cycles , vacuum distilled onto Grade I alumina and stirred for one day after which it was distilled onto activated Linde 3A Molecular Sieve.

Electronic Absorption and Emission Experiments. Electronic absorption spectra were measured on a Cary 17 spectrometer. Steady-state emission spectra were recorded on an instrument built at Caltech.[27] Excitation light from 150 W Xe or 200 W Hg(Xe) arc lamps was wavelength selected with a 220 mm Spex Minimate monochromator and chopped at 535 Hz by a PAR 125A light chopper. Emitted light was monochromated by a 500 mm Spex monochromator (variable slit control) which was scanned by a Spex 1872 Minidrive motor. Photon detection was by a Hamamatsu R955 (extended multi-alkali response) or a dry-ice cooled R406 photomultiplier tube. The signal from the PMT was amplified by a PAR 181 preamplifier and fed into a PAR 186A Synchro-het lock-in amplifier.

Emission studies entailed various sample preparations. Solutions were prepared by vacuum distillation of the

appropriate solvent into all glass cells, after which the solution was subjected to five freeze-pump-thaw cycles. Poly(methyl methacrylate) films of $(Bu_4N)_2Re_2Cl_8$ were prepared by adding a dichloromethane solution of the compound to one of PMMA, followed by slow solvent evaporation. Films were microscopically scrutinized to insure that $(Bu_4N)_2Re_2Cl_8$ had not precipitated during solvent evaporation. Samples for quantum yield measurements of $(Bu_4N)_2Re_2Cl_8$ in PMMA were prepared by the following procedure. Approximately 1 mg of $(Bu_4N)_2Re_2Cl_8$ in 0.35 ml of CH_3CN was added to 4 ml of methyl methacrylate in a 1 cm fluorescence cuvette. The solution was treated with 0.85 mg of 2,2'-azobisisobutyronitrile (a radical initiator), degassed under an argon flow, sealed from the atmosphere, and heated at 80°C for two days. After the methyl methacrylate had completely polymerized, the cell was pumped under dynamic vacuum for 48 hr. The absolute quantum yield of $Re_2Cl_8^{2-}$ in PMMA was estimated by comparison to a CH_3CN solution of $Re_2Cl_8^{2-}$ ($\phi_e=10^{-4}$) with identical absorbance (A=0.2). The corrections enumerated by Demas were applied to all quantum yield calculations.[28] The observed emission spectra were corrected for monochromator and photomultiplier response.

Emission lifetimes were measured with a time-resolved laser system constructed at Caltech, the design of which has been discussed elsewhere.[29] All dinuclear rhenium halide species were excited with the third harmonic (λ_{exc}=353 nm; 40 mj/pulse; 8 ns fwhm) from a Quanta Ray DCR-1 Nd:YAG laser

equipped with a harmonic generator and separator. Luminescence was wavelength selected with a 350 mm MacPherson monochromator and detected by an RCA 928 PMT with a 50 Ω terminating resistance (RC time constant of ∿1.5 ns). Luminescence decay signals were photographed from a Hewlett-Packard 466 storage oscilloscope. For signal averaged lifetime measurements, the signal passed through a LeCroy (model VV101ATM) amplifier to a 50 Ω impedance input of a 6500 Biomation waveform recorder. Laser triggering, data acquisition and analysis were controlled by a PDP 11/03-L Digital Computer.

Low temperature measurements employed a Cryogenic Technology Inc. (Model 20) cryocooler which was appropriately modified for use with our spectrometers. Samples were usually mounted on a quartz disk affixed to a copper block by an Apiezon H grease/Cu powder mixture which also served as a thermal conductor between block and sample. Liquid helium spectra were measured with an Andonian 0-24 variable temperature optical dewar. Sample temperature was determined with a calibrated carbon glass resistor. Polycrystalline samples of $Re_2Cl_8^{2-}$ were sandwiched between two quartz plates and mechanically mounted in the helium dewar sample compartment. Emission spectra were recorded from front surface luminescence of the crystalline sample.

Stern-Volmer Quenching Experiments. Acetonitrile solutions of $(Bu_4N)_2Re_2Cl_8$ (typically 5×10^{-4} M) and TBAP (μ=0.1 M) were

prepared on an all glass vacuum line which attained final pressures of <1 micron. The cell used for steady-state quenching experiments consisted of a 10 ml round bottom with a quartz cuvette sidearm. The two chambers were isolated from the atmosphere by a Kontes quick release valve. The cell was connected to the vacuum line *via* a glass U-tube. Acetonitrile was transferred to the cell by bulb-to-bulb distillation and was then degassed by five freeze-pump-thaw cycles. Special precautions were taken to permit quencher additions to be performed under high vacuum. Liquid quenchers, which were measured with a 250 μl Finn-pipette that was calibrated to dispense liquid with greater than 98% accuracy, were added to the U-tube and subjected to five freeze-pump-thaw cycles before bulb-to-bulb distillation into the quenching cell. Inefficient luminescence quenchers required high amine concentrations in order to observe significant changes in $Re_2Cl_8^{2-}$ luminescence. Their addition caused the solution volume to increase during the course of an experiment. The volume changes were conveniently monitored by the absorbance of $Re_2Cl_8^{2-}$ at 680 nm (ε_{680}=2340 M^{-1} cm^{-1}). A calibration curve describing the dependence of the emission intensity on $Re_2Cl_8^{2-}$ concentration was used to correct Stern-Volmer constants. All quenching experiments were performed with 660 nm excitation light (150 W Xe lamp), 5 mm entrance and exit slit widths for both monochromators and R955 PMT detection. Luminescence intensities (I_{em}) were averages of three measured spectra

at each quencher concentration. Since the luminescence band shape did not change with quencher additions, I_{em} was measured from the emission band maximum of the uncorrected spectrum. Sample orientation and instrument stability were carefully monitored during quencher experiments to insure confidence in quenching data.

Electrochemical Experiments. Cyclic voltammograms were obtained with a Princeton Applied Research (PAR) 173 potentiostat/galvanostat driven by a PAR 175 universal programmer with a Pt button working, Pt wire auxiliary, and Ag wire reference electrodes. The auxiliary electrode was concentrically wrapped around the working electrode to provide uniform current densities for scan rates greater than 500 $mV\,s^{-1}$. In these experiments, cyclic voltammograms were displayed on a Tektronix digital oscilloscope. A conventional H-cell design was used in most electrochemical experiments. A small volume cell with a 1 ml working electrode compartment, the design of which is available in these laboratories, permitted electrochemical measurements on small sample quantities. Cyclic voltammograms were typically measured on solutions which were 2 mM in compound and 0.1 M in supporting electrolyte. Solvent purity was maintained by conducting all transfers under an argon counterflow.

Electrode potentials for binuclear rhenium chloride species were related to the standard calomel reference

potential through the previously reported $Re_2Cl_8^{2-/3-}$ couple,[47] which was present in all cyclic voltammograms. Ferrocene was used as an internal standard to correct for uncompensated cell resistance. Cyclic voltammograms of dinuclear rhenium bromide compounds and aromatic amines were referenced to the ferrocene potential (0.31 V *vs.* SCE).[30]

Bulk electrolysis experiments were performed with the above electrochemical apparatus in conjunction with a PAR 179 coulometer. Pt basket working and Pt foil auxiliary electrodes facilitated electrolysis. A Hewlett-Packard Model 8450A electronic absorption spectrometer was used to record optical spectra of electrolysis products.

Crystal Structure Solution and Refinement of $NBu_4Re_2Br_9$. The crystal structure analysis of $NBu_4Re_2Br_9$ was performed by Dr. William P. Schaefer at Caltech. Preliminary oscillation and Weissenberg photographs indicated a monoclinic cell. The only systematic absences, 0k0 with k=2n+1, are consistent with space groups $P2_1$ or $P2_1/m$. Wilson statistics indicated the centric space group $P2_1/m$ and the successful solution and refinement of the structure confirmed it. A prismatic crystal with edges .309, .292 and .374 mm was mounted and carefully centered on a Syntex $P2_1$ diffractometer with the *b* axis (0.374 mm) roughly parallel to ϕ. Cell dimensions were obtained by a least-squares fit to the setting angles of five reflections (four forms each of three

and two forms of one) with $27°<2\theta<30°$. Intensity data were collected using graphite-monochromatized MoKα radiation. Reflections with $3°<2\theta<50°$ were scanned in a θ-2θ mode at 2°/min; background was counted for one-half the scan time at each end of the scan, which was from 1° below $2\theta(K\alpha_1)$ to 1° above $2\theta(K\alpha_2)$. Three reflections were measured every 100 reflections; they showed an average decrease of 7.5% and the data were corrected for this decay, for absorption, and for Lorentz and polarization factors. From the 2585 reflections scanned, 2424 independent reflections were obtained, of which 2146 had $F_o^2>0$ and 1275 had $F_o^2 > 3\sigma(F_o^2)$.

The structure was solved by Patterson and Fourier methods and refined by full-matrix least squares using programs of the CRYRM system. After the atoms of the anion were refined, we were able to pick out the cation atoms. The nitrogen atom lies on the mirror plane and two of the *n*-butyl groups lie near this plane in a disordered fashion. The other group (and its mirror image) is even less well defined. Least squares refinement of a scale factor, positional parameters for all the atoms, anisotropic thermal parameters for Re and Br atoms and isotropic thermal parameters for N and C led to an R-index of 0.108 for all positive reflections and 0.066 for those with $F_o^2>3\sigma(F_o^2)$ ($R = \Sigma(|F_o-|F_c||)/\Sigma F_o$). The goodness of fit ($=[\Sigma w(F_o^2-F_c^2)^2/(n-p)]^{\frac{1}{2}}$) is 2.13 for n = number of data = 2424 and p = number of parameters = 115; this high value reflects the

fact that the thermal motion of the anion is large and that our model for the tetrabutylammonium ion is very poor. Residual electron density near the heavy atoms and in the region of the cation is as high as 2.3 e/Å^3, the isotropic thermal parameters of the carbon atoms run as high as 32 Å and the carbon-carbon distances range from 1.12 Å to 1.49 Å. The residual peaks did not correspond to any better geometry and differing models of the cation had no effect on the refinement of the anion, so this unsatisfactory model was retained.

Photolysis Experiments. Steady-state photolysis experiments were performed in two arm evacuable cells equipped with Kontes quick release teflon valves. Tetrabutylammonium chloride was placed in one arm of the cell and $(Bu_4N)_2Re_2Cl_8$ in the other. Quencher was added to the cell against an argon counterflow after the NBu_4Cl had been dried for 4 hr. at 100°C under dynamic vacuum (<1 micron). The cell was re-evacuated and the solvent was transferred by vacuum distillation. All solutions were subjected to five freeze-pump-thaw cycles. Photolyses were performed with a 1000 W high pressure Hg(Xe) lamp and high energy light was eliminated with a series of Corning cut-off filters. In a typical experiment, 1 mM $(Bu_4N)_2Re_2Cl_8$, 10 mM quencher, and 100 mM NBu_4Cl were irradiated in CH_3CN or CH_2Cl_2 solution at 10±1°C. Photolysis products were separated from irradiated solutions by column chromatography. Florasil®

was the absorbent and CH_2Cl_2/CH_3CN solvent systems were used for elution; CH_3CN greatly reduced the elution times of all compounds from the column.

Flash photolysis experiments were performed on an instrument built at Caltech.[31] Data were collected with single 300 joule pulses from xenon flash lamps. Corning high energy cut-off filters were used to selectively irradiate the desired spectral regions of the compound of interest. Flash cells consisted of a 15 cm pathlength monitoring chamber, a 50 ml round bottom and a 1 cm quartz cuvette, each of which were constructed at a 90° angle to its neighboring compartment. Samples were prepared by bulb-to-bulb solvent distillation. Solutions were subjected to five freeze-pump-thaw cycles and blanketed with argon. The $TCNE^-$ and chloranil anion molar extinction coefficients used for back reaction rate constant calculations were measured to be: $TCNE^-$, $\varepsilon_{438} = 7.43 \times 10^3\ M^{-1}cm^{-1}$ (CH_2Cl_2); chloranil anion, $\varepsilon_{460} = 4.90 \times 10^3\ M^{-1}cm^{-1}$ (CH_3CN), and $\varepsilon_{466} = 4.92 \times 10^3\ M^{-1}cm^{-1}$ (acetone).

Other Procedures. The thermal oxidation kinetics of $Re_2Cl_8^{2-}$ (CH_2Cl_2; μ=0.1 M, NBu_4Cl) by high purity chlorine was monitored by the absorbance of the solution at 685 nm. Tetrabutylammonium chloride was dried under vacuum for 30 min.

EPR spectra were recorded on a Varian E-line Century Series X-Band spectrometer equipped with an Air Products Heli-Trans low temperature system. All EPR experiments were

performed at 10 K on frozen CH_2Cl_2 solutions which had undergone five freeze-pump-thaw cycles.

C. SPECTROSCOPY OF OCTACHLORODIRHENATE

The electronic spectroscopy of the $Re_2Cl_8^{2-}$ anion is of long-standing interest since the compound remains the prototypal quadruply bonded metal-metal dimer. The bonding in $Re_2Cl_8^{2-}$ is aptly described by the molecular orbital diagram for L_4MML_4 dimers (see Figure 1). The electronic absorption spectrum of $Re_2Cl_8^{2-}$ in acetonitrile is illustrated in Figure 2. The beautiful blue color of $Re_2Cl_8^{2-}$ solutions arises from the absorption band at 14,700 cm^{-1}. The transition associated with this band was the source of much confusion during the early years of quadruple bond chemistry. It is now agreed, however, that the absorption band arises from the orbitally and spin allowed $\delta \rightarrow \delta^*$ ($^1A_{2u} \leftarrow {}^1A_{1g}$) transition, first assigned by Cowman and Gray in 1972 on the basis of the band's temperature independence and z polarization.[32]

The higher energy absorption bands of $Re_2Cl_8^{2-}$ have also been investigated, most notable of which are those centered at 566 nm and 478 nm, first assigned to $\delta \rightarrow \pi^*$ ($^1E_{1g} \leftarrow {}^1A_{1g}$) and $\delta \rightarrow d_{x^2-y^2}$ ($^1A_{1u} \leftarrow {}^1A_{1g}$), respectively.[33] A recent study using improved crystal absorption spectra attributes the 566 nm band system to both the $\delta \rightarrow \pi^*$ and $\pi \rightarrow \delta^*$ ($^1E_{1g} \leftarrow {}^1A_{1g}$) transitions and the 478 nm profile to the orbitally allowed $\pi \rightarrow \pi^*$ ($^3A_{2u} \leftarrow {}^1A_{1g}$) transition.[34] Within the context of the photochemistry reported herein,

Figure 2. Electronic absorption spectrum of $(Bu_4N)_2Re_2Cl_8$ in acetonitrile solution at room temperature.

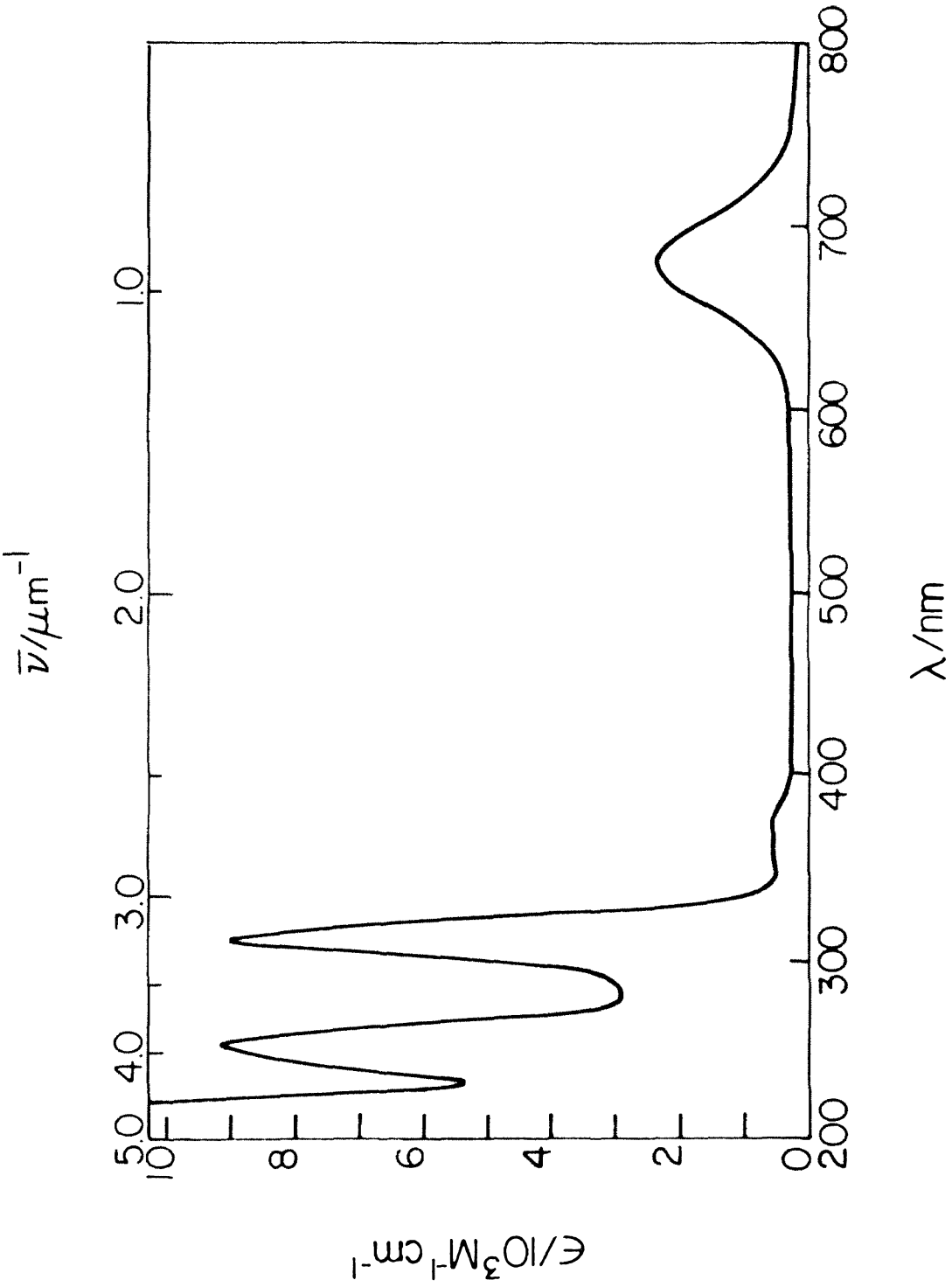
$\bar{\nu}/\mu m^{-1}$
5.0
4.0
3.0
2.0
1.0
$\epsilon/10^3 M^{-1} cm^{-1}$
10
8
6
4
2
0
200
300
400
500
600
700
800
λ/nm

it suffices to note that the transitions immediately to higher energy of $\delta \rightarrow \delta^*$ are metal localized ones involving π orbitals.

Both crystals and nonaqueous solutions containing $(Bu_4N)_2Re_2Cl_8$ luminesce in the near infrared upon excitation of the $\delta \rightarrow \delta^*$ transition. A structureless luminescence band was first reported from a single crystal of $(Bu_4N)_2Re_2Cl_8$ at 1.3 K upon 650 nm excitation and was assigned to the spin forbidden $\delta^* \rightarrow \delta$ ($^1A_{1g} \leftarrow {}^3A_{2u}$) transition.[35] Fluorescence decay from the $^1A_{2u}$ state was contested because of the lack of overlap of the emission band with the 0-0 transition in absorption and the absence of mirror symmetry between the emission and absorption ($^1A_{2u} \leftarrow {}^1A_{1g}$) profiles. Emission from $^1A_{2u}$ was not completely ruled out, however, as the authors noted that a large geometrical distortion in the $^1A_{2u}$ state could account for non-overlapping emission and absorption systems. Subsequent studies proposed, in fact, on the basis of the emissive properties of the structurally rigid $Mo_2Cl_4(PR_3)_4$ (R=alkyl)(D_{4h}) quadruple bond dimers, that the emissive state in $Re_2Cl_8^{2-}$ possessed an equilibrium geometry near D_{4d} (or D_4) symmetry (arising from the torsional rotation of the two $ReCl_4$ units about the metal-metal axis).[36] Emission was assigned to $\delta\delta^*$ (singlet) (D_4 or D_{4d}) $\rightarrow \delta^2$ ($^1A_{1g}$). This assignment is in accord with theoretical studies which place the $^3A_{2u}$ state only 3000 to 4000 cm^{-1} above the $^1A_{1g}$ ground state.[37]

Elucidation of $Re_2Cl_8^{2-}$ excited state's energy, geometry and lifetime is crucial to a complete description of $Re_2Cl_8^{2-}$ photochemistry. Recent correspondence with Professor R. D. Peacock at the University of Glasgow, in which he described a vibrationally structured emission band of $Re_2Cl_8^{2-}$, prompted us to re-examine the low temperature luminescence properties of $Re_2Cl_8^{2-}$. New information from the $Re_2Cl_8^{2-}$ emissive state is now presented.

Results

The luminescence spectrum of polycrystalline $(Bu_4N)_2Re_2Cl_8$ at 5 K is displayed in Figure 3.[38] Vibronic maxima resolve on the high energy side of the emission band. The relative intensities of the peaks are not in accord with those predicted for a single harmonic Franck-Condon progression.[39] The peak intensities do, however, suggest two vibrational progressions built on a'_0 and b'_0. The peak positions and energy spacings are shown in Table 1, with ±10 cm^{-1} uncertainty. The 288 cm^{-1} average energy spacing of both progressions may reasonably be interpreted to be the symmetric ReRe stretching vibration; the ground state $\nu_{a_{1g}}$ (ReRe) stretching frequency is 275 cm^{-1} as determined from Raman measurements.[40] The vibrational structure is unresolved at 30 K.

The emission quantum yield, ϕ_e, of crystalline $(Bu_4N)_2Re_2Cl_8$ at room temperature appears to be much

Figure 3. Uncorrected emission spectrum of polycrystalline $(Bu_4N)_2Re_2Cl_8$ at 5 K (680 nm excitation, 50 cm^{-1} resolution).

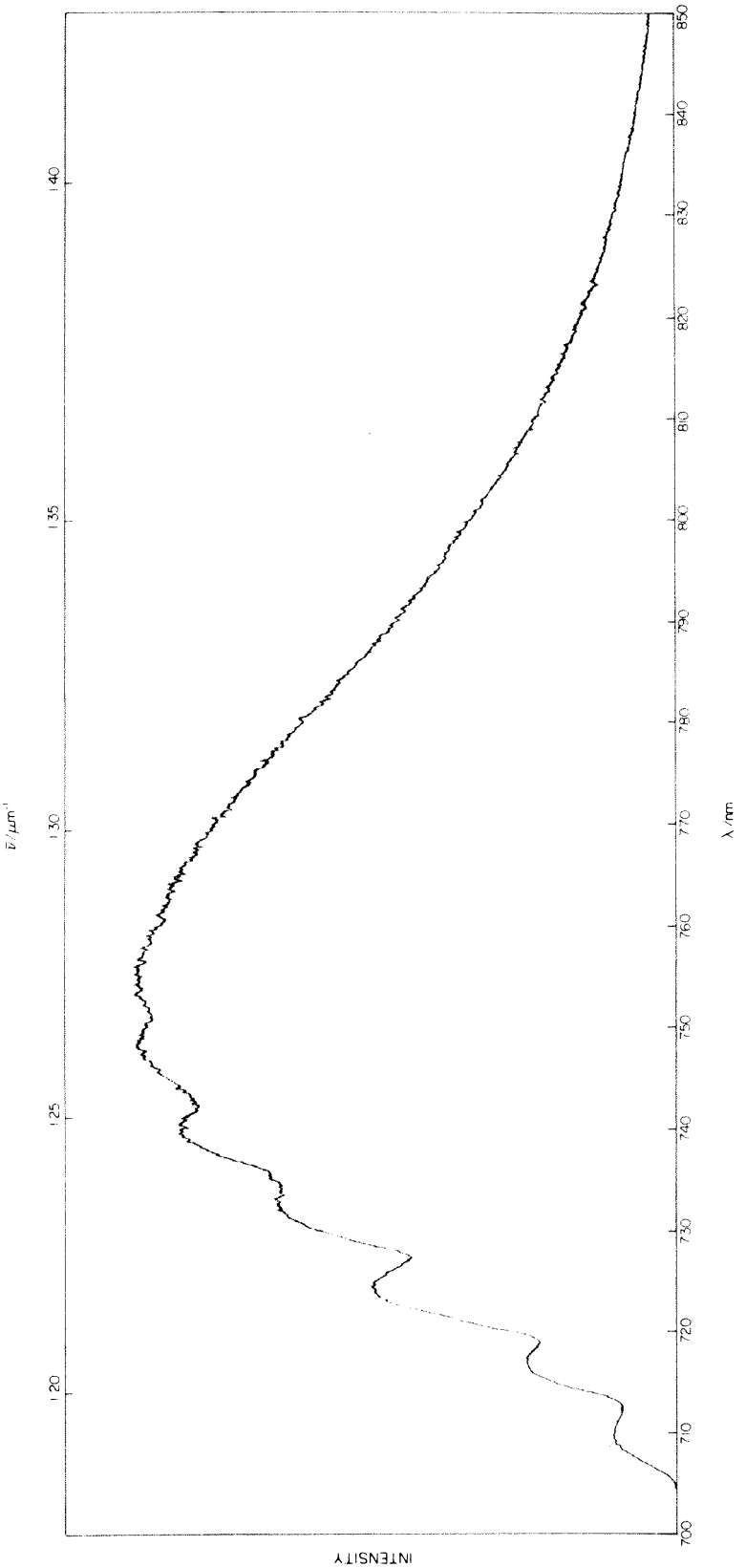
INTENSITY
$\bar{\nu}$ /μm^{-1}
1.20
1.25
1.30
1.35
1.40
λ /nm
700
710
720
730
740
750
760
770
780
790
800
810
820
830
840
850

Table 1. Vibrational Structure of the Luminescence Band of Polycrystalline $Re_2Cl_8^{2-}$ at 5 K.

Peak	nm[a]	cm^{-1}	$\Delta\bar{\nu}(a')$ cm^{-1}	$\Delta\bar{\nu}(b')$ cm^{-1}
a_0'	709.92	14,086[b]	0[c]	
b_0'	717.12	13,945		141
a_1'	724.56	13,801	285	
b_1'	732.72	13,657		288
a_2'	740.16	13,511	290	
b_2'	748.08	13,368		289

[a] Vibronic peak maxima.

[b] $\pm 10\ cm^{-1}$.

[c] The absorption (a_0'') and emission (a_0') vibronic maxima establish the pure electronic origin at 14,129 cm^{-1} (see text).

greater than solution values. Similarly, a more quantitative measurement showed ϕ_e of $Re_2Cl_8^{2-}$ in PMMA to be 20 times that of $\phi_e(CH_3CN)$ even though the emission lifetime of $Re_2Cl_8^{2-}$ was 127 ns in the PMMA film and 140 ns in CH_3CN. Miskowski *et al.* also noted that the quantum yield of $Re_2Cl_8^{2-}$ in a 2:1 2-methyltetrahydrofuran: propionitrile glass at 77 K was a factor of 75 greater than the solution value (at room temperature),[36] despite the identical lifetimes of $Re_2Cl_8^{2-}$ in the two environments (i.e. rigid *vs.* solution).[41] The emission quantum yield reflects the excited state lifetime through the relation,

$$\phi_e = \frac{k_r}{k_r+k_{nr}} = \frac{k_r}{k_{obs}} = k_r\tau_{obs} \qquad (1)$$

where k_r and k_{nr} are the radiative and nonradiative rate constants, respectively, of the excited state. The above experiments clearly demonstrate the capacity of a rigid environment to significantly increase k_{rad} relative to solution; that the observed lifetime does not change indicates $k_r << k_{nr}$, and k_{obs} is predominantly represented by k_{nr}. The temperature dependence of k_{obs} in crystalline $(Bu_4N)_2Re_2Cl_8$ is summarized in Table 2. To a first approximation, the observed lifetime may be defined by,

$$k_{obs} = \frac{k_0 + k_1 e^{-\Delta E/kT}}{1 + e^{-\Delta E/kT}} \qquad (2)$$

Table 2. Observed Emission Lifetime as a Function of Temperature in Polycrystalline $Re_2Cl_8^{2-}$.

T(K)	τ_{obs}[a] ns	$k_{obs} \times 10^{-6}$ s^{-1}
4.6	231	4.33
4.8	231	4.33
7.7	232	4.31
10.6	219	4.57
14.0	235	4.25
22.1	236	4.24
37.0	230	4.35
49.0	232	4.31
57.0	225	4.44
79.0	194	5.15
81.0	194	5.15
93.0	185	5.41
103.0	177	5.65
105.0	178	5.62
113.0	172	5.81
122.0	167	5.99
132.0	165	6.06
143.0	158	6.33
153.0	159	6.29
163.0	158	6.33
173.0	165	6.06
184.0	166	6.02
193.0	158	6.33
202.0	161	5.92
213.0	169	5.92
222.0	167	5.99
233.0	167	5.99
243.0	166	6.02
253.0	160	6.25
263.0	160	6.25

[a] ±5 ns.

where ΔE is the energy separation between two thermally equilibrated states, the lower of which is characterized by nonradiative rate constant k_0, and the upper state by k_1. A plot of k_{obs} *vs.* T is shown in Figure 4. The temperature independence of k_{obs} at small T defines k_0 to be 4.33×10^6 sec^{-1} (τ_0=232 ± 5 ns). A two parameter fit of the lifetime data in Table 2 with equation 2 (indicated by the solid line in Figure 4) yields a state energy separation of 120 ±20 cm^{-1} and k_1 to be 11.11×10^6 sec^{-1} (τ_0=90±10 ns).

The luminescence properties of other dirhenium quadruple bond complexes are less well-defined. Crystals of the cesium salt of $Re_2Cl_8^{2-}$ at 5 K show luminescence ($\lambda_{max,em}$ > 820 nm) considerably red-shifted from the emission band of the tetrabutylammonium salt. The lower energy luminescence may be attributed to the weaker metal-metal interaction of $Re_2Cl_8^{2-}$ anion due to the axial coordination of H_2O in the cesium salt's crystal lattice.[42] The effect of phosphine substitution on emission properties of molybdenum halide quadruple bond dimers[43] stimulated the investigation of $[Re_2Cl_4(PMe_2Ph)_4](PF_6)_2$. An unstructured, extremely weak emission band ($\lambda_{max,em}$ > 910 nm) is observed upon 710 nm excitation of crystalline solid at 77 K. The presence of $Re_2Cl_5(PMe_2Ph)_3$ as an impurity in these samples makes interpretations of the luminescence spectrum tenuous, at best. Interestingly, highly purified crystalline samples and solutions of $Re_2Cl_6(PEt_3)_2$ demonstrate no luminescence at room temperature nor 77 K.

Figure 4. Plot of observed rate constant (●) for luminescence decay in polycrystalline $(Bu_4N)_2Re_2Cl_8$ as a function of temperature. Two parameter fit of equation 2 with data in Table 2 ($k_0=4.30\times10^6$ s^{-1}, $\tau_0=232(\pm5)$ ns) yields $\Delta E=120(\pm20)$ cm^{-1} and $k_1=11.11\times10^6$ s^{-1} ($\tau_1=90(\pm10)$ ns). Calculated fit designated by solid line.

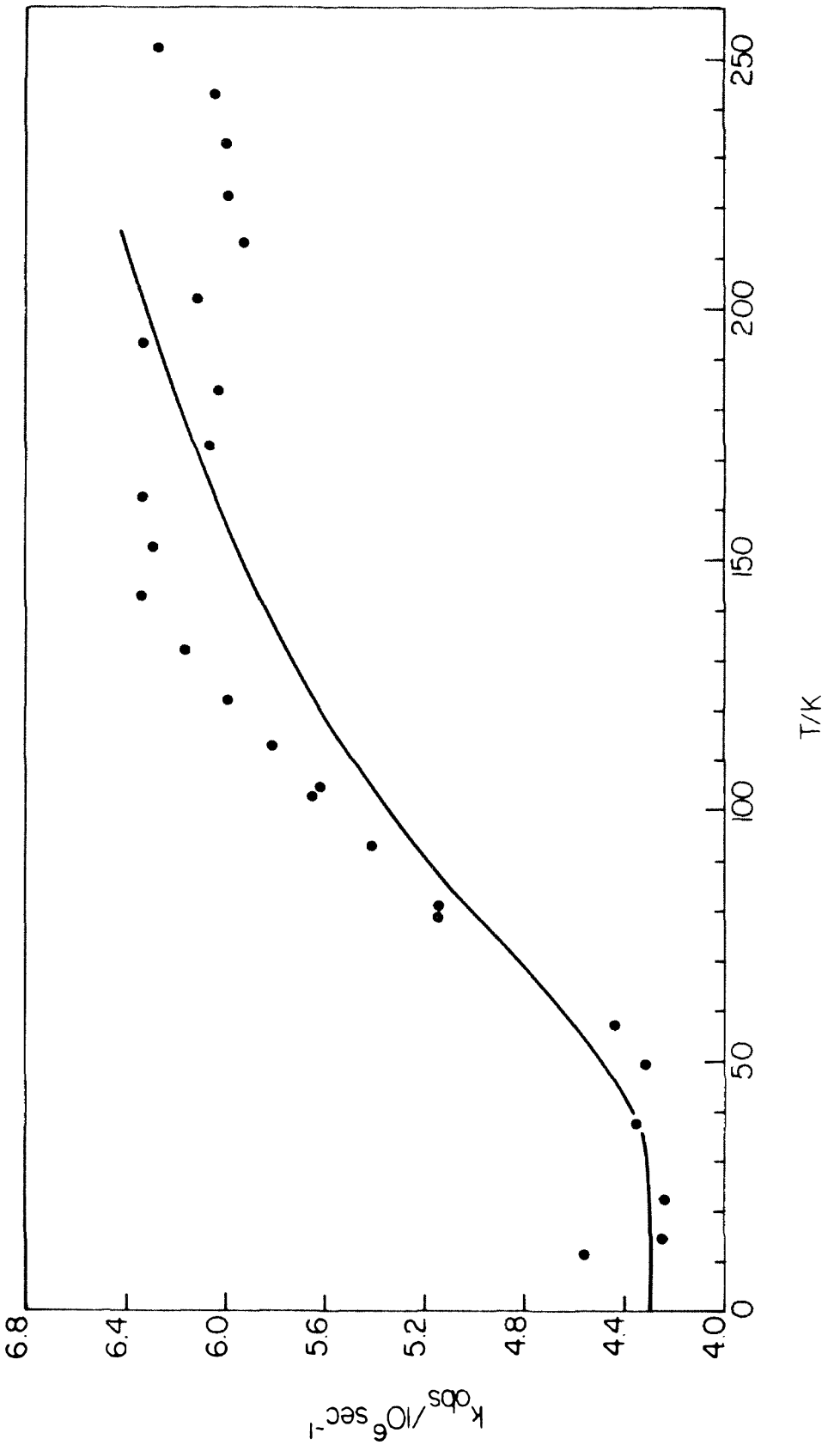
6.8
6.4
6.0
5.6
5.2
4.8
4.4
4.0
0
50
100
150
200
250
T/K
$k_{obs}/10^6 sec^{-1}$

Discussion

The structured luminescence of $Re_2Cl_8^{2-}$ permits a much stronger comparison between ground and excited state properties than was possible in past spectroscopic investigations. The vibronic structural data from Cowman's landmark investigation of the electronic absorption spectrum of $Re_2Cl_8^{2-}$ is included in Table 3 along with the luminescence data from Table 2. The luminescence spectrum may be interpreted in terms of two vibrational progressions in quanta of 288 cm^{-1}, corresponding to $\nu_{a_{1g}}$ (ReRe), built on a_0' and b_0'. Similarly, the absorption system shows two progressions in quanta of 248 cm^{-1}, also attributable to $\nu_{a_{1g}}$ (ReRe), and built on a_0 and b_0. Closer examination of the absorption spectrum reveals that the electronic origin is not well-defined. Indeed, it is bothersome that the energy spacing between v_0 and v_1 is 224 cm^{-1}, while all the other energy spacings in the progression are 249±1 cm^{-1} (see Table 3). These results suggest that the vibronic maximum of the 0-0 transition in the absorption spectrum is 25 cm^{-1} to lower energy than the previously assigned value of 14,183 cm^{-1}. Choosing 14,157 cm^{-1} as the vibronic maximum of the 0-0 transition (designated a_0'') results in a 141 cm^{-1} energy separation between a_0'' and b_0 the energy of which agrees with the ReReCl bending mode of e_g symmetry.

Table 3. Vibrational Structure of the $\delta \rightarrow \delta^*$ Absorption Band and the Luminescence Band of Polycrystalline $Re_2Cl_8^{2-}$ at 5 K.

$\delta \rightarrow \delta^*$ Absorption System:[d]					Emission System:[e]				
Peak	nm[a]	cm^{-1}	$\Delta\bar{\nu}(a)$ cm^{-1}	$\Delta\bar{\nu}(b)$ cm^{-1}	Peak	nm[a]	cm^{-1}	$\Delta\bar{\nu}(a')$ cm^{-1}	$\Delta\bar{\nu}(b')$ cm^{-1}
a_0	705.06	14,183[b]	0		a_0'	709.92	14,086[c]	0	
b_0	699.41	14,298		115	b_0'	717.12	13,945		141
a_1	694.12	14,407	224		a_1'	724.56	13,801	285	
b_1	687.65	14,542		245	b_1'	732.72	13,657		288
a_2	682.41	14,654	247		a_2'	740.16	13,511	290	
b_2	676.24	14,788		245	b_2'	748.08	13,368		289
a_3	671.00	14,903	249						
b_3	665.06	15,036		249					
a_4	660.00	15,152	248						
b_4	654.35	15,282		246					
a_5	649.29	15,401	250						
b_5	644.12	15.525		243					
a_6	639.00	15,649	248						
b_6	634.29	15,766		240					

[a]Vibronic peak maxima. [b]± 2 cm^{-1}. [c]± 10 cm^{-1}. [d]Ref. 32. [e]This work.

The first two vibronic bands of the readjusted absorption spectrum (a_0'' and b_0) and emission spectrum (a_0' and b_0') are illustrated in Figure 5. The 120 cm^{-1} breadth of the vibronic bands in the luminescence spectrum is much greater than the natural line width and can be attributed to coupling of the electronic transitions with low energy vibrational modes (e.g. lattice vibrations, torsional modes of the anion).[44] Given this assumption, the pure electronic origin will be found in the low energy tail of the absorption vibronic band and the high energy tail of emission. The symmetrical disposition of the absorption and emission vibronic bands places the pure electronic origin at 14,129 cm^{-1}. Thus, the emission spectrum clearly overlaps the electronic origin of the $^1A_{2u} \leftarrow {}^1A_{1g}$ transition.

Of course, the above analysis does not explain all of the details of the electronic absorption and emission spectra of $Re_2Cl_8^{2-}$. The disappearance of the vibrational structure near the emission band maximum, the intensity discrepancies between the absorption and emission vibronic maxima and the overall lack of mirror symmetry between the absorption and emission profiles indicate that the correct description of the excited state potential energy surface is, indeed, a complicated one. The luminescence spectrum and temperature dependence of k_{obs} appear to support Miskowski *et al.'s* proposal of a highly distorted excited state. The 120 cm^{-1} energy gap in the excited state potential energy surface

Figure 5. Electronic origin region of $Re_2Cl_8^{2-}$. Peaks a_0" and b_0 are the first two vibronic components of the $\delta \rightarrow \delta^*$ absorption system (ref. 32); peak a_0" has been relocated as described in the text and was fit to a Gaussian band shape. Peaks a_0' and b_0' are the first two vibronic components of the luminescence band. Arrow signifies pure electronic origin.

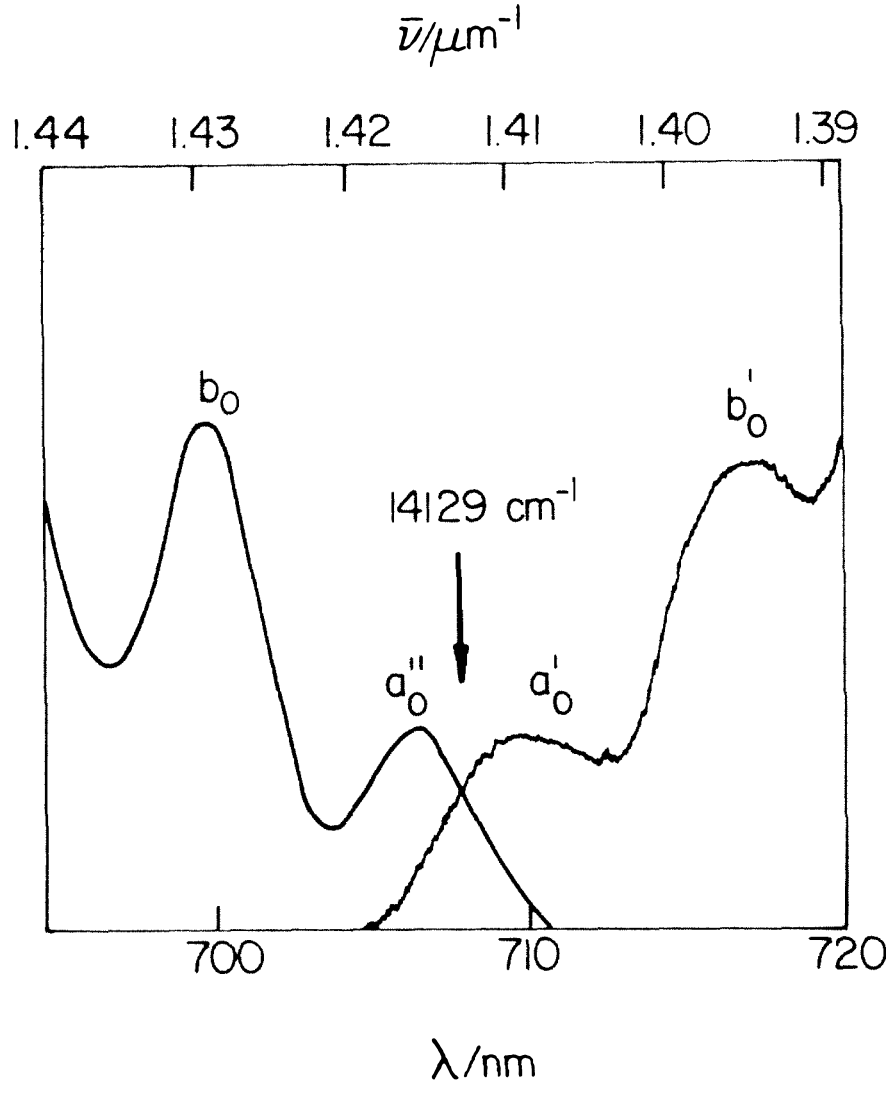
$\bar{\nu}/\mu m^{-1}$
1.44
1.43
1.42
1.41
1.40
1.39
b_0
b_0'
14129 cm^{-1}
a_0''
a_0'
700
710
720
λ/nm

(as determined from equation 2) may, in fact, represent the energy separation between the D_{4h} and D_{4d} excited states. The relaxation of $Re_2Cl_8^{2-}$ (D_{4h}) to its D_{4d} (or D_4) torsional isomer involves the activation of many coupled vibrational modes in the molecule. As the $ReCl_4$ units twist about the metal axis in the excited state, the steric interactions between the chloride ligands (which are partly manifested in a 104° ReReCl angle of the D_{4h} geometry) will decrease, thereby allowing (i) a shorter metal-metal bond distance and (ii) smaller ReReCl bond angles in the D_{4d} (or D_4) geometry. In light of these structural changes, it is interesting to note that both absorption and emission spectra possess progressions in the symmetric ReRe vibration and a 140 cm^{-1} vibrational mode corresponding to the ReReCl bending vibration.

The enigmatic $Re_2Cl_8^{2-}$ excited state still awaits its complete description. The above investigation does, however, clearly establish the luminescent excited state of $Re_2Cl_8^{2-}$ to be of $\delta\delta^*$ *singlet* character, an important consideration in $Re_2Cl_8^{2-}$ photochemistry.

D. BINUCLEAR RHENIUM HALIDE ELECTROCHEMISTRY

The electrochemical reactions of quadruply bonded halide dimers can provide a foundation from which their photoredox chemistry may be developed. Previous electrochemical studies have painted a somewhat misleading picture of $Re_2X_8^{2-}$ redox chemistry. Initially, $Re_2Cl_8^{2-}$ was reported to exhibit a two wave reduction polarogram, a reversible wave at -0.83 V *vs.* SCE and an irreversible wave at -1.44 V *vs.* SCE.[45] Unfortunately, at the time of this study, the molecular orbital analysis of the bonding in $Re_2Cl_8^{2-}$ predicted the lowest unoccupied molecular orbital to be σ nonbonding. On the basis of the incorrect molecular diagram, the polarographic waves were attributed to consecutive one-electron reductions of $Re_2Cl_8^{2-}$ to produce $Re_2Cl_8^{3-}$ and $Re_2Cl_8^{4-}$. A more detailed electrochemical study on $Re_2Cl_8^{2-}$ was reported six years later.[46] Employing a battery of electrochemical techniques, the authors concluded the initial electrochemical investigation to be correct. In addition, controlled potential electrolysis of $Re_2Cl_8^{2-}$ at -1.01 V *vs.* SCE to produce $Re_2Cl_8^{3-}$ was claimed despite a non-exponential current/time curve. An electronic absorption spectrum of the electrolyzed solution was interpreted to be $Re_2Cl_8^{3-}$. It was also reported that the cyclic voltammogram of $Re_2Br_8^{2-}$ showed two irreversible reduction waves with peak potentials at -0.70 V and -1.32 V *vs.* SCE. Much of the existing confusion associated with the

above investigations was clarified by rotating disk polarography and cyclic voltammetric studies of Cotton and Pedersen.[47] Their results showed that nonaqueous solutions of $Re_2Cl_8^{2-}$ did, indeed, undergo a one-electron quasi-reversible process at -0.840 V *vs.* SCE corresponding to $Re_2Cl_8^{3-}$ formation. From the variation of the peak current ratio of the cyclic voltammetric reduction wave with scan rate, it was estimated that $Re_2Cl_8^{3-}$ irreversibly decomposed with an unimolecular rate constant of 0.5 s^{-1}, thereby refuting the purported electronic absorption spectrum of $Re_2Cl_8^{3-}$. Evidence for reduction of the quadruple bond to $Re_2Cl_8^{4-}$ was not obtained. A large irreversible oxidation wave at $\geq$1.25 V *vs.* SCE was also reported, however, further studies directed toward the elucidation of the oxidation processes were not pursued. Presumably, the authors concluded that the oxidation wave corresponded to ligand oxidation since nonaqueous chloride solutions are oxidized to chlorine at potentials near 1.25 V *vs.* SCE. Assignment of the anodic wave to chloride oxidation is bothersome in light of the electrochemical oxidation chemistry of $M_6X_{14}^{2-}$ (M=Mo,W; X=Cl,Br) cluster compounds, which undergo simple one-electron reversible oxidations in aprotic solvents at potentials quite positive of the free halide ion.[48] These results indicate the stability of the clusters in nonaqueous solvents. There is no reason, a priori, to expect the $Re_2X_8^{2-}$ system to be any less robust than the cluster systems.

The thermal oxidation chemistry of $Re_2Cl_8^{2-}$ was first studied by Cotton and coworkers,[22] who showed $Re_2X_8^{2-}$ oxidation by halogen gas to produce confacial bioctahedral $Re_2X_9^-$. The monoanion is readily reduced by one electron to the mixed valence dimer, $Re_2X_9^{2-}$, by a variety of reducing agents. Indefinitely stable as a solid at room temperature, $NBu_4Re_2X_9$ was readily converted to $Re_2X_9^{2-}$ in methanol solutions over the period of minutes and prolonged heating finally yielded $Re_2X_8^{2-}$. The mechanism for the reaction was not determined, however, formaldehyde nor formic acid were detected as oxidation products.

The thermal reaction chemistry of $Re_2X_8^{2-}$ indicates that confacial bioctahedral dirhenium halide species may play an important role in quadruple bond electrochemistry. To this end, the electrochemical reactions of $Re_2X_8^{2-}$ and $Re_2X_9^{2-}$ are reported below. The crystal structure of $NBu_4Re_2Br_9$ is also reported.

Results

Binuclear Rhenium Chloride Systems. The cyclic voltammogram of $NBu_4Re_2Cl_9$ (~2 mM) in dichloromethane with TBAP (μ=0.1 M) supporting electrolyte is shown in Figure 6a. Scanning cathodically from 0.8 V *vs.* SCE, three reduction waves are observed of which two show anodic return waves. The irreversible component (wave B) does not show an anodic return wave for scan rates up to 500 V s^{-1}. The wave illustrated by the dashed line in Figure 6a (wave A) is

Figure 6. Cyclic voltammograms (CH_2Cl_2 solution at 22°C, 0.1 M TBAP) for: (a) $NBu_4Re_2Cl_9$ (2mM); (b) $(Bu_4N)_2Re_2Cl_8$ (2mM), and NBu_4Cl (10mM); (c) $(Bu_4N)_2Re_2Cl_8$ (2mM).

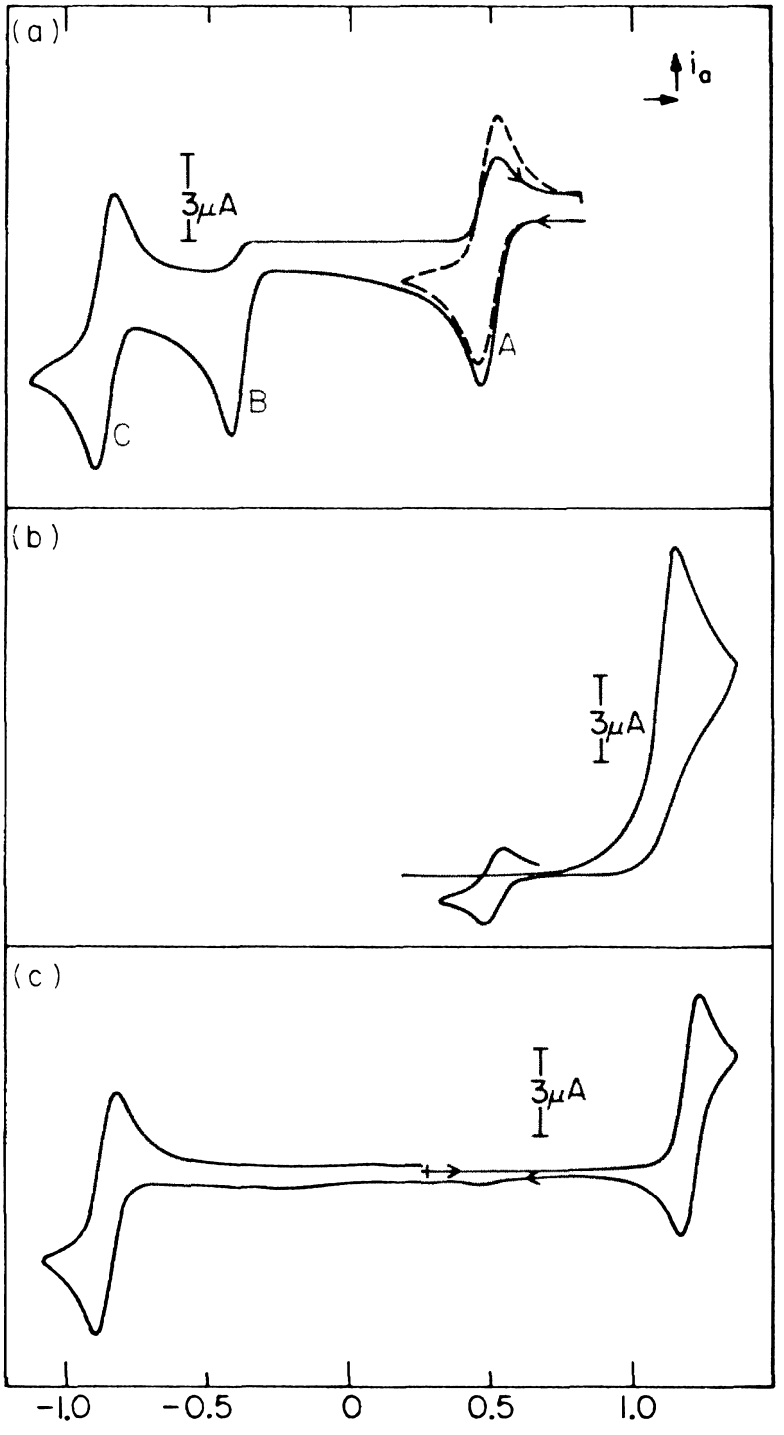
(a)
i_a
3μA
A
B
C
(b)
3μA
(c)
3μA
-1.0
-0.5
0
0.5
1.0
$E_{1/2}$/V vs SCE

obtained if the scan is reversed before wave B is reached. A reversible electrode process for wave A is indicated by linear plots of the anodic and cathodic currents *vs.* (scan rate)$^{\frac{1}{2}}$ (for scan rates of 20 to 500 mV s^{-1}), values of 1.02±0.03 for the ratio of the anodic to cathodic peak currents (i_a/i_c), and the peak separation of 65 mV.[49] Bulk electrolysis of a green CH_2Cl_2 solution of $Re_2Cl_9^-$ at 0.2 V *vs.* SCE is complete upon passage of 1.04 equivalents of electrons into solution. An optical spectrum of the resulting violet solution is identical with that of $Re_2Cl_9^{2-}$, indicating wave A to be the $Re_2Cl_9^{-/2-}$ couple with a measured half-wave potential of 0.53 V *vs.* SCE. Bulk electrolysis of the violet $Re_2Cl_9^{2-}$ solution at -0.5 V *vs.* SCE passes 1.06 equivalents of electrons into solution and an optical spectrum of the blue electrolysis product is that of $Re_2Cl_8^{2-}$. These experiments confirm that wave B corresponds to the irreversible one-electron reduction of $Re_2Cl_9^{2-}$ to form $Re_2Cl_8^{2-}$ and Cl^-. Wave C of Figure 6a, therefore, corresponds to the reversible $Re_2Cl_8^{2-/3-}$ couple at -0.85 V *vs.* SCE.

The facility at which $Re_2Cl_9^{2-}$ interconverted to $Re_2Cl_8^{2-}$ and chloride suggested to us the possibility that the reverse reaction might occur. Our initial oxidation studies on $Re_2Cl_8^{2-}$ consistently produced cyclic voltammograms similar to the one shown in Figure 6b, a large anodic current at 1.25 V (in accordance with Cotton and Pedersen's observation) with a smaller cathodic wave at 0.50 V.

Comparison to Figure 6a indicates the formation of confacial bioctahedron, suggesting the presence of Cl^- impurities in our $Re_2Cl_8^{2-}/CH_2Cl_2$ solutions. These results prompted the careful purification of $(Bu_4N)_2Re_2Cl_8$. The cyclic voltammogram of purified $(Bu_4N)_2Re_2Cl_8$ (2 mM) in CH_2Cl_2 with TBAP (μ=0.1 M) as a supporting electrolyte is shown in Figure 6c. The one-electron oxidation wave of $Re_2Cl_8^{2-}$ at 1.25 V *vs.* SCE is now observed in addition to the $Re_2Cl_8^{2-/3-}$ couple. The oxidation wave is quasi-reversible for scan rates up to 500 mV s^{-1}. At scan rates of 10 V s^{-1} to 100 V s^{-1}, i_a/i_c is equal to 1.02±0.02 indicating electrochemical reversibility. The peak separation increases monitonically with increasing scan rate (130 mV at 100 V s^{-1}), a result of either slow electron transfer kinetics at the electrode surface or uncompensated cell resistance. Observation of electrochemical reversibility for the $Re_2Cl_8^{2-}$ oxidation wave depended on sample preparation.

Addition of dry NBu_4Cl to solutions of highly purified $Re_2Cl_8^{2-}$ gives rise to the cyclic voltammogram in Figure 6b. The large anodic wave with no reversible cathodic component is observed when the potential is anodically scanned from 0.2 V *vs.* SCE. Presumably, the anodic wave corresponds to the oxidation of Cl^-, $Re_2Cl_8^{2-}$ and $Re_2Cl_9^{2-}$. Scanning to more negative potentials from the large oxidation wave yields the reversible $Re_2Cl_9^{-/2-}$ couple at 0.53 V *vs.* SCE. The production of confacial bioctahedron is observed for

scan rates up to 500 V s^{-1}. The cyclic voltammetric results in the presence of anionic donors such as Cl^- explain why the $Re_2Cl_8^{-/2-}$ couple may be observed only for highly purified samples of $Re_2Cl_8^{2-}$.

Addition of $Re_2Cl_8^{2-}$ (3 μmoles) to deaerated Cl_2-saturated (1.59 M at 20°C[50]) CH_2Cl_2 solution (5 ml) containing 0.1 M Cl^- produces $Re_2Cl_9^-$. The reaction follows first-order kinetics over three half-lives. A first-order rate constant of 10^{-3} s^{-1} is calculated from the total absorbance of the solution at 685 nm (ε_{685} ($Re_2Cl_8^{2-}$) = 2610 M^{-1} cm^{-1} and ε_{685} ($Re_2Cl_9^{2-}$) = 395 M^{-1} cm^{-1}).

Binuclear Rhenium Bromide Dimers. Dichloromethane and acetonitrile solutions of $(Bu_4N)_2Re_2Br_8$ show irreversible cyclic voltammetric waves from -2.0 to 2.0 V *vs.* SCE. Repeated recrystallizations and purification of $(Bu_4N)_2Re_2Br_8$ to remove bromide and other anionic impurities yield samples with unimproved cyclic voltammograms. The binuclear rhenium chloride chemistry suggested that the $Re_2Br_8^{2-/3-}$ couple might be measured from cyclic voltammograms of $NBu_4Re_2Br_9$ for which extremely pure compound may be obtained (see Experimental). The cyclic voltammogram of $NBu_4Re_2Br_9$ in CH_2Cl_2 with TBAP (μ=0.1 M) as supporting electrolyte is shown in Figure 7. The gross features of the voltammogram are similar to ones obtained for $NBu_4Re_2Cl_9$: a reversible $Re_2Br_9^{-/2-}$ couple at 0.41 V *vs.* SCE; followed by a large irreversible cathodic wave at -0.38 V *vs.* SCE arising

Figure 7. Cyclic voltammogram for $NBu_4Re_2Br_9$ (2mM) in CH_2Cl_2 (22°C, 0.1 M TBAP).

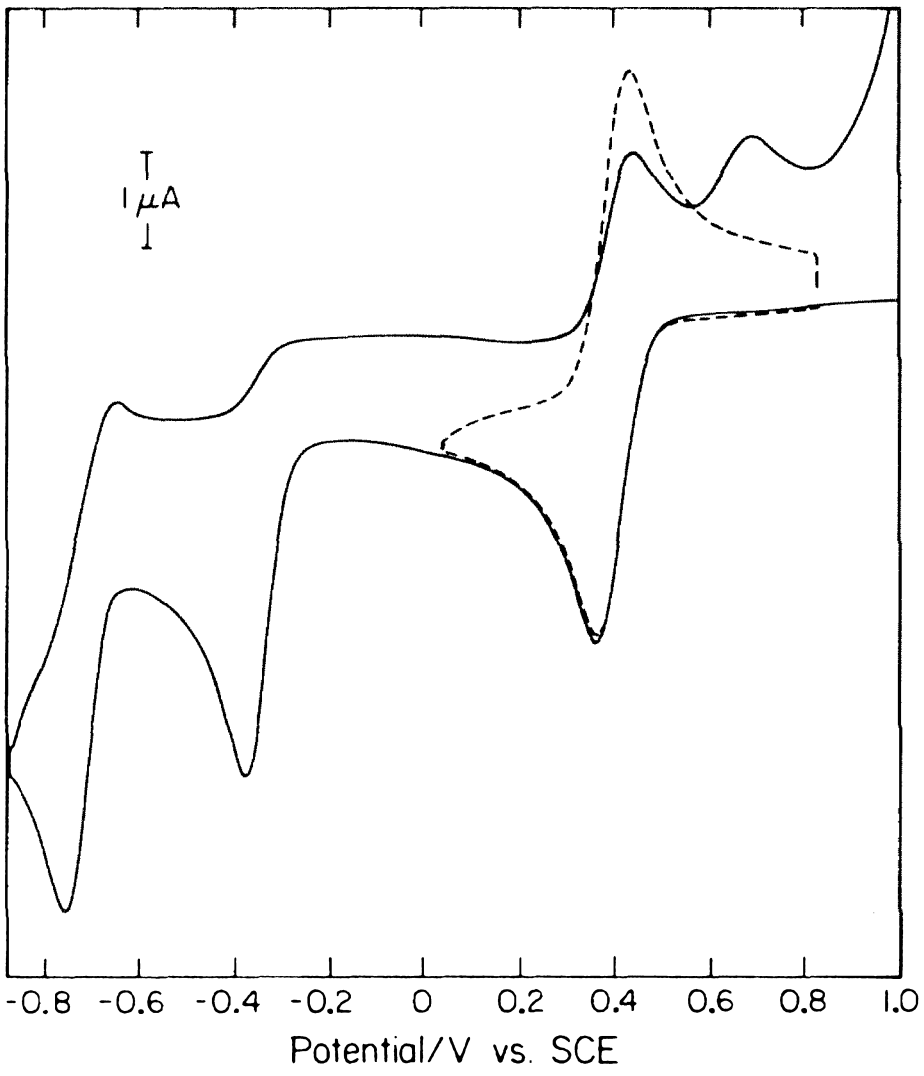
1 μA
-0.8
-0.6
-0.4
-0.2
0
0.2
0.4
0.6
0.8
1.0
Potential/V vs. SCE

from Br^- elimination from $Re_2Br_9^{2-}$ upon its reduction; and lastly, the ensuing $Re_2Br_8^{2-/3-}$ couple. Unlike $Re_2Cl_8^{2-}$, the $Re_2Br_8^{2-/3-}$ wave is irreversible with cathodic and anodic peak potentials of -0.76 V and -0.66 V *vs.* SCE, respectively. The electrochemical irreversibility does not permit the calculation of a half-wave redox potential. At scan rates of $1\,V\,s^{-1}$, i_a/i_c increases to 0.20 (from 0.03 at $100\,mV\,s^{-1}$) indicating that a reversible couple might be measured at fast scan rates.

The irreversible wave at 0.7 V *vs.* SCE in the $Re_2Br_9^-$ cyclic voltammogram is a feature not apparent in $Re_2Cl_9^-$ electrochemistry. The potential corresponds to bromide oxidation to bromine; the bromide source being the halide elimination reaction of $Re_2Br_9^{2-}$ at -0.38 V.

Crystal Structure of $NBu_4Re_2Br_9$. In light of the extensive characterization of multiply bonded rhenium halide compounds, it is surprising that the structural properties of rhenium confacial bioctahedral complexes have not been enumerated. Cotton and coworkers have found $NBu_4Re_2Cl_9$ to be structurally analogous to β-$ReCl_4$,[51] in which there are zig zag chains of Re_2Cl_9 confacial bioctahedra. Though the details of the structure were not described, the average bond lengths and distances in the compound were reported.[52]

The crystal structure analysis of $NBu_4Re_2Br_9$ is now presented. The geometric configuration of $Re_2Br_9^-$ is the expected confacial bioctahedron. The crystal structure data for $NBu_4Re_2Br_9$ are given in Table 4. The final positional

Table 4. Crystal Data for $NBu_4Re_2Br_9$.

a	=	13.973(3) Å
b	=	11.686(3) Å
c	=	10.712(4) Å
β	=	111.71(3)°
F(000)	=	1208 electrons
λMoKα	=	0.71069 Å
μ	=	195.91 cm^{-1}
F. wt.	=	1344.05
V	=	1625.1(7) Å
Space group	=	$P2_1/m$ (#11)
ρ_{calc}	=	2.73 g/cm^3

parameters for all atoms (except hydrogen) are listed in Table 5 and the anisotropic thermal parameters for Re and Br atoms are shown in Table 6. Final distances and angles for the anion are listed in Table 7. An ORTEP stereo drawing of $Re_2Br_9^-$ is illustrated in Figure 8.

The tetrabutylammonium cation is very poorly defined and probably even more distorted than our model indicates. The distances and angles in the cation are in Table 8. There was no point in finding a better model, as refinements with two different models gave the same Re and Br parameters and equally unsatisfactory C and N parameters. In lieu of this result, discussion concerning the structural analysis of the cation, for the most part, is meaningless.

Discussion

The nonaqueous electrochemistry of the binuclear rhenium halide system is conveniently depicted by the Latimer diagram in Figure 9. Fully oxidized confacial bioctahedron undergoes reversible one-electron transfer to the isostructural mixed valence species, which upon its reduction loses chloride to produce the quadruply bonded dimer. If one begins with solutions of highly purified $Re_2Cl_8^{2-}$, reversible one-electron oxidation and reduction reactions to $Re_2Cl_8^-$ and $Re_2Cl_8^{3-}$ occur. Introduction of chloride to $Re_2Cl_8^{2-}$ solution does not affect the reduction electrochemistry, however, the oxidation chemistry dramatically alters with the production of confacial bioctahedral dimer. Electrochemical production of $Re_2Cl_9^-$ from $Re_2Cl_8^{2-}$ may proceed by

Table 5. Final Parameters of All Atoms except Hydrogen in $NBu_4Re_2Br_9$ Crystal Structure.[a]

Atom	x	y	z	Ueq or B[b]	Pop[c]
Re1	829(1)	¼	2632(2)	0.0679(4)	2
Re2	2873(1)	¼	2961(2)	0.0553(3)	2
Br1	51(3)	1001(3)	3434(4)	0.135(1)	4
Br2	-642(4)	¼	554(6)	0.186(3)	2
Br3	1631(2)	943(3)	1680(3)	0.098(1)	4
Br4	2257(4)	¼	4880(5)	0.124(2)	2
Br5	4084(2)	1014(3)	4154(4)	0.109(1)	4
Br6	3619(4)	¼	1241(5)	0.126(2)	2
N	750(2)	¼	506(3)	5.5(7)	2
C11	858(3)	191(4)	582(4)	5.0(1)	2
C12	918(6)	¼	661(6)	11.0(2)	2
C13	1024(8)	¼	748(8)	17.0(3)	2
C14	1098(7)	187(8)	780(8)	17.0(3)	2
C21	699(3)	189(4)	604(4)	5.0(1)	2
C22	694(4)	¼	705(6)	12.0(2)	2
C23	633(5)	¼	792(7)	16.0(2)	2
C24	635(6)	192(7)	902(8)	13.0(3)	2
C31	715(4)	142(5)	406(6)	18.0(2)	4
C32	683(4)	92(5)	293(6)	14.0(2)	4
C33	656(6)	-3(8)	210(7)	18.0(3)	4
C44	613(6)	-59(7)	138(7)	32.0(3)	4

[a] Positional parameters of Re and Br have been multiplied by 10^4, of the remaining atoms by 10^3.

[b] $Ueq = \frac{1}{3}\sum_{ii}\sum[U_{ij}(A_i^* A_j^*)A_i A_j]$; $\sigma(Ueq) = \frac{1}{16}\frac{\sigma(U_{ii})}{U_{ii}}$ Ueq.

[c] Number of atoms in the unit cell.

Table 6. Anisotropic Thermal Parameters x 10^3 for the $Re_2Br_9^-$ Anion.

Atom	U11	U22	U33	U12	U13	U23
Re1	53(1)	68(1)	92(1)	0	37(1)	0
Re2	52(1)	51(1)	71(1)	0	32(1)	0
Br1	140(3)	86(2)	244(4)	-21(2)	144(3)	-2(3)
Br2	68(3)	309(9)	148(5)	0	0(3)	0
Br3	83(2)	96(2)	131(3)	-22(2)	56(2)	-55(2)
Br4	89(3)	209(6)	93(4)	0	53(3)	0
Br5	71(2)	78(2)	179(4)	17(2)	45(2)	39(2)
Br6	112(4)	190(6)	114(4)	0	84(3)	0

Table 7. Bond Distances and Angles in the $Re_2Br_9^-$ Anion.

Atom	Atom	Dist.(Å)	Atom	Atom	Atom	Angle(°)
Re 1 -	Br1	2.441(4)	Br1 -	Re1 -	Br1'	91.6(1)
	Br2	2.407(6)			Br2	90.7(2)
	Br3	2.540(4)			Br3	88.5(1)
	Br4	2.494(5)			Br4	86.1(2)
	Re2	2.745(2)	Br2 -	Re1 -	Br3	89.0(2)
Re 2 -	Br3	2.538(4)	Br3 -	Re1 -	Br3'	91.5(1)
	Br4	2.505(5)			Br4	94.2(1)
	Br5	2.431(4)	Br1 -	Re1 -	Br3'	179.7(1)
	Br6	2.429(5)	Br2 -	Re1 -	Br4	175.5(2)
			Br3	Re2	Br4	94.0(1)
					Br5	88.6(1)
					Br6	89.4(2)
					Br3'	91.6(1)
			Br4	Re2	Br5	87.3(1)
			Br5	Re2	Br6	89.3(2)
			Br5	Re2	Br5'	91.1(1)
			Br4	Re2	Br6	175.1(2)
			Br3	Re2	Br5'	178.7(1)
			Re1	Br3	Re2	65.5(1)
			Re1	Br4	Re2	66.6(1)

Figure 8. ORTEP stereo drawing of $Re_2Br_9^-$ ion. Atom numbering scheme is designated on molecule in lower half of the figure.

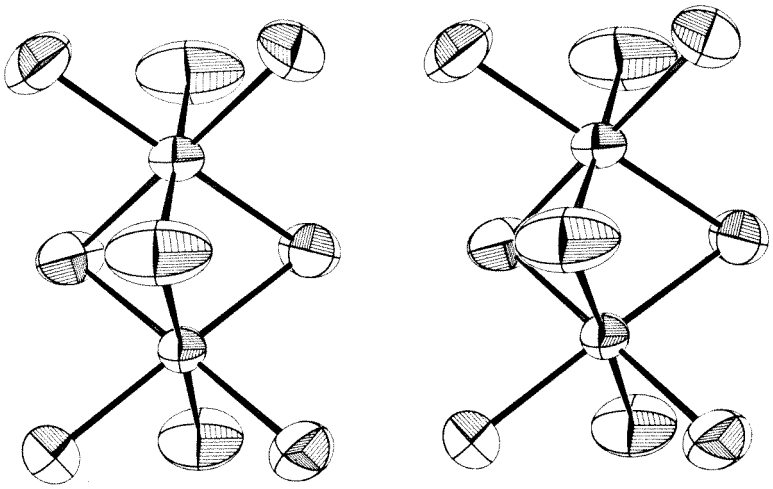

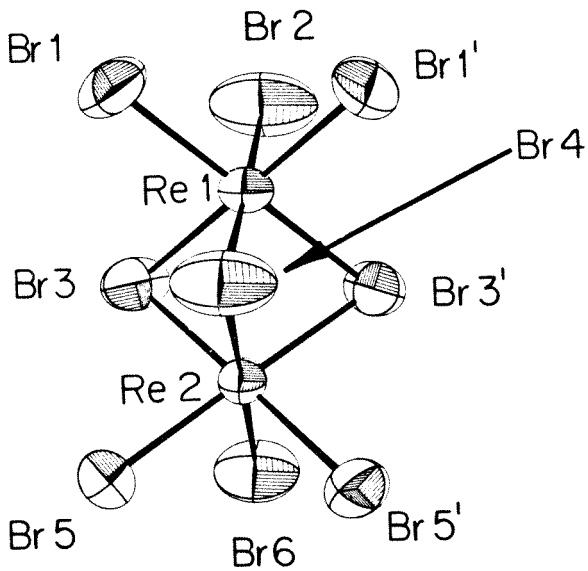
Br 1
Br 2
Br 1'
Br 4
Re 1
Br 3
Br 3'
Re 2
Br 5
Br 6
Br 5'

Table 8. Bond Distances and Angles in the NBu_4^+ Cation.

Atom	Atom	Dist.(Å)	Atom	Atom	Atom	Angle(°)
N	C11	1.59(6)	C11	N	C21	93(3)
	C21	1.64(5)			C31	87(3)
	C31	1.57(6)			$C31^1$	130(3)
C11	C12	1.16(8)	C21	N	C31	91(3)
C12	C13	1.42(12)			$C31^1$	134(3)
C13	C14	1.22(14)	C31	N	$C31^1$	105(3)
C21	C22	1.33(8)	N	C11	C12	113(5)
C22	C23	1.49(10)	C11	C12	C13	139(7)
C23	C24	1.37(11)	C12	C13	C14	141(10)
C31	C32	1.24(8)	N	C21	C22	118(4)
C32	C33	1.33(9)	C21	C22	C23	138(6)
C33	C34	1.12(12)	C22	C23	C24	136(7)
			N	C31	C32	153(5)
			C31	C32	C33	151(6)
			C32	C33	C34	155(9)

Figure 9. Latimer diagram for dirhenium octachloride and nonachloride systems with Cl^- trapping reaction (electrode potentials/V *vs*. SCE in CH_2Cl_2; 22°C).

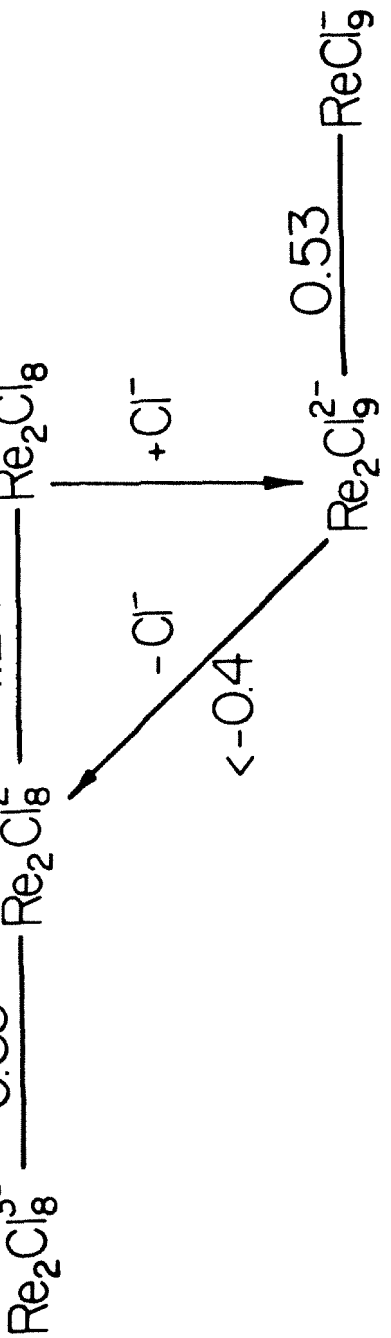
$Re_2Cl_8^-$
$Re_2Cl_8^{2-}$
$Re_2Cl_8^{3-}$
$Re_2Cl_9^{2-}$
$ReCl_9^-$
+Cl⁻
-Cl⁻
1.24
-0.85
0.53
<-0.4

either of two mechanisms. One possibility is that chloride is oxidized to chlorine at the electrode surface which in turn thermally oxidizes $Re_2Cl_8^{2-}$ to $Re_2Cl_9^-$. Alternatively, oxidation of $Re_2Cl_8^{2-}$ to $Re_2Cl_8^-$ followed by Cl^- trapping leads to confacial bioctahedron. The thermal reaction of Cl_2 with $Re_2Cl_8^{2-}$ is too slow to account for the production of $Re_2Cl_9^-$ on the electrochemical time scale, suggesting that confacial bioctahedron formation proceeds by the reaction pathway illustrated in Figure 9. From cyclic voltammetric measurements a lower limit of 10^3 M^{-1} s^{-1} may be estimated for the rate constant of the reaction of Cl^- with $Re_2Cl_8^-$, indicating it to be an efficient process.

The electrochemical reactions of the binuclear rhenium halides are nested in the facile interconversion between confacial bioctahedron and quadruple bond dimers. The salient structural features of the $Re_2X_8^{2-}$ and $Re_2X_9^-$ (X=Cl,Br) anions are summarized in Table 9. The structural characteristics of quadruple bond dimers have been discussed in excruciating detail[1a] and we eschew elaboration. The structural parameters of the $Re_2X_9^-$ species support significant metal-metal interaction. The metal-metal distances in the dirhenium nonahalide monoanions are shorter than in confacial bioctahedra in which there is pure metal repulsion.[53] Additionally, the X-Re-X angles are less than 70.5°, the angle of a structurally ideal confacial bioctahedral polyhedron. Comparison of the structural parameters of the two dimer structures in Table 9 shows that the

Table 9. Pertinent Structural Parameters for $Re_2X_8^{2-}$ and $Re_2X_9^-$ Anions.[a]

Anion	Parameter	X=Cl	X=Br
$Re_2X_8^{2-}$[b]:	Re-Re	2.222	2.228
	Re-X	2.32	2.47
	∢ Re-Re-Br	103.9	104.6
	∢ Br-Re-Br(cis)	86.7	86.4
	∢ Br-Re-Br(trans)	152.2	151.3
$Re_2X_9^-$[c]:	Re-Re	2.703	2.745
	$Re-X_t$	2.29	2.427
	$Re-X_b$	2.41	2.519
	∢ X_{br}-Re-X_{br}	91.6	94.1
	∢ X_t-Re-X_t	92.7	91.4
	∢ Re-X_b-Re	68.2	66.0

[a]Distances in Å; bond angles in (°).

[b]$Re_2Cl_8^{2-}$: NBu_4^+ salt (Cotton, F. A.; Frenz, B. A.; Stults, B. R.; Webb, T. R. J. Am. Chem. Soc. 1976, 98, 2768); $Re_2Br_8^{2-}$: Cs^+ salt (Cotton, F. A.; DeBoer, B. G.; Jeremic, M. Inorg. Chem. 1970, 9, 2143).

[c]$Re_2Cl_9^-$: NBu_4^+ salt (Cotton, F. A.; Ucko, D. A. Inorg. Chim. Acta 1972, 6, 161); $Re_2Br_9^-$: NBu_4^+ salt, this work.

octahedral coordination geometry about each metal in $Re_2X_9^-$ occurs at the expense of the strong metal-metal interaction in $Re_2X_8^{2-}$. Due to the substantial ligand admixture with the metal orbitals in $Re_2X_9^-$ species,[54] it is difficult to assess the exact strength of the metal-metal bond, however, it suffices to note that the metal interaction is greatly weakened from its $Re_2X_8^{2-}$ counterpart.

The electrochemistry of the binuclear rhenium halide systems is explained in terms of an oxidation state/structural relationship. The quadruple bond structure, in which four chlorides coordinate the metal center, is preferred when the rhenium oxidation state is +2 or +3. Oxidation of the metal core to produce a Re(IV) center, however, leads to the production of confacial bioctahedron (when Cl^- is available), where the octahedral coordination of six anionic ligands stabilizes the higher positive charge of the metal center. As we shall see, the propensity of Re(IV) to form confacial bioctahedral species is a property of the binuclear rhenium halide system which may be exploited to effect multielectron photoredox chemistry in these systems.

E. PHOTOREDOX CHEMISTRY OF OCTACHLORODIRHENATE

The extensive spectroscopic and electrochemical investigations of $Re_2Cl_8^{2-}$ suggest it to be an inorganic photoreagent with novel reactivity. First, the $\delta\delta^*$ singlet state ($^1\delta\delta^*$) may be prepared upon low energy excitation without interference from higher energy excited states. Second, the $^1\delta\delta^*$ lifetime and energy should permit $Re_2Cl_8^{2-}$ to participate in bimolecular photoreactions. The energy of $^1\delta\delta^*$, estimated from the electronic origin of $^1A_{1g} \leftarrow {}^1A_{2u}$, in conjunction with its ground state oxidation and reduction couples predict electronically excited $Re_2Cl_8^{2-}$ ($Re_2Cl_8^{2-*}$) to be both a powerful oxidant and a good reductant. The $Re_2Cl_8^{2-*}$ one-electron redox couples are represented on the modified Latimer diagram in Figure 10. Third, the electrochemical reactions of the previous section demonstrate a myriad of metal oxidation states available to the binuclear rhenium halide system. Integration of the dirhenium nonachloride dimer chemistry with $Re_2Cl_8^{2-}$ photoprocesses suggests possible multielectron photochemical reactivity of the binuclear rhenium halide system. A systematic study of the nonaqueous single and multielectron photochemistry is presented below.

Results

Luminescence Quenching. The luminescence of $Re_2Cl_8^{2-*}$ in acetonitrile solution is quenched by secondary and tertiary

Figure 10. Modified Latimer diagram for $Re_2Cl_8^{2-}$ in CH_2Cl_2 (excited state energy in eV; electrode potentials/V *vs.* SCE; 22°C).

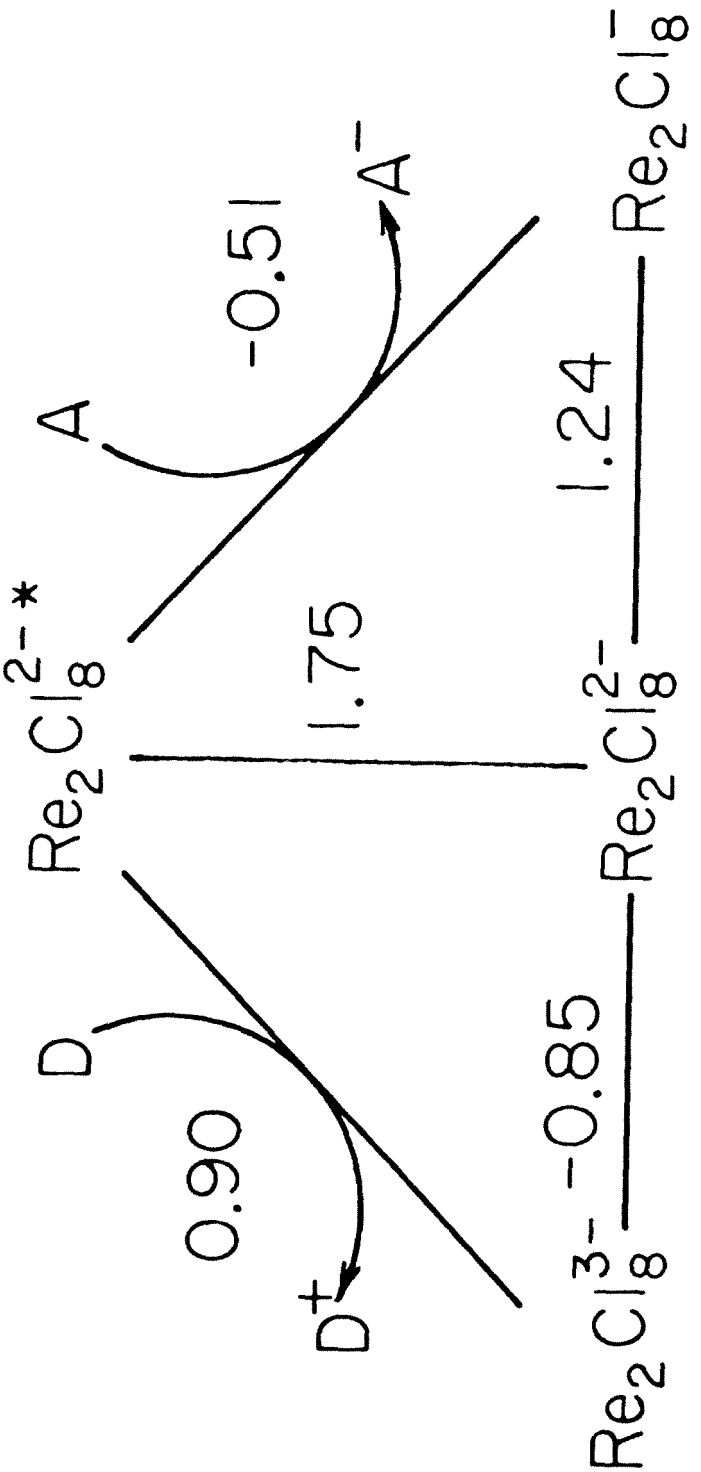
A
-0.51
A⁻
Re₂Cl₈²⁻*
1.75
1.24
Re₂Cl₈⁻
D
0.90
D⁺
Re₂Cl₈³⁻
-0.85
Re₂Cl₈²⁻

amines. Primary amines thermally reacted with $Re_2Cl_8^{2-}$ and, therefore, were not included in quenching studies. Neither the electronic absorption spectrum nor emission spectrum of $Re_2Cl_8^{2-}$ changes in the presence of the quenchers and no evidence for the formation of new chemical species was observed in flash spectroscopic or steady-state emission experiments. In order to establish the luminescence quenching mechanism of $Re_2Cl_8^{2-*}$, the quenching rate constants for the aromatic amines shown in Table 10 were determined. Due to the large discrepancies of the reported aromatic amine reduction potentials, cyclic voltammograms of acetonitrile solutions containing 1 to 2 mM quencher and TBAP (μ=0.1 M) supporting electrolyte were measured. Most of the aromatic amines, except DMA, DEA, and DPA, show electrochemically reversible reduction waves with peak separations of 68±10 mV and i_a/i_c values ranging from 0.96 to 1.05. The measured reduction potentials for aromatic amines showing electrochemically reversible behavior are shown in Table 10. These results are in good agreement with those of a previous study by Meyer *et al.*[55] The reduction potentials for amines exhibiting irreversible cyclic voltammetric waves were, therefore, taken from Meyer's study in which the thermodynamic electrode potentials for reduction were calculated from experimental data using the equation of Olmstead *et al.*[56]

The kinetics of the quenching reaction in acetonitrile solution (25°C; μ=0.1 M in TBAP) were studied using the

Table 10. Rate Constants for Quenching of $Re_2Cl_8^{2-*}$ by Aromatic Amines in Acetonitrile Solution at 25°C.

Quencher (D)	$E_{1/2}$[a]	$k_{q(obsd)}$[b] M^{-1} s^{-1}	$k_{q(corr)}$[c] M^{-1} s^{-1}
(1) *N,N,N',N'*-tetramethyl-p-phenylenediamine	0.10	5.4×10^9	7.6×10^9
(2) *N,N,N',N'*-tetramethyl-benzidine	0.36	2.2×10^9	2.5×10^9
(3) dimethoxydiphenylamine	0.58	1.1×10^9	1.2×10^9
(4) phenothiazine	0.59	8.4×10^8	8.8×10^8
(5) *N,N*-dimethyl-p-toluidine	0.70	1.3×10^7	1.3×10^9
(6) 10-methylphenothiazine	0.73	9.5×10^6	9.5×10^6
(7) diphenylamine	0.79	6.1×10^6	6.1×10^6
(8) *N,N*-diethylaniline	0.76	2.2×10^6	2.2×10^6
(9) *N,N*-dimethylaniline	0.81	1.5×10^6	1.5×10^6

[a] Reduction potentials (D^+/D, V *vs.* SCE) from cyclic voltammetric measurements in CH_3CN solutions containing 0.1 M TBAP. Reduction potentials for quenchers 7-9 taken from ref. 55.

[b] Second-order rate constants ($M^{-1}s^{-1}$), ±0.2; $[(Bu_4N)_2Re_2Cl_8]=5\times10^{-4}$ M; μ=0.1 M TBAP.

[c] Rate constants ($M^{-1}s^{-1}$) corrected for diffusion effects (see text).

Stern-Volmer relationship,

$$\frac{I_o}{I} = 1 + k_q' \tau_o [Q] \qquad (3)$$

where k_q' is the observed quenching rate constant, I_o and I are the intensities of emitted light at a fixed wavelength in the absence and presence of quencher, respectively, τ_o is the excited state lifetime of $Re_2Cl_8^{2-}$, and [Q] is the quencher concentration. In accordance with 3, Stern-Volmer analysis of $Re_2Cl_8^{2-*}$ luminescence quenching by the aromatic amines in Table 10 yields I_o/I *vs.* [Q] plots which are linear over the entire range of quencher concentrations with intercepts of 1.00±0.05 for all quenchers. The observed quenching rate constants, calculated from the slopes of these lines with τ_o equal to 0.14 μs,[12] are shown in Table 10. As expected for a quenching reaction involving a neutral reactant, k_q' s were independent of ionic strength (μ=0.01 to 0.1 M).

It is necessary to correct the observed rate constants for diffusional effects. In a steady-state system of molecules *A* and *B*, a concentration gradient will be established by a flux of unreacted *B* towards unreacted *A* and an equal flux of reacted *B* away from *A*. Noyes has shown that the reaction rate of *A* will be proportional to the average concentration of *B* undergoing collisions with *A*,[57] and has expressed this result in terms of bimolecular

rate constants,

$$1/k_q' = 1/k_q + 1/k_D \qquad (4)$$

where k_q' is defined above, k_D is the rate constant for collision of two species due to diffusion, and k_q is the second-order rate constant corrected for diffusional effects. Using the Stokes-Einstein equation, Smoluchowski has expessed k_D as,[58]

$$k_D = \frac{1}{4} \left(2 + \frac{r_1}{r_2} + \frac{r_2}{r_1}\right) \frac{8RT}{3\eta} \qquad (5)$$

where r_1 and r_2 are the radii of reacting species, R is the gas constant, T is the temperature in Kelvin and η is the viscosity of the solution. The aromatic amine radii, calculated by averaging the van der Waal radii along the three molecular axes, vary from 3.4 Å to 4.6 Å. An average radius of 3.6 Å is calculated for $Re_2Cl_8^{2-}$ using a similar procedure. A value of k_D equal to 1.9×10^{10} M^{-1} s^{-1} is calculated from 5 for all quencher radii. Substitution of k_q' and k_D into 4 yields the corrected quenching rate constants given in Table 10.

Various electron acceptors (e.g. TCNE, chloranil, $PW_{12}O_{40}^{3-}$) also quench $Re_2Cl_8^{2-*}$ luminescence in nonaqueous solutions. A transient signal attributable to $TCNE^-$ is observed upon irradiation ($\lambda > 560$ nm) of dichloromethane

solutions of TCNE (1 mM) and $(Bu_4N)_2Re_2Cl_8$ (0.1 mM) in flash spectroscopic experiments. The transient signal decayed by second-order kinetics with a rate constant of $3.2(7)x10^9$ M^{-1} s^{-1}. Quenching of $Re_2Cl_8^{2-*}$ by TCNE in acetonitrile solution also resulted in $TCNE^-$ formation, however, the signal decayed by neither first- nor second-order kinetics. A product with an electronic absorption spectrum in accordance with a TCNE charge transfer complex accumulated upon repetitive excitation of the acetonitrile solution. It is undoubtedly this secondary reaction to produce charge transfer products that leads to anomolous $TCNE^-$ decay kinetics in acetonitrile. Similar flash spectroscopic experiments on the $Re_2Cl_8^{2-}$/chloranil system revealed second-order kinetic behavior for the disappearance of the photogenerated chloranil anion. The bimolecular rate constants for transient decay were $1.8(7)x10^9$ M^{-1} s^{-1} in CH_3CN and $1.5(2)x10^9$ M^{-1} s^{-1} in acetone solutions.

The kinetics of the oxidative quenching reaction were studied by the Stern-Volmer analysis described above. For TCNE in dichloromethane, k_q was $3.3(1)x10^9$ M^{-1} s^{-1}. With chloranil in CH_3CN, the measured rate constant was $1(1)x10^9$ M^{-1} s^{-1}. The kinetics for the oxidative quenching reactions of $Re_2Cl_8^{2-*}$ as well as those for the ensuing transient decay reactions are summarized in Table 11.

Oxidative Quenching in the Presence of Cl^-. Dichloromethane and acetonitrile solutions of $Re_2Cl_8^{2-}$, oxidative quencher

Table 11. Rate Constants for Quenching of $Re_2Cl_8^{2-*}$ by Oxidative Quenchers and Their Transient Decay in Nonaqueous Solutions at 25°C.

Quencher (A)	Solvent	k_q $M^{-1}s^{-1}$	k_b $M^{-1}s^{-1}$
TCNE	CH_2Cl_2	$3.3(1)\times10^9$	$3.2(7)\times10^9$
Chloranil	CH_3CN	$1(1)\times10^9$	$1.8(7)\times10^9$
	acetone	-	$1.5(2)\times10^9$

(TCNE or chloranil, ten-fold molar excess), and Cl^- (hundred-fold molar excess) were irradiated at >660 nm. Upon irradiation, the 685 nm $Re_2Cl_8^{2-}$ absorption band disappeared with concomitant appearance of the 736 nm band of $Re_2Cl_9^{2-}$. Unfortunately, the reaction could not be monitored by optical absorption spectroscopy at higher energy, owing to intense absorption attributable to the red TCNE/Cl^- charge transfer complex. Spectral data from a typical photolysis experiment are shown in Figure 11. The photolysis reaction is quantitative on the basis of the 685 nm absorption band of $Re_2Cl_8^{2-}$ (ε_{685} = 2610 $M^{-1}cm^{-1}$ (CH_2Cl_2); ε_{680} = 2340 M^{-1} cm^{-1} (CH_3CN)) and the 736 nm band of $Re_2Cl_9^{2-}$ (ε_{736} = 1380 M^{-1} cm^{-1} (CH_2Cl_2)). Reaction rates depend on both Cl^- and quencher concentrations. Dichloromethane and acetonitrile solutions identical with those used for photolysis reactions were prepared and stored in the dark at 50°C. No reaction occurred after 24 hr. Irradiation (λ > 660 nm for two days) of $Re_2Cl_8^{2-}/Cl^-$ (hundred-fold molar excess) and $Re_2Cl_8^{2-}$/TCNE (ten-fold molar excess) in CH_2Cl_2 and CH_3CN did not lead to the production of $Re_2Cl_9^{2-}$. In addition to optical absorption spectra, the photolysis reaction mixtures were also characterized by EPR and electrochemical measurements. EPR spectra of photolyzed solutions with TCNE as the oxidative quencher show the characteristic 9 line signal of the radical anion.[59] The EPR spectrum of a frozen CH_2Cl_2 solution of $Re_2Cl_9^{2-}$ displays a weak axial doublet signal with

Figure 11. Spectral changes upon irradiation (λ>660 nm) of a dichloromethane solution of $(Bu_4N)_2Re_2Cl_8$ (0.6 mM), TCNE (6 mM), and NBu_4Cl (60 mM) at 10(0.5)°C: ——, initial spectrum; ----, spectrum of photolyzed solution.

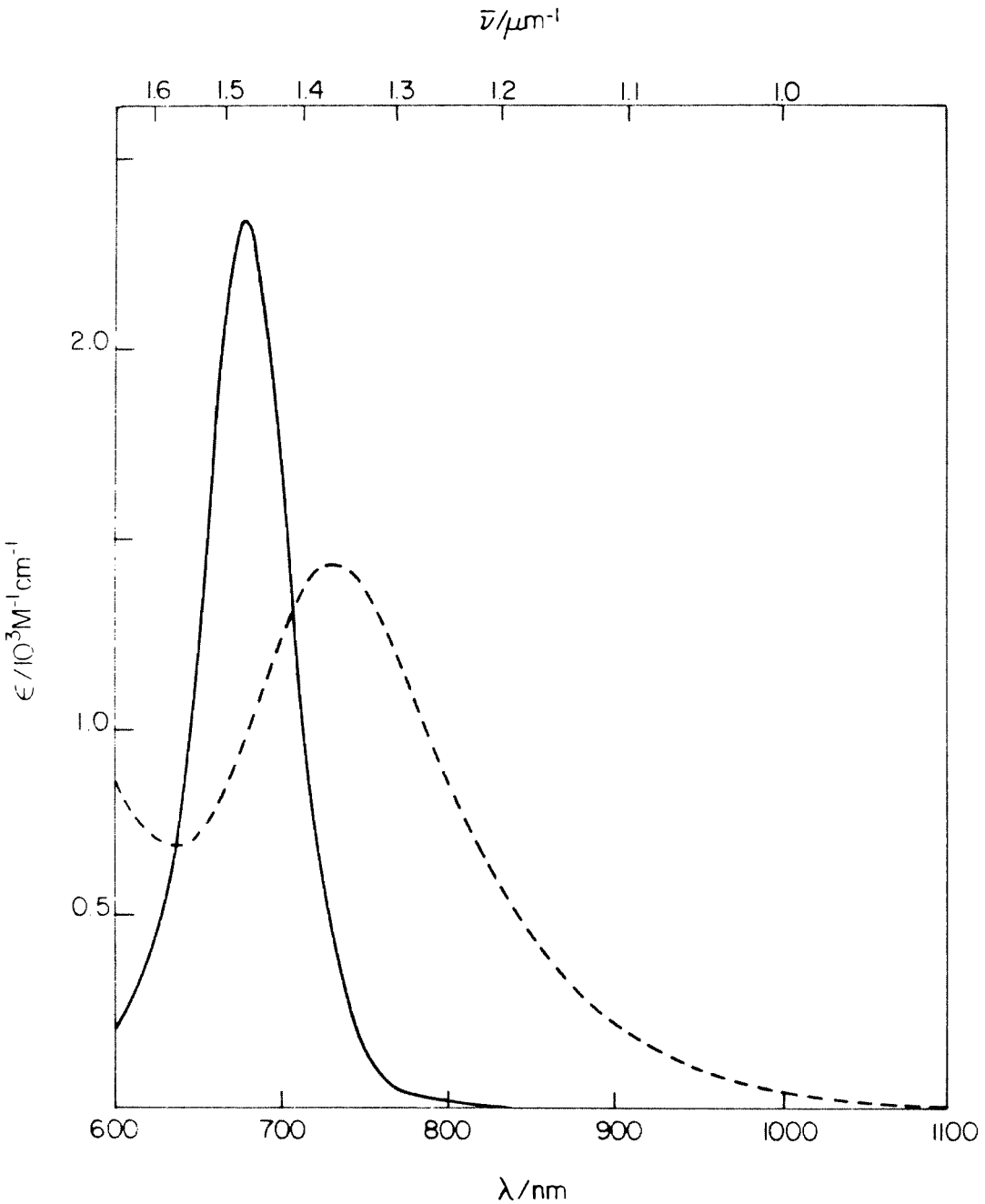
$\bar{\nu}/\mu m^{-1}$
1.6
1.5
1.4
1.3
1.2
1.1
1.0
2.0
1.0
0.5
$\epsilon/10^3 M^{-1} cm^{-1}$
600
700
800
900
1000
1100
λ/nm

$g_{\perp} = 2.00$ and $g_{\parallel} = 1.93$. Unfortunately, these g values are near that of the TCNE radical anion, thereby preventing the detection of the $Re_2Cl_9^{2-}$ species in the photolysis reaction mixture. A cyclic voltammogram of the photolysis mixture with TCNE as a quencher is shown in Figure 12. The $TCNE^{0/-}$ couple at 0.35 V *vs.* SCE[60] and the $Re_2Cl_9^{-/2-}$ couple at 0.53 V are both observed.

Irradiation (λ > 660 nm) of dichloromethane solutions (10(1)°C) of $(Bu_4N)_2Re_2Cl_8$ (1 mM), DDQ (10 mM) and NBu_4Cl (100 mM) led to the disappearance of the 685 nm absorption band of $Re_2Cl_8^{2-}$ and the production of a species with a weak absorption system that extended to 1000 nm. Discrete features in the optical absorption spectrum of the photolysis reaction mixture could not be distinguished from those of the burgundy colored DDQ/Cl^- charge transfer complex. The 736 nm band of $Re_2Cl_9^{2-}$ did not appear as a product during the four hour photolysis reaction. Cyclic voltammograms of the photolysis reaction mixture showed only one, large reversible wave at 0.6 V *vs.* SCE, attributable to the $DDQ^{0/-}$ redox couple.[61] In order to characterize the reaction, the photolysis solution was chromatographed on Florasil® using CH_2Cl_2 as an eluant. A green band immediately separated from a series of yellow and red bands upon introduction of the photolyzed solution onto the column. An optical absorption spectrum of the green product showed it to be $Re_2Cl_9^-$ ($\varepsilon_{321} = 22{,}500\ M^{-1}\ cm^{-1}$) in greater than 80% yield. Addition of acetonitrile to the

Figure 12. Cyclic voltammogram of a photolyzed CH_2Cl_2 solution of $(Bu_4N)_2Re_2Cl_8$ (1 mM), TCNE (10 mM), and NBu_4Cl (100 mM). Scan rate, 200 mV s^{-1}.

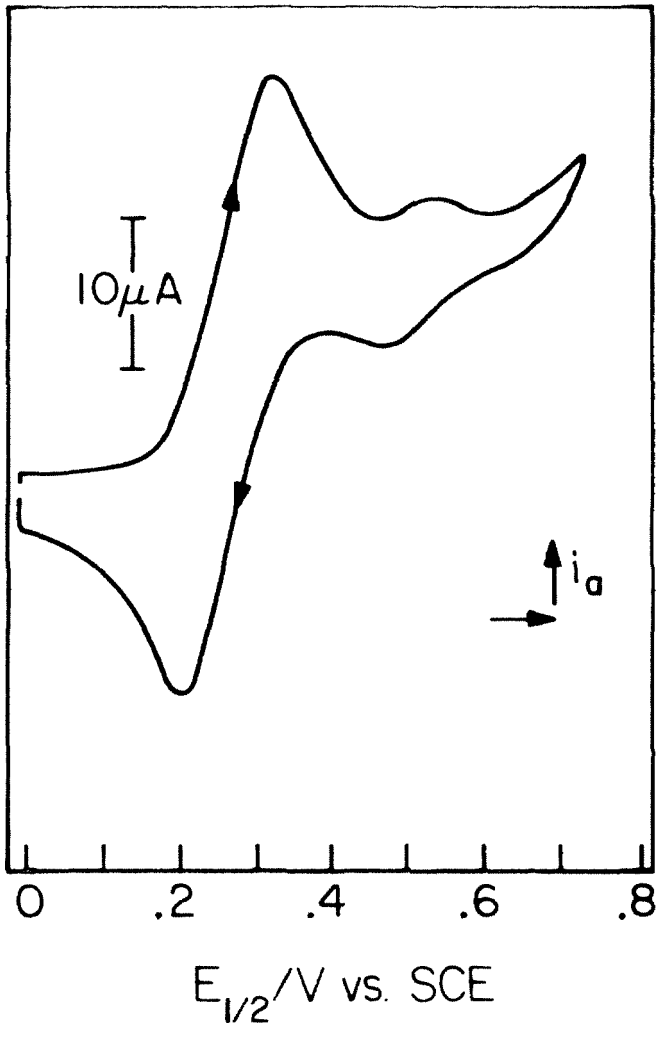
10μA
i_a
0
.2
.4
.6
.8
$E_{1/2}$/V vs. SCE

CH_2Cl_2 facilitated the elution of the green band from the column. The remaining yellow and red bands were all DDQ products.[62] A note of caution about the chromatographic separation of $Re_2Cl_9^-$ from photolysis solutions should be interjected at this point. Prolonged exposure (~0.5 hr.) of $Re_2Cl_9^-$ on Florasil® promotes reduction of the monoanion to $Re_2Cl_9^{2-}$, which has a much greater retention time than $Re_2Cl_9^-$. The time between introduction of the photolyzed solution onto the column and $Re_2Cl_9^-$ collection should, therefore, be minimized. Solutions identical with those used for photolysis experiments slowly reacted in the dark at 22°C after 5 days. Chromatographic separation of the components in the solution on Florasil® showed $Re_2Cl_9^-$ product formation.

Dichloromethane solutions of $Re_2Cl_9^{2-}$ immediately react with DDQ to produce $Re_2Cl_9^-$ in quantitative yield.

$PtCl_6^{2-}$ Quenching. The absorption spectrum of a dichloromethane solution containing $(Bu_4N)_2Re_2Cl_8$ (1 mM) and $(Bu_4N)_2PtCl_6$ (10 mM) is shown in Figure 13. In addition to the $Re_2Cl_8^{2-}$ absorption profile, the absorption band arising from the lowest energy excited state of $PtCl_6^{2-}$ at 465 nm is also evident. The absorption spectrum does not change after storage of the solution in the dark at 50°C for 7 days. Irradiation of the solution (10(0.5)°C) with a 1000 W Hg(Xe) lamp equipped with a 3-67 Corning high energy cut-off filter (% T_{540} = 1.0, % T_{555} = 50) results in the production of the absorption spectrum illustrated by the dashed

Figure 13. Spectral changes upon irradiation (λ>590 nm) of a dichloromethane solution of $(Bu_4N)_2Re_2Cl_8$ (1 mM) and $(Bu_4N)_2PtCl_6$ (10 mM) at 10(0.5)°C: ———, initial spectrum; -----, spectrum of photolyzed solution.

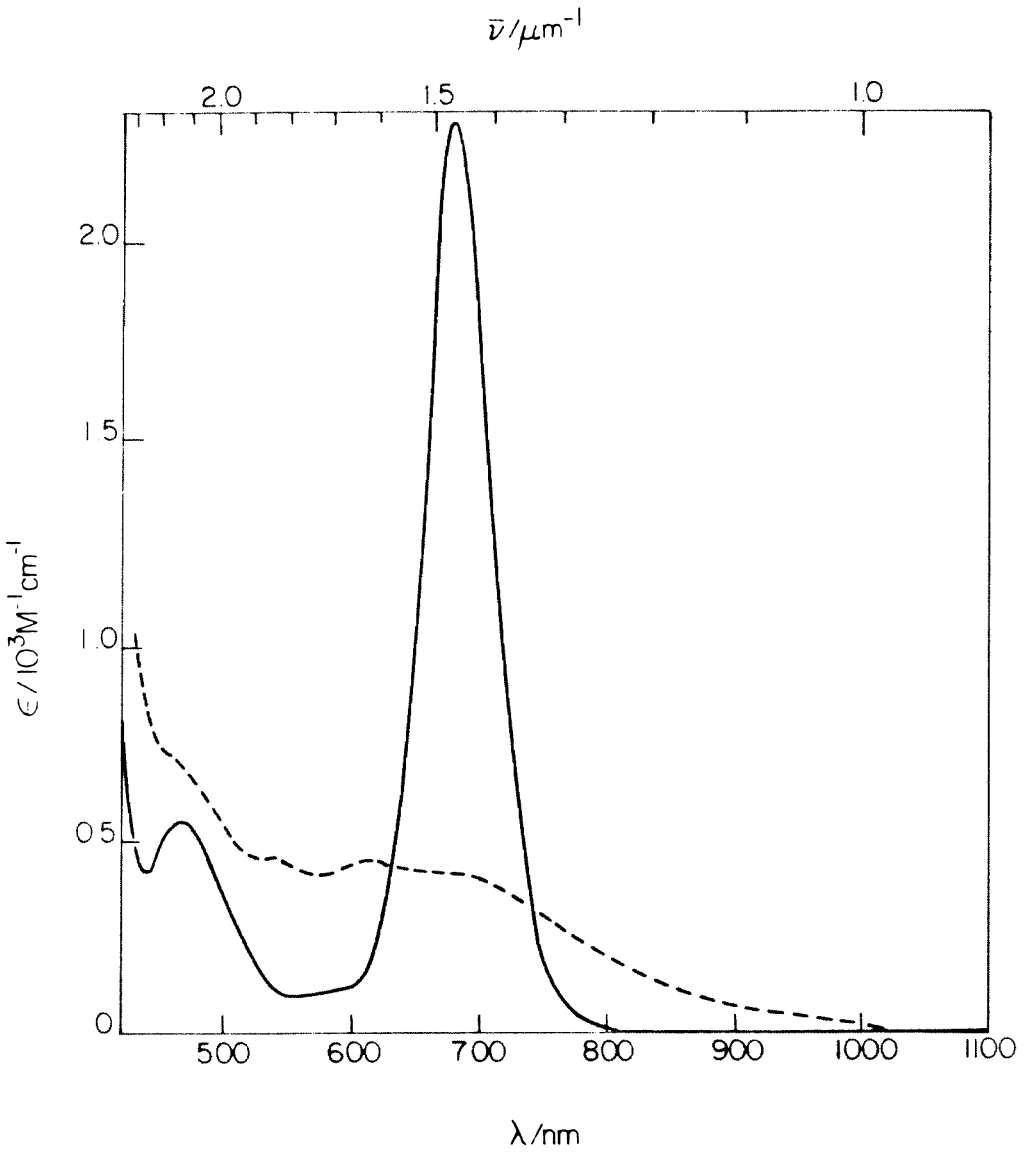
$\bar{\nu}/\mu m^{-1}$
2.0
1.5
1.0
2.0
1.5
1.0
0.5
0
$\epsilon/10^3 M^{-1}cm^{-1}$
500
600
700
800
900
1000
1100
λ/nm

line in Figure 13 after 12 hr. The rate of the photolysis reaction decreases significantly upon longer wavelength excitation of the solution. Qualitative photochemical experiments show that the photolysis reaction goes to completion after 4 days with 2-62 Corning filtered (% T_{595} = 1.0, % T_{605} = 50) excitation. A negligible reaction is observed after 4 days when the excitation light is filtered by a 2-58 Corning filter (% T_{630} = 1.0, % T_{645} = 50). Solutions irradiated with 3-73 Corning filtered (% T_{420} = 1.0, % T_{435} = 50) light react completely in minutes. In the above photolysis reactions, the $(Bu_4N)_2Re_2Cl_8$ and $(Bu_4N)_2PtCl_6$ concentrations were 1 mM and 10 mM, respectively.

Optical absorption spectra of photolyzed solutions which were stored in the dark show the reappearance of the 685 nm band of $Re_2Cl_8^{2-}$. After four months, the concentration of $Re_2Cl_8^{2-}$ was 80% of its original, pre-irradiated value. Dichloromethane solutions of $(Bu_4N)_2Re_2Cl_8$ (1 mM) and $(Bu_4N)_2PtCl_6$ (10 mM) do not show appreciable absorbance at 685 nm after storage for two months in the dark, suggesting that $Re_2Cl_8^{2-}$ production occurs from the back reaction of the photoproducts.

The photolysis reaction was again characterized by chromatographic separation of the photoproducts on Florasil®. The green band of $Re_2Cl_9^-$ immediately separates from the remaining components when CH_2Cl_2 is the eluant. In all photolysis experiments, $Re_2Cl_9^-$ is produced in quantitative yield as determined from its ultraviolet

absorption band (ε_{321} = 22,500 M^{-1} cm^{-1}). The large molar excess of $PtCl_6^{2-}$ prevented the detection of the platinum photolysis reduction product, which is presumably $PtCl_4^{2-}$ since platinum metal was not observed as a reaction product in any photolysis reaction.

The photolysis reaction rate is enhanced as the $(Bu_4N)_2PtCl_6$ concentration is increased relative to that of $(Bu_4N)_2Re_2Cl_8$. Radical trapping reagents such as duroquinone and galvinoxyl radical do not appear to inhibit the reaction rate. Dichloromethane solutions of $(Bu_4N)_2Re_2Cl_8$ (1 mM), $(Bu_4N)_2PtCl_6$ (10 mM and 100 mM), and NBu_4Cl (100 mM) do not react upon irradiation with Corning 3-67 filtered excitation.

The steady-state luminescence of $Re_2Cl_8^{2-*}$ (λ_{exc} = 660 nm) is not significantly quenched in 100 mM $PtCl_6^{2-}$ solutions. The inability to detect quenching at these concentrations with our instrument indicates a quenching rate constant of less than 10^6 M^{-1} s^{-1}. The low solution quantum yield of emission from $Re_2Cl_8^{2-}$ precluded the investigation of the wavelength dependence of the quenching reaction.

Dichloromethane solutions of $PtCl_6^{2-}$ exhibit a transient signal in the 350-400 nm spectral region upon ultraviolet irradiation of the solutions in flash spectroscopic experiments. The transient absorption spectrum, displayed in Figure 14, is in accordance with the spectrum of a Pt(III) intermediate produced by homolytic

Figure 14. Transient difference spectrum of $(Bu_4N)_2PtCl_6$ in dichloromethane recorded 1.25 ms after flash irradiation (λ>360 nm).

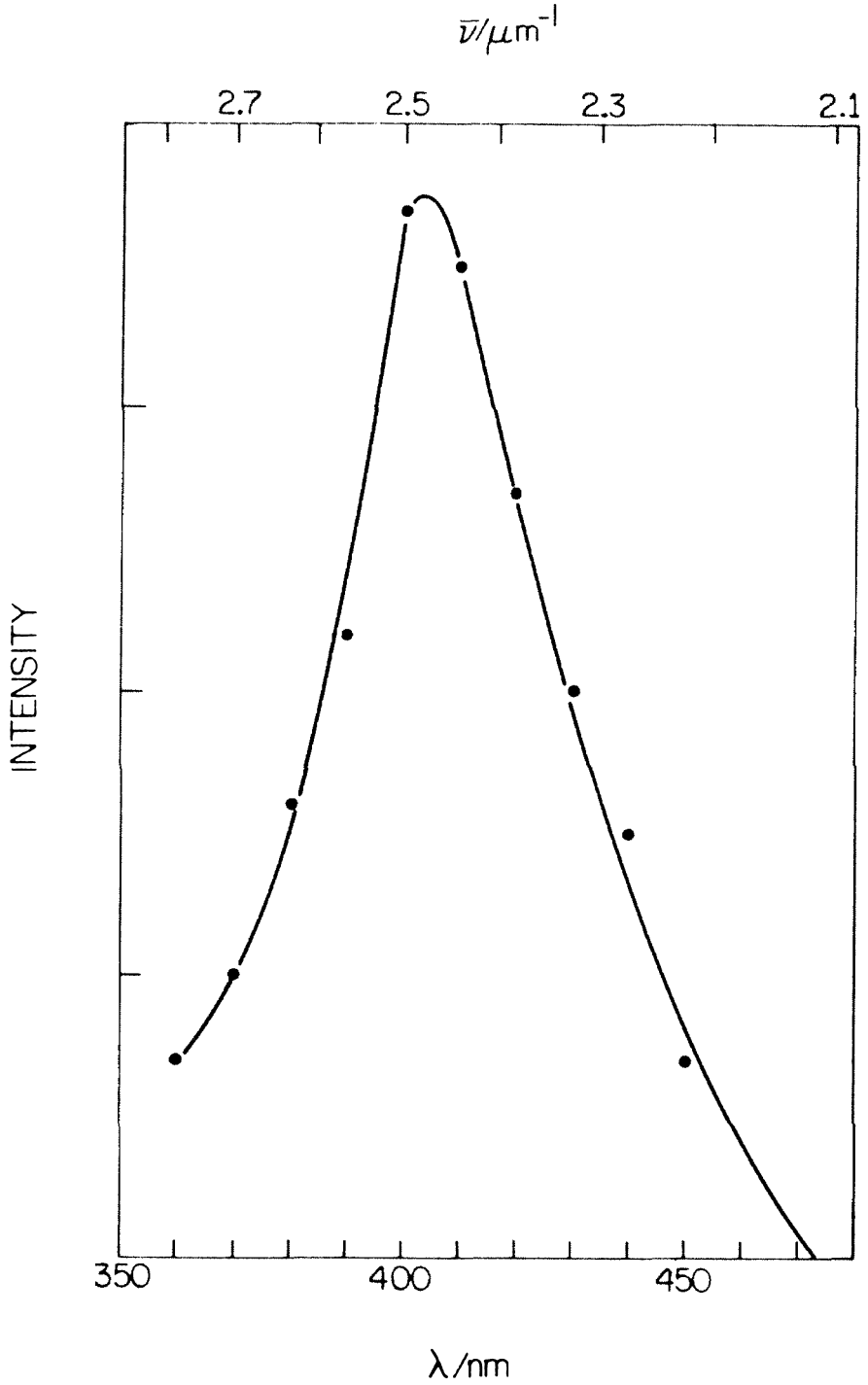
$\bar{\nu}/\mu m^{-1}$
2.7
2.5
2.3
2.1
INTENSITY
350
400
450
λ/nm

dissociation of a Pt-Cl bond in $PtCl_6^{2-}$.[63] Flash photolysis of $PtCl_6^{2-}$ with Corning 3-67 glass filtered excitation shows no transient formation.

Discussion

Luminescence quenching of an electronically excited transition metal complex (M^*) may occur by a variety of mechanisms,[64] most important of which are: (i) static quenching, (ii) dynamic energy transfer, and (iii) chemical reaction, especially electron transfer. Static quenching arises from the chemical or physical association between ground state metal complex (M) and quencher (Q) (M|Q, the concentration of which is defined by an equilibrium constant for association). Formation of M|Q results in net quenching when the excited state of the associated complex, $M^*|Q$, does not possess the same emissive properties as M^* (which is usually the case). Generally, this quenching mechanism is only important for systems involving ground state molecules of opposite charge. Since the electronic absorption and emission spectra of $Re_2Cl_8^{2-}$ did not change upon quencher addition, in any circumstance, static quenching of $Re_2Cl_8^{2-}$ luminescence was ruled out. The remaining two mechanisms for $Re_2Cl_8^{2-}$ luminescence quenching are described by reactions 2, 3 and 5 in Figure 15. Energy transfer from $Re_2Cl_8^{2-*}$ to Q produces $Re_2Cl_8^{2-}$ and Q^* (which thermally deactivates), therefore, resulting in $Re_2Cl_8^{2-}$ luminescence quenching. As we can

Figure 15. Possible luminescence quenching mechanisms of electronically excited $Re_2Cl_8^{2-}$: energy transfer (reaction 2); oxidative electron transfer (reaction 3); and reductive electron transfer (reaction 5). Thermal back electron transfer reactions are designated by 4 and 6. A, oxidative quencher; D, reductive quencher; Q, quencher.

$$Re_2Cl_8^{2-} \xrightarrow{h\nu\,(\lambda>660nm)} Re_2Cl_8^{2-*} \qquad (1)$$

energy transfer:

$$Re_2Cl_8^{2-*} + Q \xrightarrow{k_q} Re_2Cl_8^{2-} + Q^* \qquad (2)$$

oxidative quenching:

$$Re_2Cl_8^{2-*} + A \xrightarrow{k_q} Re_2Cl_8^{-} + A^- \qquad (3)$$

$$Re_2Cl_8^{-} + A^- \xrightarrow{k_b} Re_2Cl_8^{2-} + A \qquad (4)$$

reductive quenching:

$$Re_2Cl_8^{2-*} + D \xrightarrow{k_q} Re_2Cl_8^{3-} + D^+ \qquad (5)$$

$$Re_2Cl_8^{3-} + D^+ \xrightarrow{k_b} Re_2Cl_8^{2-} + D \qquad (6)$$

see in reaction 2 of Figure 15, energy transfer is a chemically non-productive quenching mechanism and, in the context of $Re_2Cl_8^{2-}$ photochemical reactivity, is not as important as the electron transfer quenching mechanism in which $Re_2Cl_8^{2-*}$ is (i) oxidatively quenched by an electron acceptor, A (reaction 3 in Figure 15), or (ii) reductively quenched by an electron donor molecule, D (reaction 5 in Figure 15). Typically, the large thermodynamic driving force for recombination of the electron transfer quenching products leads to the rapid back reactions depicted by reactions 4 and 6 in Figure 15. Of course, the ubiquitous "back reaction" is a problem which plagues photochemical energy storage cycles.[65]

It is the goal of the photochemist to distinguish which quenching mechanism is operative in the system under investigation. In our case, the oxidative quenching studies clearly demonstrate that $Re_2Cl_8^{2-*}$ is quenched by an electron transfer mechanism since the electron transfer products of the acceptor molecules (A^- in reactions 3 and 4 in Figure 15) are detected in flash spectroscopic experiments. Of course, the decay of the transient signal in the TCNE and chloranil flash photolysis studies corresponds to the facile back reaction described by reaction 4 in Figure 15, the kinetics of which are defined by the bimolecular rate constants in Table 11. Our observations that the rates of both the quenching and back reactions are near the diffusion controlled limit suggest

that very little internuclear reorganization is associated with electron transfer involving the δ and δ^* orbitals of the octachlorodirhenate system.

The mechanism for $Re_2Cl_8^{2-}$ luminescence quenching by aromatic amines is less well-defined than for the oxidative quenchers, since D^- is not directly observed in flash spectroscopic experiments. Two pieces of evidence support an electron transfer quenching mechanism. First, energy transfer quenching by the aromatic amines chosen for this study is energetically unfavorable. Energy transfer may occur by a coulomb (Förster mechanism[66]) or exchange interaction (Dexter mechanism[67]). Both mechanisms relate the magnitude of the rate constant for energy transfer to the integrated overlap of the experimental emission curve of the electronically excited donor with an absorption curve of the acceptor. As the spectral overlap approaches zero, so does the rate constant for energy transfer. The lowest energy singlet absorption bands of the aromatic amines in Table 10 are in the ultraviolet spectral region, well removed from the $Re_2Cl_8^{2-}$ emission curve, thereby obviating energy transfer quenching with the amine singlet states. Knowledge of the lowest energy triplet states is sparse, however, available data indicate energy transfer with the triplet states to be a highly endothermic process[68] and not able to efficiently compete with an electron transfer quenching mechanism. A second, more substantial piece of evidence supporting an electron transfer quenching reaction

by the aromatic amines comes *via* a Marcus analysis of the free energy correlation of the observed quenching rate constants in Table 10. The analysis is outlined below.

Steady-State Quenching Analysis. A model describing the electron transfer luminescence quenching mechanism of $Re_2Cl_8^{2-*}$ by the aromatic amines is shown in Figure 16. This kinetic scheme was first proposed by Rehm and Weller to describe the fluorescence quenching reactions between various organic acceptor and donor molecules.[69] As shown in Figure 16, excitation of the $^1A_{2u} \leftarrow {}^1A_{1g}$ transition produces $Re_2Cl_8^{2-*}$ which may either decay back to ground state or form an associated complex with a ground state donor molecule (i.e. aromatic amine). The equilibrium constant for the associated complex is given by $K_{12} = k_{12}/k_{21}$. Within the associated complex, electron transfer quenching occurs with a rate described by k_{23}. The electron transfer products may back react with a rate constant of k_{32} to regenerate $Re_2Cl_8^{2-*}$ within the activated complex. Competing with this process are all modes of deactivation of the associated complex, which include back electron transfer to produce ground state species. For convenience, all deactivation modes are described by the single rate constant k_{30}. Application of the Stern-Volmer equation and the steady-state approximation to the kinetic scheme in Figure 16 yields the following expression for the quenching rate constant,

Figure 16. Model for electron transfer reaction of $Re_2Cl_8^{2-*}$ with aromatic amines.

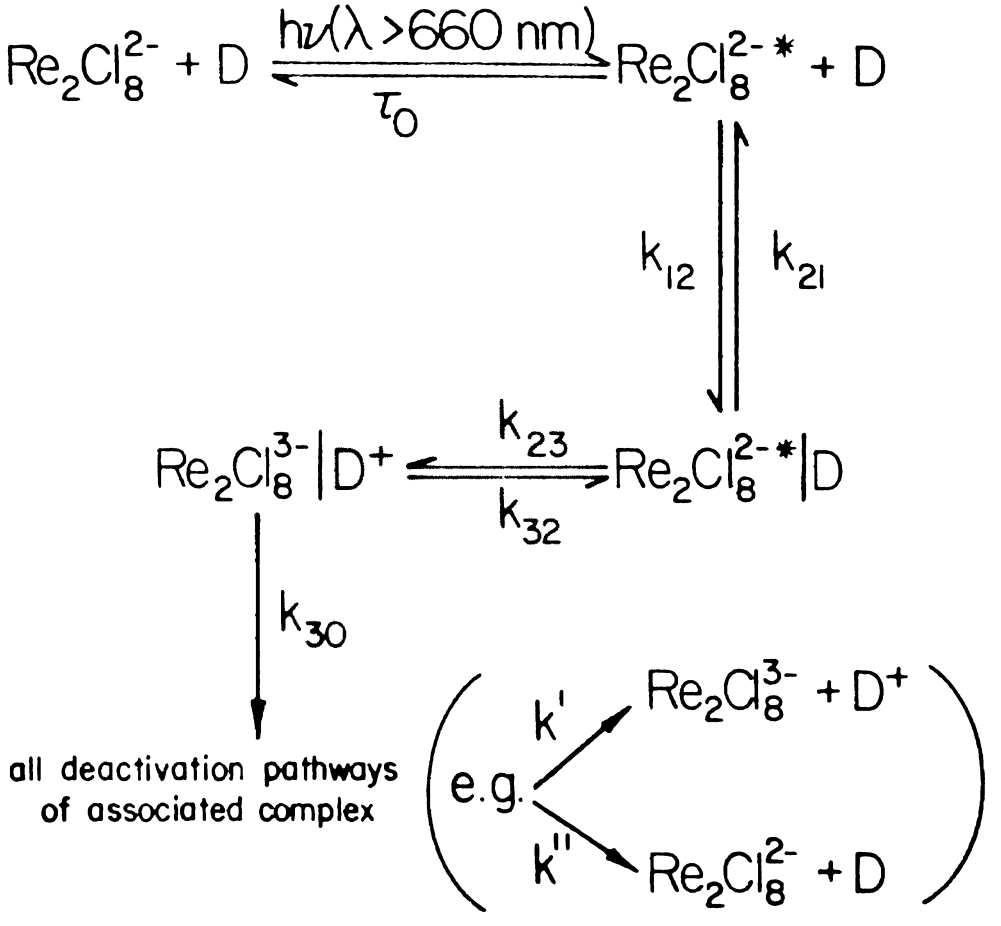
$Re_2Cl_8^{2-} + D \rightleftharpoons Re_2Cl_8^{2-*} + D$
$h\nu(\lambda > 660\ nm)$
τ_0
k_{12}
k_{21}
$Re_2Cl_8^{3-}|D^+ \rightleftharpoons Re_2Cl_8^{2-*}|D$
k_{23}
k_{32}
k_{30}
all deactivation pathways of associated complex
e.g.
k'
$Re_2Cl_8^{3-} + D^+$
k''
$Re_2Cl_8^{2-} + D$

$$k_q = \frac{k_{12}}{1 + \frac{k_{21}}{k_{23}}\left(1 + \frac{k_{32}}{k_{30}}\right)} \quad . \qquad (6)$$

With the assumption that precursor complex formation is established by a rapid pre-equilibrium step and that electron transfer within the complex is rate determining (i.e. $k_{21} >> k_{23}$), 6 reduces to

$$k_q = \frac{K_{12}k_{30}k_{23}}{k_{30} + k_{32}} \quad . \qquad (7)$$

Marcus has shown that the rate constant for electron transfer within the precursor complex,

$$k_{23} = (k_B T/h)\exp(-\Delta G_{23}^{*}/RT) \qquad (8)$$

depends upon the activation energy arising from solvent polarization and vibrational changes associated with the inner sphere reorganization of the electron transfer species.[70] More specifically,

$$\Delta G_{23}^{*} = \lambda/4 + \Delta G_{23}/2 + \Delta G_{23}^{2}/4\lambda \qquad (9)$$

where ΔG_{23} is the standard free energy change for the electron transfer quenching reaction within the associated complex and λ is the sum of the inner sphere (λ_i) and outer sphere (λ_o) reorganization energies for the electron transfer process. From simple thermodynamics, the standard free energy change for one-electron reductive quenching of $Re_2Cl_8^{2-*}$ by the aromatic amines may be calculated from the following expression,

$$\Delta G_{23}(V) = -[E_{1/2}(Re_2Cl_8^{2-*/3-}) - E_{1/2}(D^+/D)] + w_p - w_r - \Delta E_{0,0} \qquad (10)$$

where $E_{1/2}(Re_2Cl_8^{2-*/3-})$ and $E_{1/2}(D^+/D)$ are the standard electrode potentials of the species involved in the electron transfer reaction; w_p and w_r are the electrostatic energy work terms associated with bringing together the products and reactants, respectively, from an infinite separation distance to the distance of the reacting species in the activated complex; and $E_{0,0}$ is the difference in zero point vibrational energies of the reactant and product electron transfer potential energy surfaces. Substitution of 8 and 9 into 7 yields

$$k_q = \frac{K_{12}k_{30}(k_BT/h)}{k_{30} + k_{32}} \exp\left[-\frac{\lambda}{4}\left(1+\frac{\Delta G_{23}}{\lambda}\right)^2 / RT \right]. \qquad (11)$$

Due to the large driving force of the back reaction in the associated complex to give ground state products, it is unlikely that back electron transfer to $Re_2Cl_8^{2-*}$ could be competitive with the former process (i.e. $k_{30} >> k_{32}$) and, therefore, 11 reduces to

$$k_q = K_{12} \frac{k_B T}{h} \exp\left[- \frac{\lambda}{4} \left(1 + \frac{\Delta G_{23}}{\lambda}\right)^2 / RT \right] . \qquad (12)$$

Taking the logarithm of 12 and rearranging, produces,

$$RT\ln k_q = \left[RT\ln K_{12} \frac{k_B T}{h} - \frac{\lambda}{4} \right] - \frac{\Delta G_{23}}{2} \left(1 + \frac{\Delta G_{23}}{2\lambda}\right) \qquad (13)$$

and when $|\Delta G_{23}|$ is much less than the outer and inner sphere reorganizational energies, 13 becomes

$$RT\ln k_q \cong \left[RT\ln K_{12} \frac{k_B T}{h} - \frac{\lambda}{4} \right] - \frac{\Delta G_{23}}{2} . \qquad (14)$$

For a structurally and electronically similar series of quenchers (as is our series of quenchers in Table 10), K_{12} and λ will be relatively constant for the electron transfer reaction. As Meyer and coworkers have pointed out,[55] when $\Delta G_{23}=0$, k_q is the rate constant of the thermoneutral electron transfer reaction between the excited state and quencher. Defining this rate constant as $k_q(0)$ and substituting it into 14 gives,

$$RT\ln k_q = RT\ln k_q(0) - \Delta G_{23}/2 \qquad (15)$$

Substitution of 10 into 15 and rearranging, gives,

$$RT\ln k_q = RT\ln k_q(0) - \frac{1}{2} E_{1/2}(D^+/D) + \frac{1}{2}[E_{1/2}(Re_2Cl_8^{2-*/3-}) - w_p + w_r] \qquad (16)$$

where the zero point energy correction has been ignored. Note that the expression in the brackets is a constant. From 16 we see that a plot of logarithm of the quenching rate constants in Table 10 *vs.* the quencher reduction potentials should yield a straight line of slope -0.5 if the aromatic amines are quenching $Re_2Cl_8^{2-*}$ by an electron transfer mechanism. Such a plot is shown in Figure 17 where the quenchers are indicated by their assigned number in Table 10. A linear regression fit of quenchers 3-10 yields a straight line with slope -0.61, in excellent agreement with the prediction from Marcus theory. We conclude, therefore, that electron transfer is the predominant quenching mechanism of $Re_2Cl_8^{2-*}$ luminescence by the aromatic amines. The absence of electron transfer products in flash kinetic experiments suggests formation of a strongly associated ion-pair, $Re_2Cl_8^{3-}|D^+$, upon electron transfer quenching. Ion-pair intermediates have

Figure 17. Plot of log k_q *vs.* $E_{1/2}$ (D^+/D); conditions and quencher numbering as in Table 10.

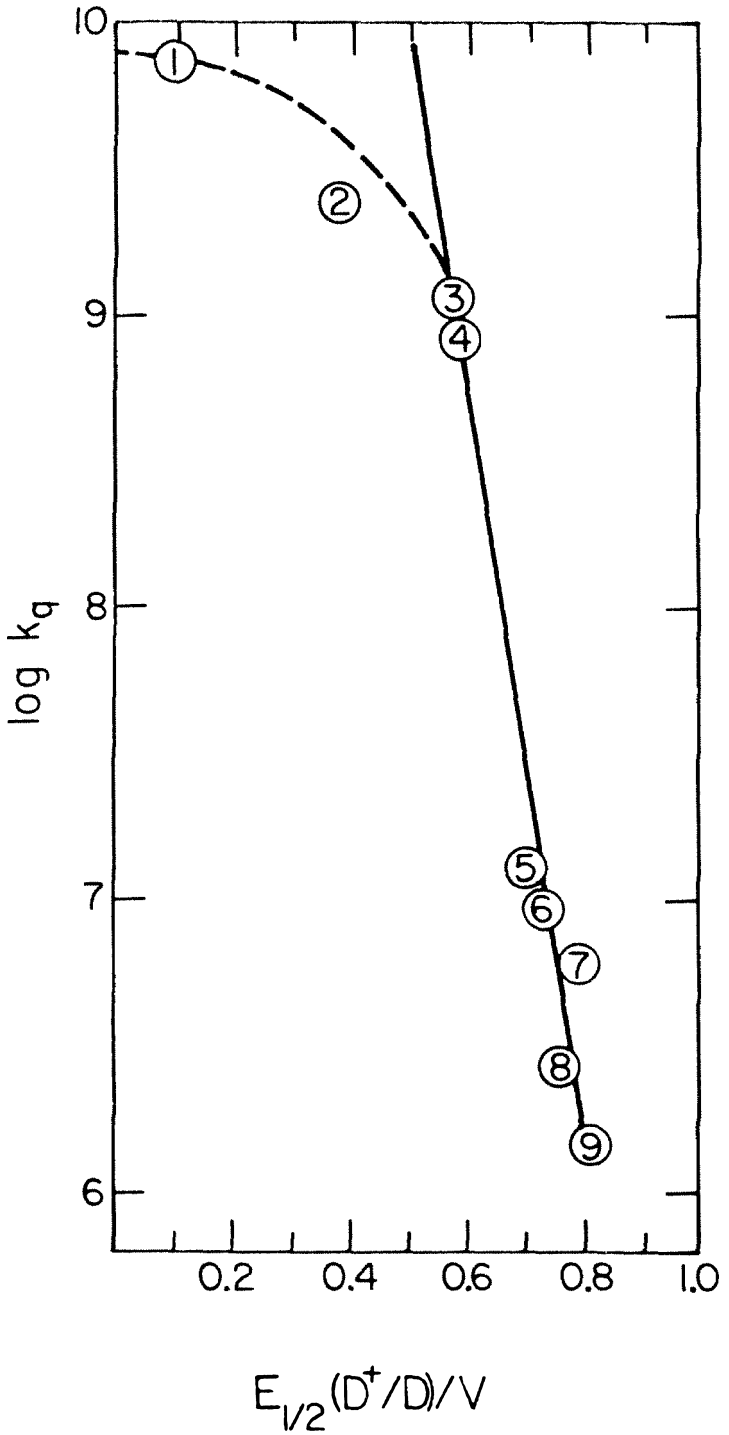
10
9
8
7
6
log k_q
0.2
0.4
0.6
0.8
1.0
$E_{1/2}(D^+/D)/V$
1
2
3
4
5
6
7
8
9

been proposed previously to explain the lack of transient formation in the oxidative quenching reactions of $Ru(bpy)_3^{2+}$ by nitroaromatic acceptors.[71] The fact that separated $Re_2Cl_8^{3-}$ and D^+ are not observed in flash spectroscopic experiments indicates unusually efficient back electron transfer.

The curvature of the line at small $E_{1/2}(D^+/D)$ values (i.e. large thermodynamic driving force of the electron transfer reaction) in Figure 17 is expected for one or both of two reasons. First, the assumption that $|\Delta G_{23}| << 2\lambda$ is no longer valid for quenching reactions exhibiting large thermodynamic driving potentials and 13 must be used in the Marcus analysis. From 13 we see that k_q will ultimately decrease as ΔG_{23} becomes large and negative. This electron transfer regime is known as the "inverted region", first predicted by the classical electron transfer theories of Marcus,[70b,c] and later supported by quantum theories.[72] Experimental studies have shown little or no decrease of the rate constant in the "inverted region". There are many mechanisms which have been postulated to explain the failure to observe the inverted region,[73] most important of which are the accessibility of low-lying electronically excited product states (which effectively decrease the driving force of the electron transfer reaction) and/or different reaction mechanisms (e.g. atom transfer reactions) which become competitive with electron transfer at large driving potentials. A second explanation of the

curvature is the asymptotic approach of the quenching rate constant to the diffusion controlled limit as the driving force of the reaction increases. Eventually, at very large driving force, k_q should become independent of ΔG_{23} and be dominated solely by diffusional effects.

The above quenching studies confirm the excited state reactivity of $Re_2Cl_8^{2-}$ originally inferred from the modified Latimer diagram in Figure 10. The $Re_2Cl_8^{2-}$ excited state undergoes facile electron transfer reactions with acceptor and donor molecules to produce the powerful oxidizing agent, $Re_2Cl_8^{-}$, and reducing agent, $Re_2Cl_8^{3-}$, respectively. The $Re_2Cl_8^{2-/3-*}$ reduction potential of 0.90 V *vs.* SCE is consistent with the low k_q values measured for quenchers 5-9 (Table 10). The ability to photochemically generate $Re_2Cl_8^{-}$ is an important result, because this species permits an interface through which confacial bioctahedral rhenium halide chemistry may be coupled to quadruple bond photochemistry.

Cl^- Trapping Photochemistry. The one-electron oxidative quenching chemistry of $Re_2Cl_8^{2-}$ in conjunction with the binuclear rhenium halide electrochemistry suggest the intriguing possibility of photochemically induced multi-electron transfer chemistry. Combination of Figures 9 and 10 yields the modified Latimer diagram illustrated in Figure 18, which predicts that photochemically generated $Re_2Cl_8^{-}$ may react with Cl^- to produce $Re_2Cl_9^{2-}$ which can undergo further oxidation in the presence of a thermo-

Figure 18. *Modified Latimer diagram for the* $Re_2Cl_8^{n-}$ (n=1,2,3)/Cl^-/$Re_2Cl_9^{n-}$ (n=1,2) system (electrode reduction potentials/V *vs.* SCE; excited state energy in eV). A, oxidative quencher; D, reductive quencher.

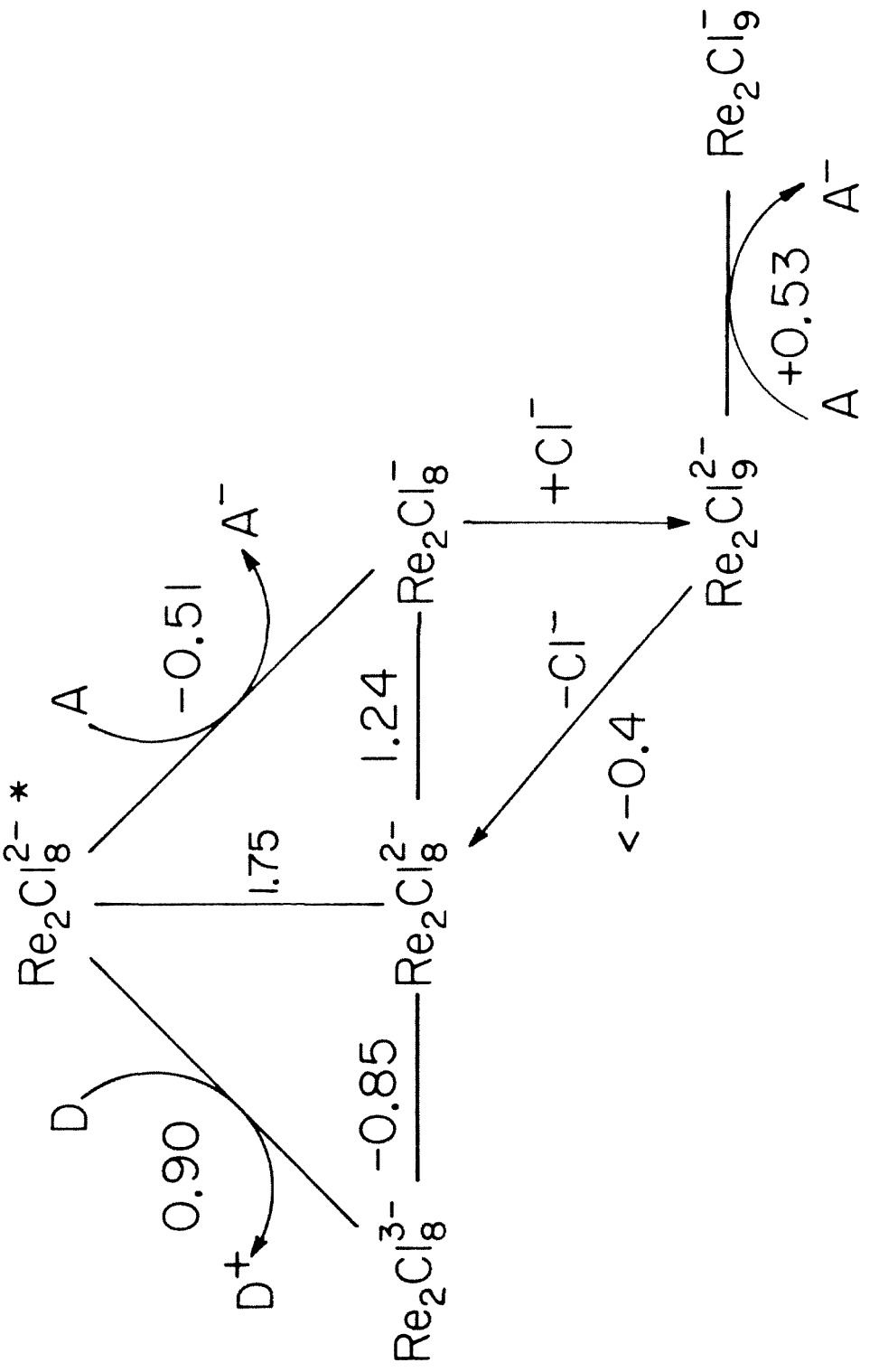
$Re_2Cl_8^{2-}$ *
A
−0.51
A^-
1.75
$Re_2Cl_8^-$
1.24
$Re_2Cl_8^{2-}$
+Cl^-
$Re_2Cl_9^-$
A
+0.53
A^-
$Re_2Cl_9^{2-}$
−Cl^-
< −0.4
$Re_2Cl_8^{2-}$
D
0.90
D^+
$Re_2Cl_8^{3-}$
−0.85
$Re_2Cl_8^{2-}$

dynamically accommodating quencher. The reaction pathway hinges on the ability of the Cl^- trapping reaction to circumvent the diffusion controlled back reaction between $Re_2Cl_8^-$ and A^-.

The photochemical production of confacial bioctahedron from $Re_2Cl_8^{2-}$ in the presence of Cl^- and oxidative quencher (TCNE, chloranil, and DDQ) clearly demonstrates that the Cl^- trapping reaction efficiently competes with the extremely fast back reaction of the photochemically generated monoanions. The rate determining step for the overall reaction could be either Cl^- trapping of $Re_2Cl_8^-$ or production of $Re_2Cl_8^-$ by excited state quenching since both Cl^- and quencher concentrations markedly affect the photochemical rate of $Re_2Cl_9^{2-}$ production. As predicted by Figure 18, the pathway for oxidative photochemistry of $Re_2Cl_8^{2-}$ proceeds through the excited state to the highly reactive $Re_2Cl_8^-$ intermediate which is trapped to $Re_2Cl_9^{2-}$. The reaction stops at the mixed valence species because TCNE and chloranil cannot oxidize $Re_2Cl_9^{2-}$ to fully oxidized confacial bioctahedron. In the DDQ experiment, however, the reduction potential of 0.60 V *vs.* SCE enables this quencher to further react with $Re_2Cl_9^{2-}$ to produce $Re_2Cl_9^-$. The overall reaction is

$$Re_2Cl_8^{2-} + 2DDQ + Cl^- \xrightarrow[CH_2Cl_2]{h\nu(\lambda>660\ nm)} Re_2Cl_9^- + 2DDQ^- . \quad (1)$$

Thus, a single low energy photon facilitates a two-electron oxidation that is (at least) kinetically difficult to bring about thermochemically.

The striking feature of the photochemical pathway is, certainly, the efficiency of the Cl^- trapping reaction. The thermodynamics of the trapping reaction may be determined from the thermal reaction chemistry of the $Re_2Cl_8^{2-}/Cl^-/A$ system and the reduction potentials of the quenchers and binuclear rhenium halide species. That dichloromethane solutions of $Re_2Cl_8^{2-}$ and Cl^- react with DDQ (to $Re_2Cl_9^-$) and not TCNE establishes the redox couple for the half-reaction, $E_{1/2}$(**2**),

$$Re_2Cl_9^- + 2e^- \rightarrow Re_2Cl_8^{2-} + Cl^- \qquad (\mathbf{2})$$

to lie in the potential range, $0.88 < E_{1/2}(\mathbf{2}) < 1.23$ V *vs.* SCE. From the simple thermodynamic cycle,

$$Re_2Cl_8^{2-} \xrightarrow[vs.\ SCE]{1.25\ V} Re_2Cl_8^- + Cl^- \underset{k_{-1}}{\overset{k_1}{\rightleftharpoons}} Re_2Cl_9^{2-} \qquad (\mathbf{3})$$

$$-0.70 \text{ to } -0.35 \text{ V } vs. \text{ SCE}; \quad +Cl^-$$

the equilibrium constant for the Cl^- trapping reaction is calculated to be 10^9-10^{15} M^{-1}. The thermodynamic driving force for $Re_2Cl_8^-$ reaction with Cl^- (ΔG = -15 to -21 kcal mol^{-1})

is, therefore, comparable to that of the $Re_2Cl_8^-/A^-$ back reactions ($\Delta G = -15$ kcal mol^{-1} for DDQ and -21 kcal mol^{-1} for TCNE), demonstrating the tendency of the Re(IV) oxidation state to be stabilized by the octahedral chloride ligation of the confacial bioctahedral geometry.

The Cl^- trapping photochemistry corresponds to oxidative addition of chlorine across the metal-metal bond of $Re_2Cl_8^{2-}$. As described above, the reaction pathway proceeds by single-electron transfer steps. A more efficient reaction of the electronically excited molecule would be to effect the oxidative addition chemistry in a single multielectron step. Our strategy was to quench $Re_2Cl_8^{2-*}$ directly to $Re_2Cl_9^-$ by a chlorine transfer reagent.

$PtCl_6^{2-}$ Quenching Photochemistry. Excited state atom transfer chemistry can involve a multielectron transfer process, an important reaction in solar energy storage cycles.[74] Furthermore, the accompanying structural rearrangement of the atom transfer reaction could create significant kinetic barriers to the energy wasting back reaction. The irradiation of dichloromethane solutions of $Re_2Cl_8^{2-}$ and $PtCl_6^{2-}$ to produce $Re_2Cl_9^-$, indeed, suggests such an atom transfer process. One may envisage $PtCl_6^{2-}$, with its two-electron couple, to react with $Re_2Cl_8^{2-*}$ *via* a chlorine-bridged intermediate to produce $Re_2Cl_9^-$ (and $PtCl_4^{2-}$ and Cl^-). In this reaction, the chlorine bridge atom, which was originally bonded to platinum, remains at

the rhenium metal core to form the confacial bioctahedral product. Fleming *et al.* have determined that upon ultraviolet irradiation of $Re_2Cl_8^{2-}$, 20% of the upper excited states decay to an intermediate which does not correspond to the $\delta\delta^*$ singlet state.[12] The geometry of intermediate was postulated to be a chlorine-bridged species which is structurally analogous to a confacial bioctahedron in which a solvent molecule occupies the open coordination site. Such an intermediate would be ideally suited for chlorine atom transfer to $Re_2Cl_9^-$.

An obvious complication with explaining the observed photochemistry of $Re_2Cl_8^{2-}$ and $PtCl_6^{2-}$ by the speculated chlorine atom transfer mechanism described above arises from the known photoreactivity of $PtCl_6^{2-}$. The electronic absorption spectrum of $PtCl_6^{2-}$ displays two bands at 465 nm and 358 nm which have been assigned to the singlet-triplet ($^3T_{1g} \leftarrow {}^1A_{1g}$) and singlet-singlet ($^1T_{1g} \leftarrow {}^1A_{1g}$) ligand field transitions, respectively, while the intense absorption band at 265 nm arises from a *LMCT* transition.[75] Crystals of $PtCl_6^{2-}$ at 4.2 K show vibrationally structured luminescence resulting from the $^3T_{1g}$ state.[76] From the published emission spectrum, the electronic origin of the lowest energy excited state lies at 590 nm. The $PtCl_6^{2-}$ anion undergoes photoaquation and photocatalyzed Cl^- exchange upon ultraviolet and visible irradiation.[77] Both reactions are believed to proceed by a chain mechanism, probably involving a Pt(III) chain propagating intermediate (most

likely $PtCl_5^{2-}$) which is produced from the charge transfer state.[78] The photoreactivity from visible excitation is believed to arise from the tail of the charge transfer band in the visible spectral region.

In light of the possible photoreactivity of $PtCl_6^{2-}$, the $Re_2Cl_8^{2-}/PtCl_6^{2-}$ photochemistry was studied as a function of the excitation light's wavelength. A mechanism involving electron or atom transfer chemistry of the $\delta\delta^*$ singlet state of $Re_2Cl_8^{2-}$ is obviated by the observation that the reaction rate for $Re_2Cl_9^{2-}$ production is negligible when irradiations are carried out with wavelengths > 620 nm. Acceleration of the photolysis reaction with light > 560 nm suggests that the photoreactivity is derived from either the $\delta\pi^*$ and/or $\pi\delta^*$ states of $Re_2Cl_8^{2-}$ (possibly leading to formation of the high energy isomer suggested by Fleming *et al.*) or a $PtCl_6^{2-}$ excited state. For solutions used in this study, the $Re_2Cl_8^{2-}$ absorbance does not increase significantly from 400-560 nm (due to the inner filter effect of $PtCl_6^{2-}$) while that of $PtCl_6^{2-}$ does; that the photochemical reaction rate accelerates from 10 hr. with λ > 560 nm to minutes with λ > 400 nm indicates $PtCl_6^{2-}$ photoreactivity and argues against a reaction pathway involving a high energy excited state of $Re_2Cl_8^{2-}$. The suggestion that the photochemistry is derived from $PtCl_6^{2-}$ necessitates the postulation of an extremely efficient photoprocess. (Recall that even though the electronic origin of the lowest energy excited state of $PtCl_6^{2-}$ is at

590 nm, the photoreaction went to completion with Corning 2-62 filtered light (% T_{595} = 1.0; % T_{605} = 50)). The flash photolysis experiments of $PtCl_6^{2-}$ do not support Pt(III) production as the initial photoprocess. Instead, chloride inhibition of the $Re_2Cl_8^{2-}/PtCl_6^{2-}$ photochemistry suggests heterolytic Pt-Cl bond cleavage of $PtCl_6^{2-}$ to produce a coordinatively unsaturated Pt(IV) intermediate. The precedence for such a reaction comes from $PtBr_6^{2-}$ photoaquation chemistry which is believed to proceed *via* direct heterolysis of the Pt(IV)-Br bond.[80] The apparent efficiency of the $PtCl_6^{2-}$ reactivity almost certainly involves the production of a Pt(III) chain propagating intermediate, suggesting the results of the radical trapping experiments to be meaningless.

Despite the mechanism, the overall reaction,

$$Re_2Cl_8^{2-} + PtCl_6^{2-} \longrightarrow Re_2Cl_9^{-} + PtCl_4^{2-} + Cl^{-} \qquad (4)$$

is calculated to be endergonic ($\Delta G(4)$ = 7 to 15 kcal/mol^{-1}). This is supported by the thermal back reaction chemistry of photolyzed solutions. It is surprising that the weak absorption of the $PtCl_6^{2-}$ ligand field states could lead to such efficient photoreactivity especially since $PtCl_6^{2-}$ ligand field photochemistry is without precedence. In light of these results, further investigation of $Re_2Cl_8^{2-}/PtCl_6^{2-}$ photochemistry is warranted. Quantitative experiments describing the wavelength dependence of the

reaction quantum yield for $Re_2Cl_9^-$ production are essential. Furthermore, other potential chlorine atom transfer quenchers with lowest energy excited states well removed from the low energy excited states of $Re_2Cl_8^{2-}$ should also be investigated.

The photochemistry reported herein indicates the diverse reactivity available to quadruply bonded transition metal complexes as inorganic photoreagents. When one considers the large number of existing quadruply bonded metal complexes, a long photochemical road lies ahead. One avenue of research with particular promise is the oxidative addition photochemistry associated with the multiple metal-metal bond.

F. REFERENCES

1. (a) Cotton, F. A.; Walton, R. A. "Multiple Bonds Between Metal Atoms"; Wiley: New York, 1982. (b) Chisholm, M. H.; Rothwell, I. P. Prog. Inorg. Chem. 1982, 29, 1. (c) Chisholm, M. H. "Reactivity of Metal-Metal Bonds"; American Chemical Society: Washington, D.C., 1981; ACS Symp. Ser. No. 155. (d) Templeton, J. L. Prog. Inorg. Chem. 1979, 26, 211. (e) Chisholm, M. H.; Cotton, F. A. Acc. Chem. Res. 1978, 11, 356.
2. (a) Bertrand, J. A.; Cotton, F. A.; Dollase, W. A. J. Am. Chem. Soc. 1963, 85, 1349. (b) Cotton, F. A.; Haas, T. E. Inorg. Chem. 1964, 3, 10.
3. (a) Cotton, F. A.; Curtis, N. F.; Johnson, B. F. G.; Robinson, W. R. Inorg. Chem. 1965, 4, 326. (b) Cotton, F. A.; Harris, C. B. Inorg. Chem. 1965, 4, 330. (c) Cotton, F. A. Inorg. Chem. 1965, 4, 334.
4. (a) Ref. 1(a), Chapter 8. (b) Trogler, W. C.; Gray, H. B. Acc. Chem. Res. 1978, 11, 232, and references therein. (c) Cotton, F. A. Chem. Soc. Rev. 1983, 12, 35.
5. (a) Martin, D. S.; Newman, R. A.; Fanwick, P. E. Inorg. Chem. 1982, 21, 3400. (b) Manning, M. C.; Trogler, W. C. Inorg. Chem. 1982, 21, 2797.
6. Hay, P. J. J. Am. Chem. Soc. 1978, 100, 2897.

7. (a) Ebner, J. R.; Walton, R. A. Inorg. Chem. 1975, 14, 1987. (b) Glicksman, H. D.; Walton, R. A. Inorg. Chem. 1978, 17, 3197. (c) Brant, P.; Walton, R. A. Inorg. Chem. 1978, 17, 2674.

8. (a) Brant, P.; Salmon, D. J.; Walton, R. A. J. Am. Chem. Soc. 1978, 100, 4424. (b) Salmon, D. J.; Walton, R. A. J. Am. Chem. Soc. 1978, 100, 991.

9. Cotton, F. A.; Foxman, B. M. Inorg. Chem. 1968, 7, 2135.

10. Cotton, F. A.; Frenz B. A.; Ebner, J. R.; Walton, R. A. Inorg. Chem. 1976, 15, 1630.

11. Geoffroy, G. L.; Gray, H. B.; Hammond, G. S. J. Am. Chem. Soc. 1974, 96, 5565.

12. Fleming, R. H.; Geoffroy, G. L.; Gray, H. B.; Gupta, A.; Hammond, G. S.; Kliger, D. S.; Miskowski, V. M. J. Am. Chem. Soc. 1976, 98, 48.

13. Erwin, D. K.; Geoffroy, G. L.; Gray, H. B.; Hammond, G. S.; Solomon, E. I.; Trogler, W. C.; Zagars, A. A. J. Am. Chem. Soc. 1977, 99, 3620.

14. Trogler, W. C.; Erwin, D. K.; Geoffroy, G. L.; Gray, H. B. J. Am. Chem. Soc. 1978, 100, 1160.

15. Trogler, W. C.; Gray, H. B. Nouv. J. Chim. 1977, 1, 475.

16. The one exception, which has enjoyed mass popularity, may be found in: Wambaugh, J. "The Delta Star"; William Morrow: New York, 1983.

17. (a) Gray, H. B.; Maverick, A. W. Science 1981, 214, 1201. (b) Eidem, P. K.; Maverick A. W.; Gray, H. B.

Inorg. Chim. Acta **1981**, 50, 59. (c) Maverick, A. W.; Gray, H. B. Pure Appl. Chem. **1980**, 52, 2339.

18. Cotton, F. A.; Curtis, N. F.; Robinson, W. R. Inorg. Chem. **1965**, 4, 1696.

19. Barder, T. J.; Walton, R. A. Inorg. Chem. **1982**, 21, 2510.

20. Cotton, F. A.; DeBoer, B. G.; Jeremic, M. Inorg. Chem. **1970**, 9, 2143.

21. Prepared in an analogous manner to $[ReCl_3P(C_6H_5)_3]_n$ in Ref. 18, with PEt_3 in place of PPh_3.

22. Bonati, F.; Cotton, F. A. Inorg. Chem. **1967**, 6, 1353.

23. Wu, H. J. Biol. Chem. **1920**, 43, 189.

24. Maverick, A. W. Ph.D. Dissertation, California Institute of Technology, **1982**.

25. (a) K^+TCNE^-: Webster, O. W.; Mahler, W.; Benson, R. E. J. Am. Chem. Soc. **1962**, 84, 3678. (b) Na^+ chloranil$^-$: Torrey, H. A.; Hunter, W. H. J. Am. Chem. Soc. **1912**, 34, 702.

26. Brändström, A.; Berntsson, P.; Carlsson, S.; Djurhuus, A.; Gustavii, K.; Junggren, U.; Lamm, B.; Samuelsson, B. Acta Chem. Scand. **1969**, 23, 2202.

27. Rice, S. F. Ph.D. Dissertation, California Institute of Technology, **1982**.

28. Demas, J. N.; Crosby, G. A. J. Phys. Chem. **1971**, 75, 991.

29. Nocera, D. G.; Winkler, J. R.; Yocom, K. M.; Bordignon, E.; Gray, H. B. to be published.

30. (a) Gagné, R. R.; Koval, C. A.; Lisensky, G. C. Inorg. Chem. 1980, 19, 2854. (b) Ref. 49, p. 701.

31. Milder, S. J.; Goldbeck, R. A.; Kliger, D. S.; Gray, H. B. J. Am. Chem. Soc. 1980, 102, 6761.

32. Cowman, C. D.; Gray, H. B. J. Am. Chem. Soc. 1973, 95, 8177.

33. Trogler, W. C.; Cowman, C. D.; Gray, H. B.; Cotton, F. A. J. Am. Chem. Soc. 1977, 99, 2993.

34. Bursten, B. E.; Cotton, F. A.; Fanwick, P. E.; Stanley, G. C. J. Am. Chem. Soc. 1983, 105, 3082.

35. Trogler, W. C.; Solomon, E. I.; Gray, H. B. Inorg. Chem. 1977, 16, 3031.

36. Miskowski, V. M.; Goldbeck, R. A.; Kliger, D. S.; Gray, H. B. Inorg. Chem. 1979, 18, 86.

37. Hay, P. J. J. Am. Chem. Soc. 1982, 104, 7007, and references therein.

38. Luminescence spectrum is uncorrected for monochromater and photomultiplier tube response.

39. (a) Herzberg, G. "Molecular Spectra and Molecular Structure, I. Spectra of Diatomic Molecules"; 2nd edition, Van Nostrand Rheinhold Company: New York, 1950. (b) Ansbacher, F. Z. Naturforschg. 1959, 14a, 889.

40. (a) Clark, R. J. H.; Franks, M. L. J. Am. Chem. Soc. 1976, 98, 2763. (b) Clark, R. J. H.; Stead, M. J. Inorg. Chem. 1983, 22, 1214.

41. Dr. V. M. Miskowski, personal communication.

42. Cotton, F. A.; Hall, W. T. Inorg. Chem. 1977, 16, 1867.

43. Hopkins, M. D.; Gray, H. B. to be published.

44. Ballhausen, C. J. "Molecular Electronic Structures of Transition Metal Complexes"; McGraw-Hill: Great Britain, 1979.

45. Cotton, F. A.; Robinson, W. R.; Walton, R. A. Inorg. Chem. 1967, 6, 1257.

46. Hendriksma, R. R.; van Leeuwen, H. P. Electrochimica Acta 1973, 18, 39.

47. Cotton, F. A.; Pedersen, E. Inorg. Chem. 1975, 14, 383.

48. (a) Maverick, A. W.; Gray, H. B. J. Am. Chem. Soc. 1981, 103, 1298. (b) Maverick, A. W.; Najdzionek, J. S.; MacKenzie, D.; Nocera, D. G.; Gray, H. B. J. Am. Chem. Soc. 1983, 105, 1878.

49. Bard, A. J.; Faulkner, L. R. "Electrochemical Methods"; Chapter 6, Wiley: New York, 1980.

50. Vdovichenko, V. T.; Kondratenko, V. I. Khim. Prom. 1967, 43, 290.

51. Bennett, M. J.; Cotton, F. A.; Foxman, B. M.; Stokely, P. F. J. Am. Chem. Soc. 1967, 89, 2759.

52. Cotton, F. A.; Ucko, D. A. Inorg. Chim. Acta 1972, 6, 161.

53. Summerville, R. H.; Hoffmann, R. J. Am. Chem. Soc. 1979, 101, 3821.

54. Trogler, W. C. Inorg. Chem. 1980, 19, 697.

55. Bock, C. R.; Connor, J. A.; Gutierrez, A. R.; Meyer, T. J.; Whitten, D. G.; Sullivan, B. P.; Nagle, J. K. J. Am. Chem. Soc. **1979**, 101, 4815.

56. Olmstead, M. L.; Hamilton, R. G.; Nicholson, R. S. Anal. Chem. **1969**, 41, 260.

57. Noyes, R. M. Prog. React. Kinet. **1961**, 1, 129.

58. Smoluchowski, M. Z. Phys. Chem. **1917**, 92, 129.

59. Phillips, W. D.; Rowell, J. C.; Weissman, S. I. J. Chem. Phys. **1960**, 33, 626.

60. The $TCNE^{0/-}$ couple in CH_3CN reported to be 0.24 V *vs.* SCE (Peover, M. E. Trans. Far. Soc. **1962**, 58, 2370).

61. The $DDQ^{0/-}$ couple in CH_3CN reported to be 0.51 V *vs.* SCE (Peover, M. E. Nature **1961**, 191, 702).

62. Addition of DDQ/Cl^- solution to Florasil® gave rise to five bands that were all identified by optical absorption spectroscopy.

63. Wright, R. C.; Laurence, G. S. J. Chem. Soc., Chem. Comm. **1972**, 132.

64. (a) Balzani, V.; Moggi, L.; Manfrin, M. F.; Bolletta, F. Coord. Chem. Rev. **1975**, 15, 321. (b) Turro, N. J. "Modern Molecular Photochemistry"; Benjamin/Cummings: Menlo Park, California, **1978**.

65. (a) See, for example, Whitten, D. G. Acc. Chem. Res. **1980**, 13, 83. (b) Matsuo, T. Pure Appl. Chem. **1982**, 54, 1693.

66. Förster, T. "Fluorenzenz Organische Verbindungen"; Gottingen: Vandenhoech and Ruprech, **1951**.

67. Dexter, D. L. J. Chem. Phys. 1953, 21, 836,

68. For example, selected triplet energies of quenchers used in this study are: PTH, 2.62 eV (Alkaitis, S. A.; Grätzel, M.; Henglein, A. Ber. Bunsenges. Phys. Chem. 1975, 79, 541); DPA, 3.12 eV (Terenin, A.; Ermolaev, V. Trans. Faraday Soc. 1956, 52, 1042); DEA, 2.95 eV (Dubroca, C.; Lozano, P. Chem. Phys. Lett. 1974, 24, 49); DMA, 2.99 eV (Lim, E. C.; Chakrabarti, S. K. Chem. Phys. Lett. 1967, 1, 28).

69. (a) Rehm, D.; Weller, A. Ber. Bunsenges. Phys. Chem. 1969, 73, 834. (b) Rehm, D.; Weller, A. Isr. J. Chem. 1970, 8, 259.

70. (a) Marcus, R. A. J. Chem. Phys. 1956, 24, 966 and 979. (b) Marcus, R. A. Discuss. Faraday Soc. 1960, 29, 21. (c) Marcus, R. A. J. Chem. Phys. 1965, 43, 679 and 2654. (d) Marcus, R. A. Ann. Rev. Phys. Chem. 1964, 15, 155. (e) For a review on classical, semi-classical and quantum theories of electron transfer, see Sutin, N. Prog. Inorg. Chem. 1983, 30, 441.

71. Bock, C. R.; Meyer, T. J.; Whitten, D. G. J. Am. Chem. Soc. 1975, 97, 2909.

72. (a) Van Duyne, R. P.; Fischer, S. F. Chem. Phys. 1974, 5, 183. (b) Ulstrup, J.; Jortner, J. J. Chem. Phys. 1975, 63, 4358. (c) Kestner, N. R.; Logan, J.; Jortner, J. J. Phys. Chem. 1974, 78, 2148.

73. (a) Siders, P.; Marcus, R. A. J. Am. Chem. Soc. 1981, 103, 748 and references therein. (b) See, also Meyer, T. J. Prog. Inorg. Chem. 1983, 30, 389.

74. Nocera, D. G.; Maverick, A. W.; Winkler, J. R.; Che, C.-M.; Gray, H. B. in "Inorganic Chemistry: Toward the 21th Century", Chisholm, M. H. ed.; American Chemical Society: Washington, D.C., 1983; ACS Symp. Ser. No. 211.

75. Swihart, D. L.; Mason, W. R. Inorg. Chem. 1970, 9, 1749.

76. (a) Douglas, I. N.; Nicholas, J. V.; Wybourne, B. G. J. Chem. Phys. 1968, 48, 1415. (b) Eyring, G.; Schmidtke, H.-H. Ber. Bunsenges. Phys. Chem. 1981, 85, 597.

77. (a) Rich, R. L.; Taube, H. J. Am. Chem. Soc. 1954, 76, 2608. (b) Cox, L. E.; Peters, D. G.; Wehry, E. L. J. Inorg. Nucl. Chem. 1972, 34, 297.

78. (a) Balzani, V.; Manfrin, F.; Moggi, L. Inorg. Chem. 1967, 6, 354. (b) Balzani, V.; Carassiti, V. J. Phys. Chem. 1968, 72, 383.

CHAPTER III

MOLYBDENUM(II) AND TUNGSTEN(II) HALIDE CLUSTER IONS

A. INTRODUCTION

Luminescent polynuclear metal complexes having a core of more than two metals represent an important class of inorganic photoreagents. The high density of redox centers in a single molecule logically adapt such species to multielectron photochemical reactions. While the search for new polynuclear inorganic photoreagents has produced a score of viable binuclear metal complexes (see Chapters I and II), few higher nuclearity clusters have been prepared that possess the long-lived excited states in solution that are a prerequisite for bimolecular photoredox chemistry. To date, the known systems number only two: $H_4Re_4(CO)_{12}$ and $M_6X_{14}^{2-}$ (M=Mo,W; X=Cl,Br,I).

Graff and Wrighton[1] have observed emission from the lowest energy excited state of $H_4Re_4(CO)_{12}$ in the solid state and 3-methylpentane at 77 K and room temperature. The excited state lifetime (20 ns in 3-methylpentane; 1.02 μs in solid; room temperature) exhibits a marked hydrogen isotope dependence, increasing 20-30% when ^1H is replaced by ^2H. Quenching studies with conventional energy transfer reagents identify the emissive state to be triplet in character. Though these photophysical properties portend the use of this cluster in energy storage cycles and catalysis, its photochemistry has not been investigated.

In these laboratories, Maverick's initial studies on $Mo_6Cl_{14}^{2-}$, $Mo_6Br_{14}^{2-}$, and $W_6Cl_{14}^{2-}$ have spearheaded an attack

on the elucidation of the spectroscopic, electrochemical, and photochemical properties of the $M_6X_{14}^{2-}$ ions.[2] The idealized structure of the molybdenum and tungsten halide clusters consists of an octahedral core of metal atoms coordinated by eight face-bridging halides and six axial halides (Figure 1). The electronic absorption spectra of the $M_6X_{14}^{2-}$ clusters are characterized by an intense broad absorption band in the ultraviolet which extends well into the visible spectral region.[3] The pronounced red shift of the ultraviolet absorption bands along the halide series, Cl^- to Br^- to I^-, in both the molybdenum and tungsten clusters indicates that the intense absorptions are associated with LMCT transitions. The absence of vibrational fine structure in the absorption profiles of $M_6X_{14}^{2-}$ clusters has severely hampered a complete description of the electronic structure of these complexes. However, the temperature dependence of the magnetic susceptibility of $Mo_6Cl_{14}^{2-}$ clearly demonstrates a $^1A_{1g}$ ground electronic state,[2b] which is in agreement with numerous theoretical descriptions of the electronic structure of these clusters.[4]

Maverick's studies on $Mo_6Cl_{14}^{2-}$, $Mo_6Br_{14}^{2-}$ and $W_6Cl_{14}^{2-}$ reveal an exciting new class of photoreceptors for light-induced chemical reactions.[2] First, ultraviolet or visible irradiation of the clusters in the solid state or aqueous and nonaqueous solutions produces an intense red luminescence. The extremely long-lived excited states of the cluster ions (τ_0 = 180 μs for $Mo_6Cl_{14}^{2-}$ in CH_3CN) (*vide supra*) make them

Figure 1. Idealized structure of $M_6X_{14}^{2-}$ ions:
● = Mo(II), W(II); ○ = Cl,Br,I.

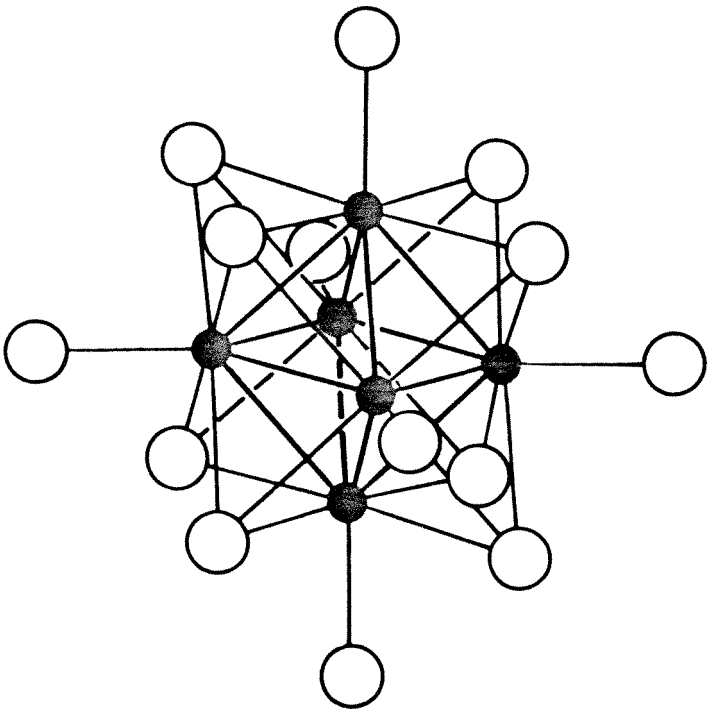

ideal photoreagents for bimolecular chemistry. Second, electrochemical studies have shown that the cluster ions undergo facile one-electron oxidation in aprotic solvents (*vide supra*) to produce powerful oxidizing agents. These electrochemical and photophysical investigations of $Mo_6Cl_{14}^{2-}$ correctly implied that the $Mo_6Cl_{14}^{-}$ ion could be generated photochemically, by electron transfer quenching reactions between the excited $Mo_6Cl_{14}^{2-}$ ion and a variety of electron acceptors. The high density of the redox centers in the cluster cores of these species makes them bright prospects for photoinduced multielectron transfer chemistry.

The potential multielectron photochemistry of the $M_6X_{14}^{2-}$ clusters (and especially their application to energy conversion cycles), compelled us to continue our assault on the chemistry of these cluster systems. The studies reported herein are two-fold. New data on the photophysical properties of $M_6X_{14}^{2-}$ excited states is outlined in Section C and discussed in the light of some recent theoretical studies on the electronic structures of the cluster ions. In Section D, the electrochemical reactions of the five clusters are examined. As demonstrated by the binuclear rhenium halide systems of Chapter II, the electrochemical reactivity of a system can provide invaluable guidelines to its prospective photochemistry. In addition to the $M_6X_{14}^{2-}$ redox chemistry, the discovery of electrogenerated chemiluminescence (ECL) from $Mo_6Cl_{14}^{2-}$ further augments the remarkable properties of these inorganic photoreagents and

these electrochemical properties are outlined in Section D.

B. EXPERIMENTAL

Materials. Molybdenum dichloride was purchased from Cerac Inc. as a fine yellow powder. The compound was heated with constant boiling HCl and filtered while hot to remove the black amorphous residue which remained undissolved. NBu_4Cl was added to the hot filtrate to afford $(Bu_4N)_2Mo_6Cl_{14}$ as a yellow powdery precipitate which was collected and washed several times with ethanol and ether. The powder was dissolved in CH_2Cl_2 and the solution was dried over $MgSO_4$, filtered, and allowed to evaporate in air at room temperature. Large prismatic crystals grew over a period of two weeks. *Anal. Calcd. for* $(Bu_4N)_2Mo_6Cl_{14}$: C, 24.69; H, 4.66; N, 1.80. Found: C, 24.67; H, 4.56; N, 1.79.

Molybdenum diiodide was obtained from Alfa Ventron as a black powder (at purportedly 99% purity). Only after several washings was the commercial sample freed from iodine. The remaining black solid was heated in boiling ethanol and the solution was treated with NBu_4I. The residue was collected and extracted with CH_2Cl_2 to produce a red solution. Evaporation of the CH_2Cl_2 produced an orange-red amorphous solid with a "seaweed-like" appearance. Imbedded in this solid, were burgundy crystals which were manually extracted. Unfortunately, the small quantity of sample did not permit elemental analysis.

The method of Dorman and McCarley[5] was used with slight modifications to prepare tungsten dibromide. A quartz reaction

tube containing 0.250 g of Al powder (Merck) and 2.40 g of reagent grade NaBr was dried at 150°C for 4 hr. under a dynamic vacuum. The tube was blanketed with argon, stoppered, transferred to a glove box and loaded with 3.00 g of $AlBr_3$ (Aldrich Chemical Co.) and 3.30 g of WBr_5 (Alfa Ventron). After removal from the nitrogen atmosphere, the quartz vessel was evacuated and sealed under a dynamic vacuum. The tube was placed in a high temperature furnace and heated to 200°C for 6 hr., after which the temperature was slowly raised over a 3 hr. period to 450°C and the reaction was allowed to equilibrate for 8 hr. The temperature was then raised during a 1 hr. period to 550°C. The reaction proceeded at this temperature for 1 day. Upon cooling, the tube was cracked open (*CAUTION!* tube occasionally explodes releasing vile and odiferous fumes) to yield a fused black solid which was leached with water to remove alkali salts. The black residue that remained was washed with ether, dried, heated with ethanol for 1 hr. and filtered. NBu_4Br (Eastman) was added to the yellow filtrate to produce a powder after 10 min. The precipitate was collected, taken up with CH_3CN, dried over $MgSO_4$ and filtered. Slow evaporation of the CH_3CN yielded orange-yellow crystals. *Anal.* Calcd. for $(Bu_4N)_2W_6Br_{14}$: C, 14.20; H, 2.69; N, 1.03. Found: C, 14.16; H, 2.53; N, 1.07.

Tungsten diiodide was prepared by the method of Hogue and McCarley.[6] To a quartz reaction tube, 1.00 g of

$(NH_4)_2W_6Cl_{14}$, 9.97 g of KI, and 3.64 g of LiI were added. The tube was evacuated, heated at 140°C for 2 hr. under a dynamic vacuum and sealed. The reaction was initiated by heating the quartz vessel to 550°C over a 1½ hr. period. After 1 hr., the tube was allowed to cool and its contents were collected in air (*CAUTION!*). The black solid was repeatedly washed with diethyl ether to remove iodine and with water to remove alkali salts. After drying, the black residue was heated with ethanol and filtered. Treatment of the yellow-orange filtrate, after concentration, with NBu_4I (Eastman) yielded a yellow powder. Well-developed orange cubic crystals may be grown upon slow evaporation of acetonitrile solutions of the compound. *Anal.* Calcd. for $(Bu_4N)_2W_6I_{14}$: W, 32.78; I, 52.80; C, 11.42; H, 2.16; N, 0.83. Found: W, 32.41; I, 52.50; C, 11.51; H, 2.14; N, 0.80.

The tetrabutylammonium salts of molybdenum bromide, prepared by the method of Sheldon,[3] and tungsten chloride were obtained from Andrew M. Maverick.

The $W_6Br_{14}^-$ anion was prepared by electrochemical and chemical oxidation reactions. Bulk electrolysis of yellow dichloromethane solutions of $(Bu_4N)_2W_6Br_{14}$ at 0.90 V *vs.* SCE was complete after 1.05 equivalents of electrons had passed through the solution. A cyclic voltammogram of the red electrolyzed solution showed only a single wave corresponding to the $W_6Br_{14}^{-/2-}$ couple at 0.77 V *vs.* SCE. The anodic and cathodic peak currents of the cyclic

voltammetric wave were identical to those of the pre-electrolyzed solution indicating complete conversion of $W_6Br_{14}^{2-}$ to $W_6Br_{14}^{-}$. The electrolyzed solution was removed from the electrochemical cell and layered with light petroleum ether and after 1 week, deep red crystals had formed. Crystal faces appeared grainy under microscopic investigation. X-ray diffraction photographs suggested a short-range crystal order, however, the ill-defined diffraction spots indicated a poor crystalline material. Oxidation of $W_6Br_{14}^{2-}$ by $NOPF_6$ was found to be a more practical synthetic route to $W_6Br_{14}^{-}$. Addition of a molar excess of $NOPF_6$ to $W_6Br_{14}^{2-}$ in dichloromethane caused the yellow solution to turn red within minutes. The reaction was terminated after the cessation of NO evolution. All attempts at growing x-ray structural quality crystals ended in failure. This may be attributed to the susceptibility of the monoanion to undergo reduction; $W_6Br_{14}^{-}$ had only short term stability in alcohols, CH_3CN, acetone, and most other nonaqueous solvents. $NBu_4W_6Br_{14}$ crystals with reflective faces were grown from CH_3CN solutions which were cooled to -60°C (in which the compound was stable for days), however, x-ray diffraction photographs again showed a poorly defined crystalline material. The tetraethylammonium salt of $W_6Br_{14}^{-}$ gave crystals with similarly unsatisfactory crystallographic properties.

Solvents and supporting electrolytes were prepared by the procedures described in Chapter II.

Analyses of $(Bu_4N)_2Mo_6Cl_{14}$ and $(Bu_4N)_2W_6Br_{14}$ were performed by L. Henling at Caltech. The $(Bu_4N)_2W_6I_{14}$ analysis was performed at Galbraith Laboratories in Knoxville, Tennessee.

Methods and Instrumentation. Absorption, emission, and lifetime experiments employed the instrumentation described in Chapter II. Absolute quantum yields for the cluster ions were determined by comparison with $Ru(bpy)_3^{2+}$ at 436 nm[7] using the corrections described by Demas and Crosby.[8] Emission spectra were corrected for monochromator and photomultiplier tube (R406) response as described by Drushel *et al.*[9] Solutions for emission and lifetime experiments, prepared by solvent distillation on a high vacuum manifold, were subjected to five freeze-pump-thaw cycles. Lifetime measurements were made using the frequency doubled Nd:YAG fundamental at a gain which was slightly above lasing threshold. At higher laser powers, non-exponential emission decay signals were observed. This was probably due to both multiphoton excitation and local sample heating.

Electrochemical measurements were made using the three electrode system and PAR apparatus described in Chapter II. A conventional H-cell design was employed in cyclic voltammetric measurements. For the electrochemical experiments involving the synthesis of the cluster monoanions, however, the specially designed high vacuum electrochemical cell in Figure 2 was used. The auxiliary electrode compartment

Figure 2. High vacuum electrochemical cell.

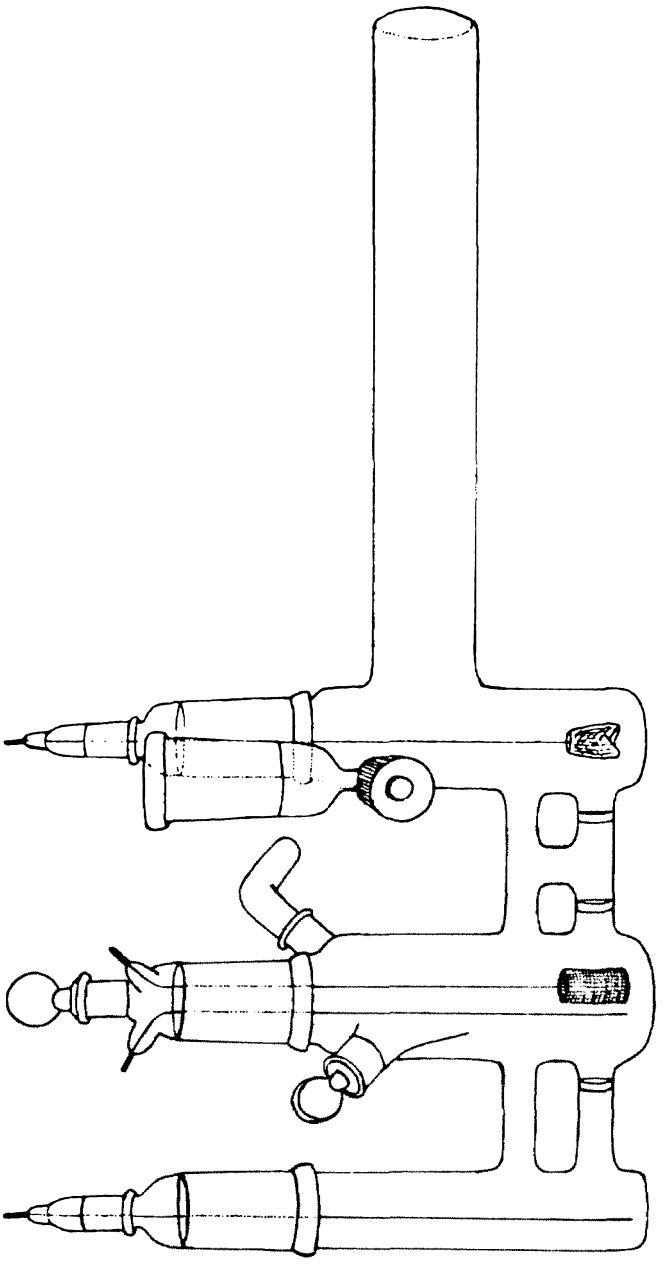

is separated from that of the working electrode by a double fritted chamber. The cell was incorporated with Pt wire and Pt basket working electrodes, a Pt mesh auxiliary electrode and an Ag wire reference electrode. In a typical experiment, the supporting electrolyte was added to the sidearm tube, the cell was assembled and evacuated under a high vacuum manifold. Solvent was vacuum distilled into the sidearm and the cell was isolated from an external atmosphere by a high vacuum teflon valve. The contents of the sidearm were thoroughly mixed and the cell was slowly tipped to fill the cell compartments. A cyclic voltammogram of the solvent background was recorded before sample was introduced into the working electrode compartment from the charging tube. The above procedure permitted all experiments to be performed under rigorously oxygen and H_2O free conditions.

ECL experiments utilized the same high vacuum cell and the detection system of the previously described emission spectrometer. A cyclic square wave potential program was employed to generate ECL transients. The lifetime of the ECL experiment was determined by the time for diffusion of the byproducts generated at the auxiliary electrode into the working electrode compartment. These auxiliary electrode "impurities" efficiently quenched the cluster ion luminescence.

All redox couples were referenced to a ferrocene internal standard and related to the SCE reference using a value of 0.31 V *vs.* SCE for the $Fc^{+/0}$ couple.[10]

EPR measurements (12 K) of electrochemically generated $M_6X_{14}^-$ ions were recorded on the Varian E-line Century Series spectrometer X-band with the Air Products Heli-Trans cooling system. Upon completion of an electrolysis reaction, solution was syringed from the working electrode compartment under an argon counterflow and added to an argon purged EPR tube equipped with a high vacuum valve. The solution was subjected to five freeze-pump-thaw cycles and the EPR spectrum was immediately measured.

C. ELECTRONIC STRUCTURE AND PHOTOPHYSICS

The electronic structure and bonding in $M_6X_{14}^{2-}$ cluster ions has been the subject of many theoretical treatments. Most studies concur with a bonding scheme of 12 Mo d levels which are filled with 24 electrons to form the 12 metal-metal bonds of the octahedron core and a diamagnetic ground state. The finer details of cluster bonding such as molecular orbital energies and composition, however, have eluded a unified description. Only recently, with the correlation among three independent theoretical studies, has a consonant analysis of the cluster ion's electronic structure begun to emerge. An SCF-SW-Xα calculation by Siefert *et al.* on $Mo_6X_8^{4+}$ (X=F,Cl,Br,I) determined that the valence orbitals were metal localized with a highest occupied molecular orbital (HOMO) of e_g symmetry.[11] Dr. David Tyler's research group at Columbia University personally communicated that their SCF-SW-Xα calculation on $Mo_6Cl_{14}^{2-}$ confirmed Siefert's e_g HOMO level and further determined that the lowest unoccupied molecular orbital (LUMO) has a_{2g} symmetry and lies 3.0 eV above the HOMO. Hughbanks and Hoffmann recently carried out an extended Hückel analysis on the $Mo_6S_8^{4-}(S^{2-})_6$ "Cheverel phase" species, which is isoelectronic and isostructural with the $M_6X_{14}^{2-}$ (i.e. $M_6X_8^{4+}(X^-)_6$) ions.[12] Their calculated frontier molecular orbitals were comprised of metal based Mo d orbitals and, in agreement with Tyler *et al.*'s

results, the HOMO and LUMO levels were found to be of e_g and a_{2g} symmetries, respectively. These three studies provide a foundation from which $M_6X_{14}^{2-}$ electronic structure may be probed. The data presented here are an extension of Maverick's initial investigations and may be understood in terms of the most recent theoretical models of $M_6X_{14}^{2-}$ bonding and structure.

Results and Discussion

The $M_6X_{14}^{2-}$ ions exhibit intense luminescence in solution and solid state. The emission quantum yields for the tetrabutylammonium salts in acetonitrile are shown in Table 1 and their luminescence spectra are illustrated in Figure 3. The large emission quantum yield of $W_6I_{14}^{2-}$ is atypical of transition metal complexes and even more remarkable when one considers the all-inorganic nature of the cluster compound. As Maverick hypothesized on the basis of the $Mo_6Cl_{14}^{2-}$ and $Mo_6Br_{14}^{2-}$ data, the relatively constant energies of the luminescence bands of molybdenum halide clusters may be ascribed to metal localized HOMO and LUMO levels. This hypothesis cannot explain the tungsten clusters' luminescence, however, which exhibit a monotonic increase of the emission band energies along the Cl^- to I^- halide series. Apparently, the larger radial extension of the 5d metal orbitals leads to greater ligand admixture in the frontier molecular orbitals in the tungsten clusters than in the molybdenum clusters.

Table 1. Emission Spectroscopic Data for $(Bu_4N)_2M_6X_{14}$

$(Bu_4N)_2M_6X_{14}$ M,X	$\bar{\nu}_{em,max}/cm^{-1}$ (fwhm/μm^{-1})	ϕ_e [a,b]	$\tau/\mu s$ [c] Solid (5 K)	Solid (300 K)	CH_3CN (300 K)
Mo,Cl	12,250(0.43)	0.19[e]	320	115	180
Mo,Br	12,000(0.44)	0.23[e]	180	71	110
Mo,I[d]	12,500(0.47)	0.059	--	--	45
W,Cl	11,250(0.35)	0.017[e]	90	6	2
W,Br	12,750(0.37)	0.12	50	13	15
W,I	14,000(0.35)	0.39	20	12	30

[a]Acetonitrile solution at 300 K. [b]Excitation wavelength 436 nm. Quantum yield measured relative to $[Ru(bpy)_3]Cl_2$ in degassed H_2O (ϕ_e(436 nm)) = 0.042 ±0.002: Ref. 7. [c]Lifetimes measure with 2nd harmonic (532 nm) from Nd:YAG laser (pulse width 8 ns fwhm). [d]No sample analysis for $(Bu_4N)_2Mo_6I_{14}$. [e]Ref. 2b.

Figure 3. Corrected emission spectra for the tetrabutylammonium salts of the $M_6X_{14}^{2-}$ anions in CH_3CN at room temperature (excitation wavelength 436 nm): (a) $Mo_6Cl_{14}^{2-}$, ———; $Mo_6Br_{14}^{2-}$, -----; $Mo_6I_{14}^{2-}$, ·····; and (b) $W_6Cl_{14}^{2-}$, ———; $W_6Br_{14}^{2-}$, -----; $W_6I_{14}^{2-}$, ·····. Peak maxima are normalized to an arbritrary value.

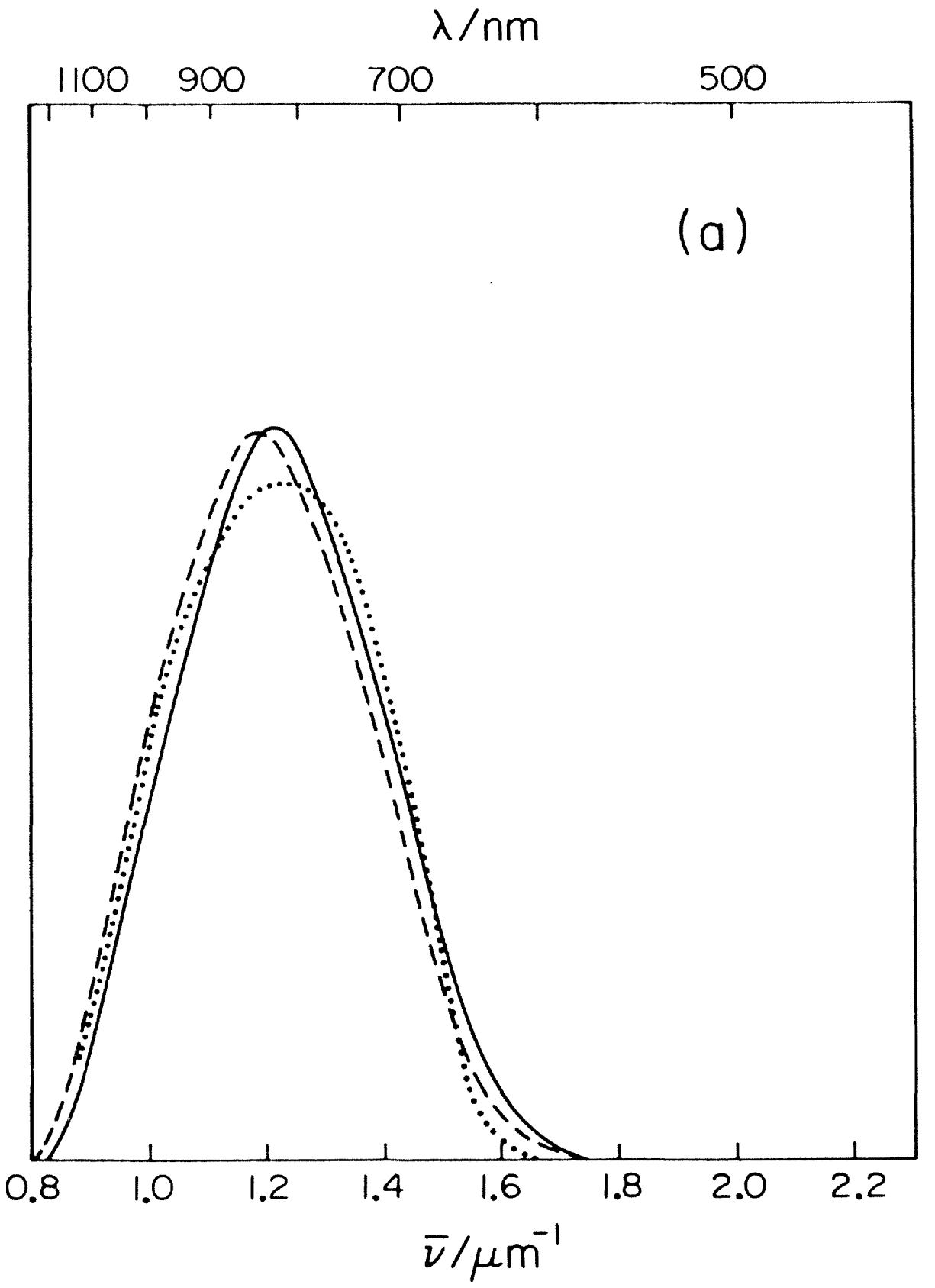
λ/nm
1100
900
700
500
(a)
0.8
1.0
1.2
1.4
1.6
1.8
2.0
2.2
$\bar{\nu}/\mu m^{-1}$

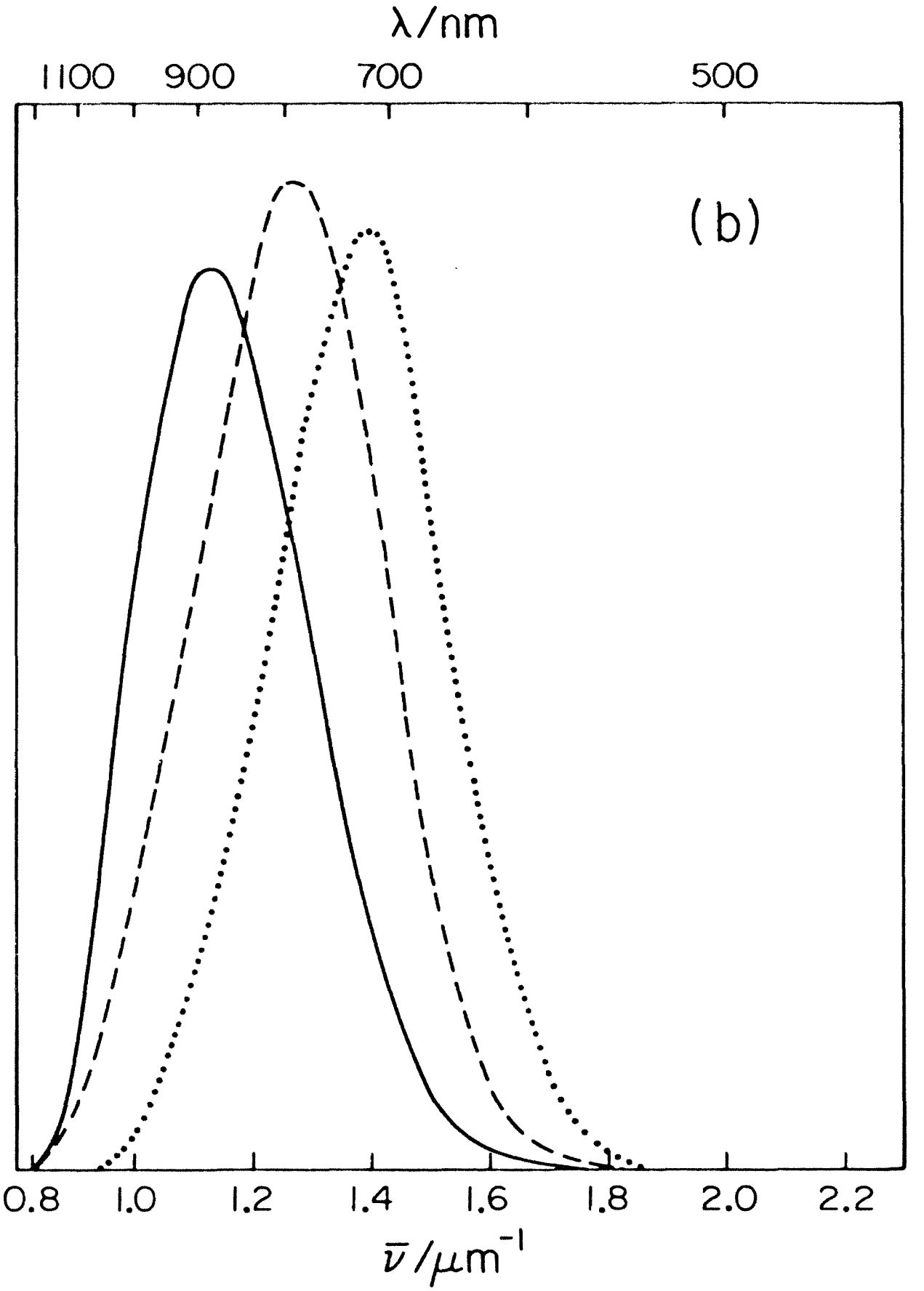
λ/nm
1100
900
700
500
(b)
0.8
1.0
1.2
1.4
1.6
1.8
2.0
2.2
$\bar{\nu}/\mu m^{-1}$

The excited state lifetimes of the cluster ions are extraordinarily long, both in solution and solid state (Table 1). Excluding $W_6Cl_{14}^{2-}$ ion, the cluster lifetimes are greater in solution than those in crystalline samples, and upon cooling to 5 K, the solid state lifetimes increase by a factor of 2 to 4; the $W_6Cl_{14}^{2-}$ lifetime at 5 K is 15 times its room temperature value. The long cluster lifetimes may be explained by the absence of high energy vibrational modes for deactivation in these all-inorganic cluster ions. Accordingly, the Raman spectrum of the tetrabutylammonium salt of $Mo_6Cl_{14}^{-}$ (Figure 4) in acetonitrile was examined since this cluster ion is expected to have the highest energy vibrational modes of the six $M_6X_{14}^{2-}$ anions. Though ten normal modes of vibration in the $M_6X_{14}^{2-}$ ion are permitted as fundamentals in the Raman spectrum in O_h symmetry ($3a_{1g} + 3e_g + 4t_{2g}$) albeit six Raman bands (indicated by arrows in Figure 4) are observed. The Raman band at 380 cm^{-1} is from CH_3CN solvent; a spectrum of the cluster ion in dichloromethane (which does not scatter between 300-500 cm^{-1}) shows no Raman peaks between 350-500 cm^{-1} verifying that the 318 cm^{-1} peak in the highest energy Raman band in $Mo_6Cl_{14}^{2-}$. The depolarization ratios of zero for the 235 cm^{-1} and 318 cm^{-1} bands (Figure 5) identifies two of the expected three totally symmetric vibrational fundamentals. These results notably contrast the previous reported Raman spectrum of $Mo_6Cl_{14}^{2-}$ which included in addition to the six peaks observed above: a strong depolarized

Figure 4. Raman spectrum of $(Bu_4N)_2Mo_6Cl_{14}$ in CH_3CN at room temperature (solvent spectrum subtracted). Excitation 5145 Å, resolution 0.50 cm^{-1}, 15 signal averages. Raman bands of the compound are indicated by the arrows, all other bands are due to solvent; peak energies are in cm^{-1}.

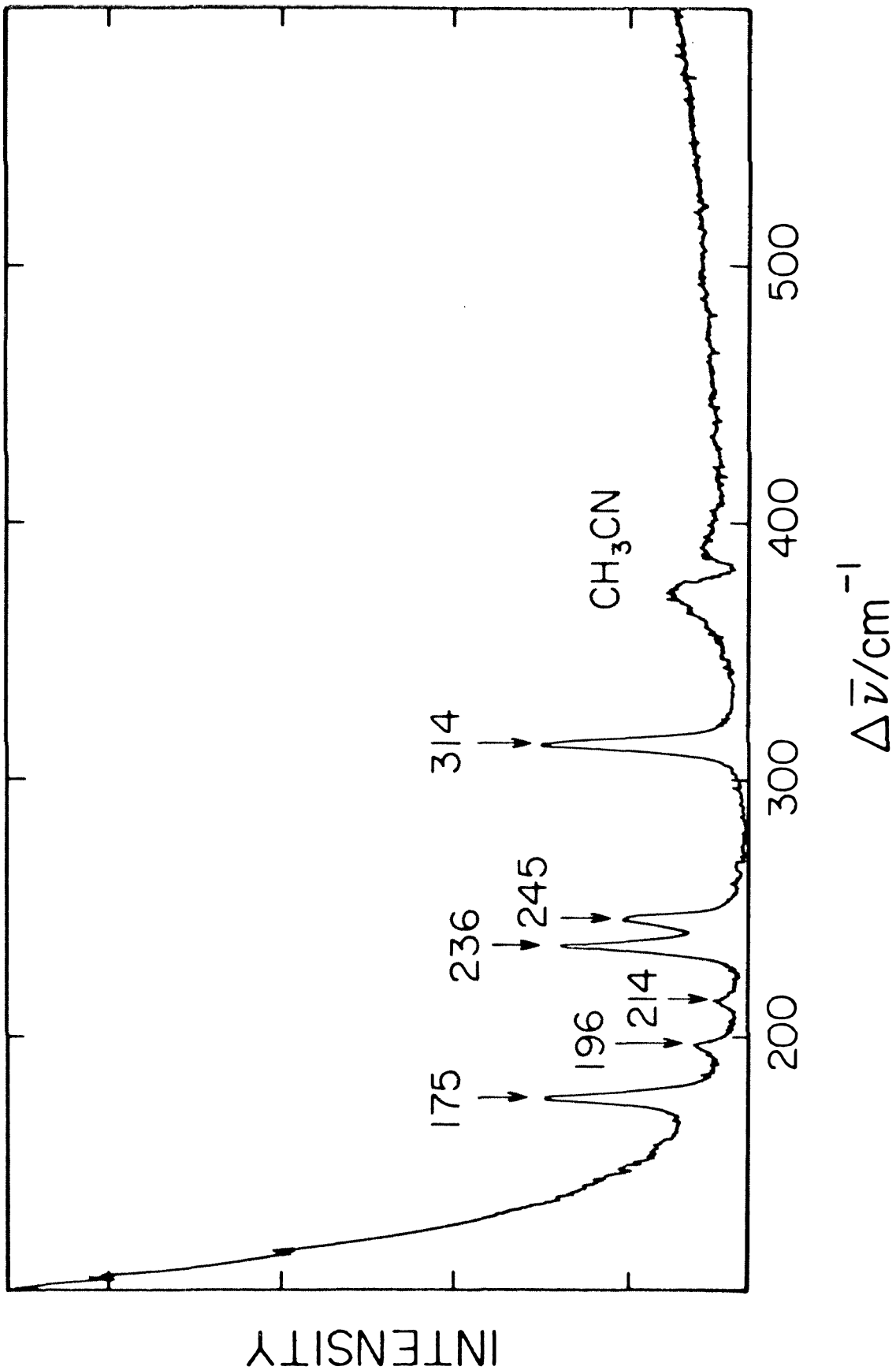
INTENSITY
200
300
400
500
$\Delta\bar{\nu}/cm^{-1}$
175
196
214
236
245
314
CH_3CN

Figure 5. Polarized Raman spectrum for $Mo_6Cl_{14}^{2-}$, as the tetrabutylammonium salt in acetonitrile at room temperature. Excitation wavelength 5145 Å , resolution 0.75 cm^{-1}, 15 signal averages. (a) $I_{\parallel}$ polarization, (b) $I_{\perp}$ polarization. Peak (depolarization ratio): a (0.75); b (0.99); c (0.85); d (0); e (0.79); f (0).

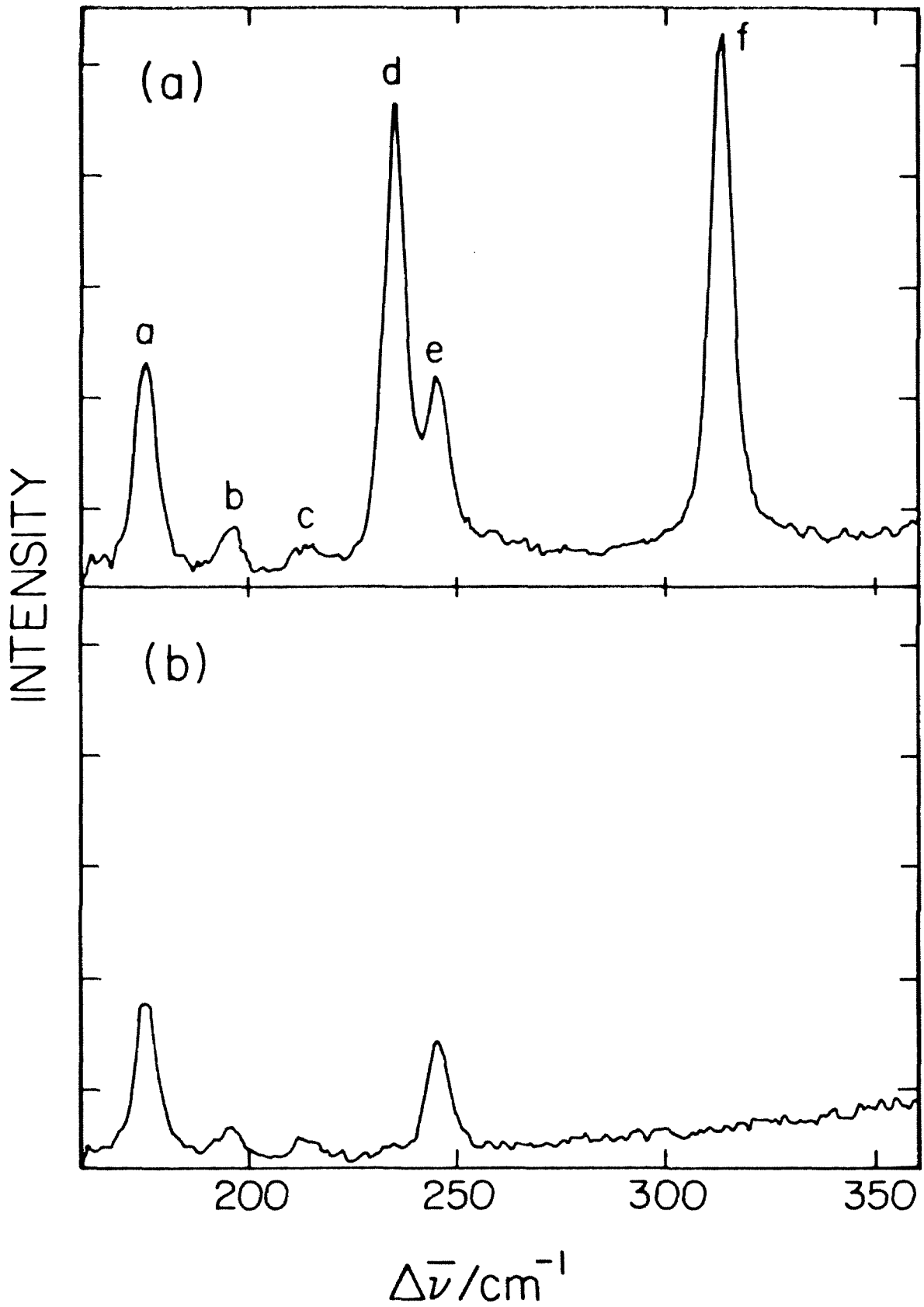
(a)
(b)
a
b
c
d
e
f
INTENSITY
200
250
300
350
$\Delta\bar{\nu}/cm^{-1}$

peak at 92 cm^{-1}, a weak totally polarized line at 402 cm^{-1} (which the authors assigned to the third a_{1g} fundamental), and two weak bands at 225 cm^{-1} and 310 cm^{-1}.[13] The absence of these bands in our studies, especially the intense band at 92 cm^{-1}, challenges the validity of the $Mo_6Cl_{14}^{2-}$ vibrational analysis which was based on the Raman spectrum. Resonance enhancement of $Mo_6Cl_{14}^{2-}$ Raman bands was not observed upon higher energy excitation. The Raman spectra of the remaining cluster ions all show fewer peaks than $Mo_6Cl_{14}^{2-}$ and, as predicted, the highest energy vibrational modes in the remaining five clusters were below 318 cm^{-1}. The absence of high energy vibrational modes in all-inorganic compounds, as demonstrated by the $M_6X_{14}^{2-}$ cluster ions, may be an important criterion for the design of new inorganic photoreceptors possessing long-lived excited states.

The experimental results reported here, in conjunction with those of Maverick's initial investigations, support the recent theoretical models of the $M_6X_{14}^{2-}$ ions. The lowest energy excited state is predicted to arise from the promotion of an electron from a filled e_g to an a_{2g} molecular orbital ($^3E_g \leftarrow {}^1A_{1g}$ and $^1E_g \leftarrow {}^1A_{1g}$). The large energy difference between the principal absorption and emission bands of the cluster ions and their long emission lifetimes strongly suggest a lowest energy excited state with triplet character. A ^3E_g excited state may be perturbed by both spin-orbit coupling and a Jahn-Teller distortion;[14] the T_{1g} and T_{2g} spin orbit components of the ^3E_g in O_h symmetry can be further

lowered in symmetry by a tetragonal distortion to give (A_{2g},E_g) and (B_{2g},E_g), respectively (in a D_{4h} point group; (A_2,E) and (B_2,E) in C_{4v}). (The same results are obtained from a tetragonal distortion of ^3E_g to give $^3A_{1g}$ and $^3B_{1g}$, which further split into (A_{2g},E_g) and (B_{2g},E_g), respectively, with a spin orbit perturbation). Thus, the theoretical models predict several thermally equilibrated excited states of the cluster ions, all of which have ^3E_g parentage. Such a model explains Maverick's observation of the luminescence band red shift (much greater than kT) of the cluster ions at low temperature. Furthermore, that the cluster lifetimes show parallel behavior between the molybdenum and tungsten series at 5 K and not at room temperature can be ascribed to the thermal population of higher energy excited states at elevated temperatures.

The most compelling experimental evidence in support of the recent theoretical model of the cluster ions' electronic structures come from the EPR measurements on electrochemically generated $M_6X_{14}^-$ (M=Mo,W; X=Cl,Br) anions in frozen dichloromethane solutions. Their EPR spectra are shown in Figure 6. In all cases, the cyclic voltammogram of the electrolyzed solution was unchanged from that of the pre-electrolyzed solution. The electrochemical generation of pure $W_6I_{14}^-$ was precluded by the presence of an anodic wave only 160 mV more positive than the $W_6I_{14}^{-/2-}$ couple (*vide supra*). As Maverick noted, the EPR signal of $Mo_6Cl_{14}^-$ may be ascribed to an axially symmetric S=1/2 system with $g_\perp$=2.11 and

Figure 6. X-band (9.280 GHz) EPR spectra of electrochemically generated $M_6X_{14}^-$ ions in frozen dichloromethane solutions at 11 K: (a) $Mo_6Cl_{14}^-$; (b) $Mo_6Br_{14}^-$; (c) $W_6Cl_{14}^-$; (d) $W_6Br_{14}^-$.

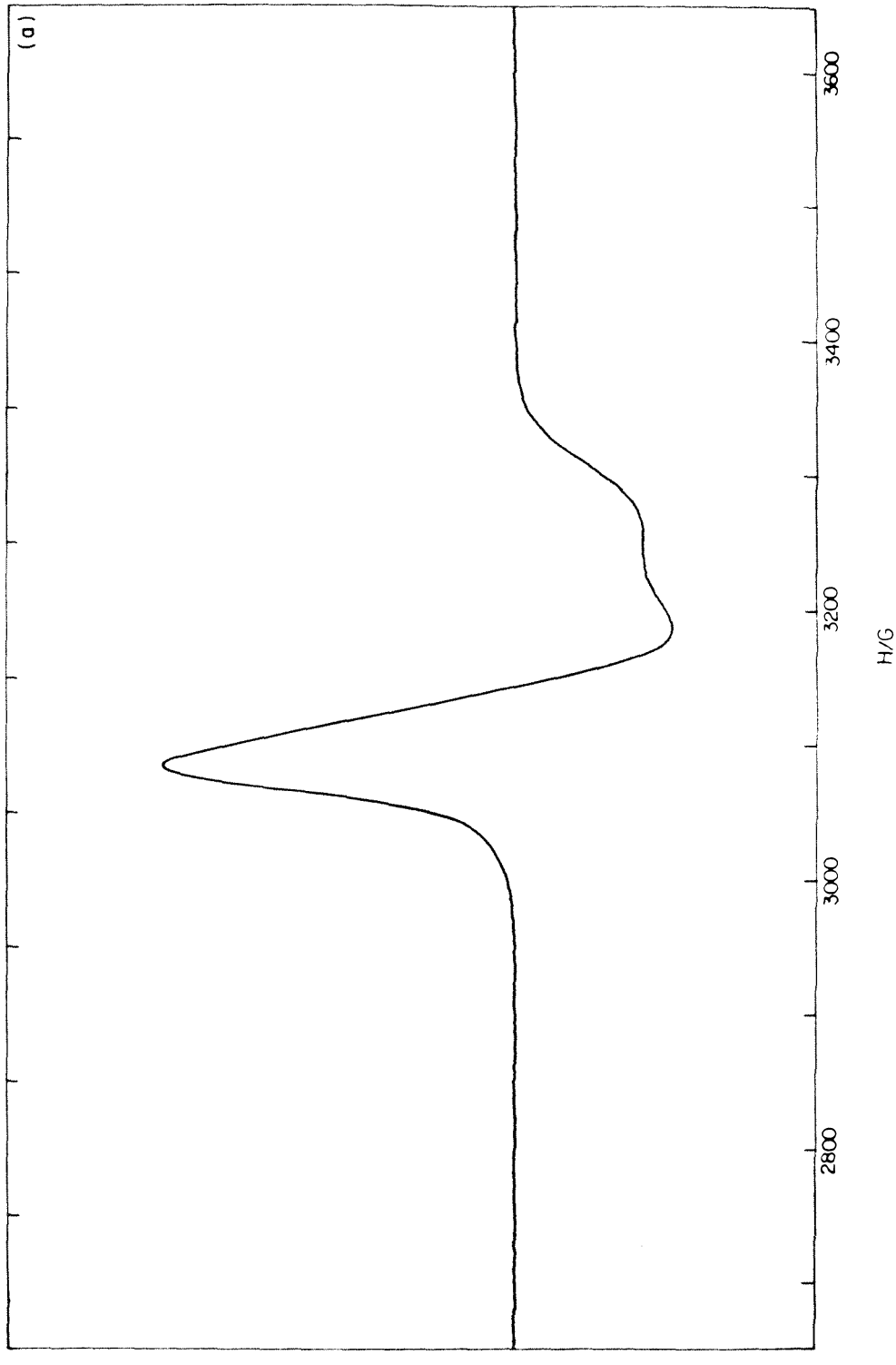
(a)
2800
3000
3200
3400
3600
H/G

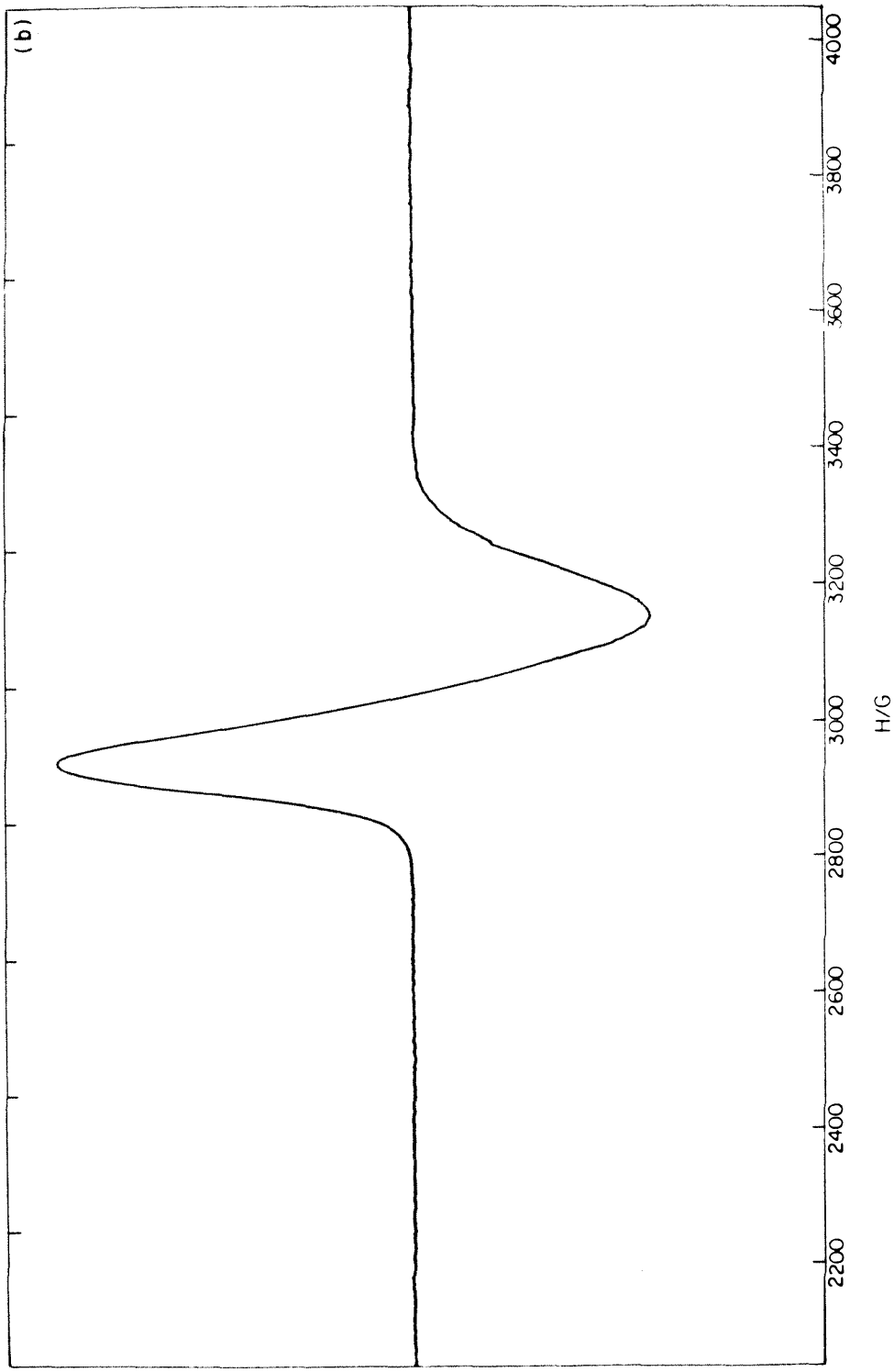
(b)
2200
2400
2600
2800
3000
3200
3400
3600
3800
4000
H/G

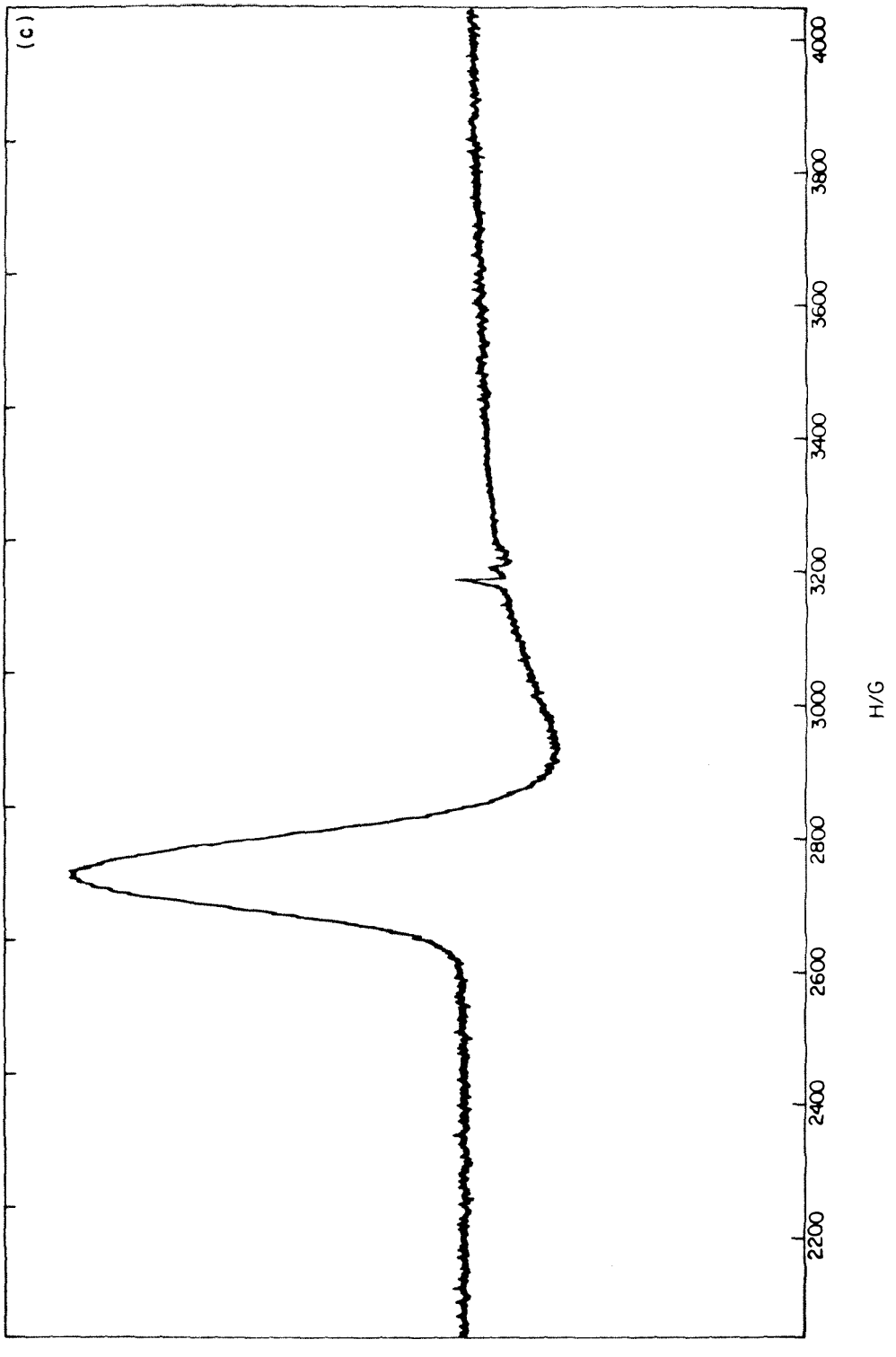
(c)
2200
2400
2600
2800
3000
3200
3400
3600
3800
4000
H/G

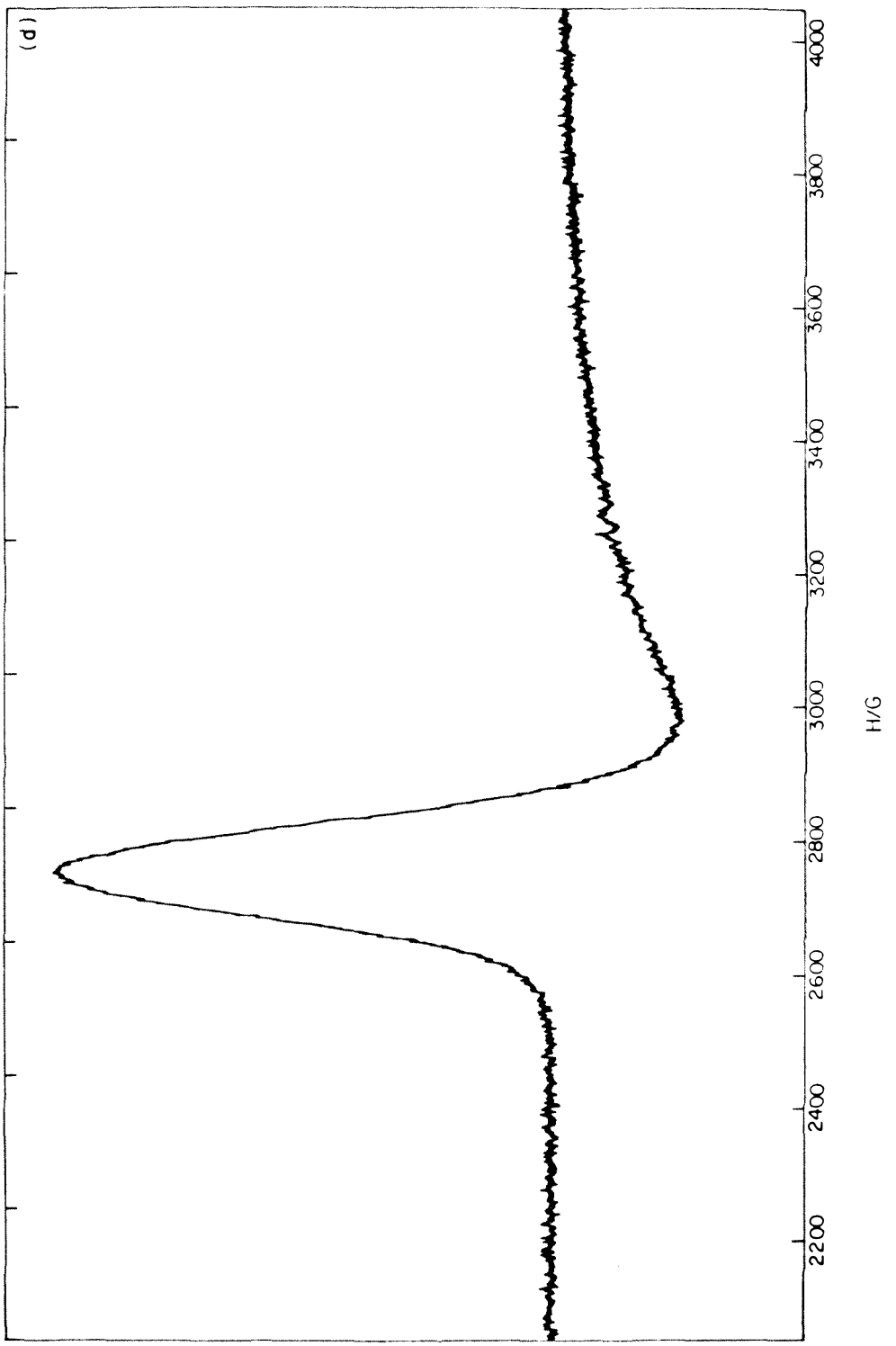
(d)
2200
2400
2600
2800
3000
3200
3400
3600
3800
4000
H/G

$g_{||} = 2.02$. The $g_{||}$ components of the other cluster spectra are not resolved and admittedly, in the case of $Mo_6Br_{14}^-$, an axial distortion, if present at all, is extremely small. The $g_\perp$ components are 2.18, 2.33 and 2.30 for $Mo_6Br_{14}^-$, $W_6Cl_{14}^-$ and $W_6Br_{14}^-$, respectively. An attractive explanation for the distorted axial signal is that the e_g orbital is depopulated to produce a ^2E_g parent state (O_h symmetry) which undergoes a tetragonal distortion to give a $^2A_{1g}$ (D_{4h}) or $^2A_1$ (C_{4v}) ground state. Unfortunately, the absence of $g_{||}$ in the $M_6X_{14}^-$ EPR spectra vitiates a full analysis of the g tensors; and a computer fit will be required to extract $g_{||}$ from the spectra in Figure 6. Nevertheless, the qualitative features of the $M_6X_{14}^-$ EPR spectra are adequately explained by the current theoretical model of the electronic structure of the $M_6X_{14}^-$ anions.

Numerous areas of research on the $M_6X_{14}^{2-}$ ion electronic structure remain to be explored. First, the documentation of the temperature dependence of the cluster ion lifetimes would be invaluable to determining the existence of several thermally accessible long-lived excited states. The dramatic increase in excited state lifetime that results from cooling $W_6Cl_{14}^{2-}$ to 5 K distinguishes this ion from other cluster analogs and suggests a markedly different electronic structure. One explanation of this behavior may be that the $W_6Cl_{14}^{2-}$ excited state more closely approaches the strong coupling limit in non-radiative decay theory while the other cluster excited states are described adequately in terms of

the weak coupling limit.[15] At low temperatures the cluster excited state lifetimes decrease monotonically along the halide series implying these polynuclear excited states to follow energy gap law behavior.[16] Low temperature spectroscopic investigation of the absorption and emission bands in conjunction with lifetime and quantum yield data are needed for a complete analysis of the mechanisms of nonradiative decay in these molecules. A second potentially promising avenue of research is to probe the structures of the ground state $M_6X_{14}^-$ ions and the $M_6X_{14}^{2-}$ excited states. As discussed previously, a ^2E_g ground state in $M_6X_{14}^-$ anion and a ^3E_g $M_6X_{14}^{2-}$ excited state are both expected to undergo tetragonal distortions. The successful isolation of the $W_6Br_{14}^-$ anion by methods described above should permit unequivocal determination of the ground state geometry by crystal structure analysis. Though initial attempts at growing x-ray structural quality crystals have failed, there remains a plenitude of counter cations and crystallizing techniques to be investigated. The longevity of the $M_6X_{14}^{2-}$ excited states permits the direct interrogation of $M_6X_{14}^{2-*}$ by novel time-resolved spectroscopic techniques. Efforts are underway in the labs of Dr. William H. Woodruff at the University of Texas at Austin to measure the time-resolved resonance Raman (TR^3) spectrum of the excited cluster ions. Due to the high symmetry of the ground state ions, the depolarization ratios of the totally symmetric vibrational fundamentals of the excited state molecule will be particularly

sensitive to excited state distortions. In another rather unique experiment exploiting the long-lived excited state of $Mo_6Cl_{14}^{2-}$, Dr. Thor Rhodin and his colleagues at Cornell University are attempting to measure the excited state EXAFS spectrum of $Mo_6Cl_{14}^{2-}$ in acetonitrile solution at room temperature. As demonstrated by these two experiments, the extraordinarily long-lived excited states of the cluster ions admit a variety of novel experimental techniques aimed at the elucidation of the electronic structure of these polynuclear metal complexes.

D. ELECTROCHEMISTRY

The $Mo_6Cl_{14}^{2-}$, $Mo_6Br_{14}^{2-}$ and $W_6Cl_{14}^{2-}$ ions have been shown to undergo facile one-electron oxidations in aprotic solvents to produce the powerful oxidants, $M_6X_{14}^{-}$. The cyclic voltammetric waves of the $Mo_6Cl_{14}^{2-}$ and $Mo_6Br_{14}^{2-}$ oxidation reactions are well positive to those for free halide oxidation, confirming the robust nature of the $M_6X_{14}^{2-}$ species. In the $W_6Cl_{14}^{2-}$ voltammogram, an additional anodic wave was observed at a potential which preceded solvent decomposition; that $W_6Cl_{14}^{2-}$ is the only ion of the three examined whose $M_6X_{14}^{-/2-}$ wave was well before solvent decomposition implies that further electrochemical reactivity of the cluster ions may be observed in highly purified solvent environments. On the basis of these initial electrochemical results, the experiments presented herein are developed along two lines of research. First, the single-electron oxidation chemistry of the $M_6X_{14}^{2-}$ polynuclear complexes is extended to include $W_6Br_{14}^{2-}$ and $W_6I_{14}^{2-}$.[17] Second, the electrochemistry of $M_6X_{14}^{2-}$ ions is interrogated using the high vacuum cell (Figure 2) with the goal of observing further electrochemical reactivity of polynuclear complexes without interference from solvent impurities (e.g. H_2O and oxygen).

Results and Discussion

Electrochemistry of $M_6X_{14}^{2-}$. Cyclic voltammograms of the cluster ions in acetonitrile and dichloromethane (0.1 M

NBu_4TFMS or TBAP, 25°C) show single-electron oxidation waves. Figure 7 illustrates the cyclic voltammogram of $W_6Br_{14}^{2-}$, which is typical of all $M_6X_{14}^{2-}$ species and lists the $M_6X_{14}^{-/2-}$ redox couples of the five cluster ions in acetonitrile and dichloromethane solutions. Linear plots of the anodic and cathodic currents *vs.* (scan rate)$^{\frac{1}{2}}$ (for scan rates of 50 to 1000 mV s^{-1}), i_a/i_c ratios of 1.00 ±0.10, and peak separations of 65 ±5 mV (as determined from ferrocene's peak separation) for all $M_6X_{14}^{2-}$ complexes examined indicate a reversible electrode process.[18]

The trends of the $M_6X_{14}^{-/2-}$ redox couples in Figure 7 may be justified with rationale common to classical inorganic chemistry. The monotonic decrease of the $M_6X_{14}^{-/2-}$ redox couple along the halide series (i.e. $E_{1/2}$ ($M_6X_{14}^{-/2-}$): X=Cl>Br>I) for both the molybdenum and tungsten series is neatly explained by the greater reducing power of iodide relative to bromide relative to chloride. In addition, the smaller $E_{1/2}$ ($M_6X_{14}^{-/2-}$) potential of a particular ion in CH_2Cl_2 as compared to the one for CH_3CN solution is consistent with CH_3CN's greater capacity to solvate $M_6X_{14}^{2-}$ relative $M_6X_{14}^{-}$. It is interesting to note that the redox couples for $M_6X_{14}^{-/2-}$ ions in CH_2Cl_2 are, consistently, 200 mV lower than those in CH_3CN solution.

The high vacuum electrochemical cell permitted the redox chemistry of the cluster ions to be investigated at potentials as low as -2.2 V *vs.* SCE and as high as 2.2 V *vs.* SCE in CH_3CN solution. The five cluster ions all show rich

Figure 7. (a) Cyclic voltammogram of $(Bu_4N)_2W_6Br_{14}$ in CH_3CN (0.1 M TBAP, 25°C). (b) Half-wave potentials of the $M_6X_{14}^{-/2-}$ couple for the cluster ions in CH_3CN and CH_2Cl_2 (electrode potentials/V *vs.* SCE).

(a)

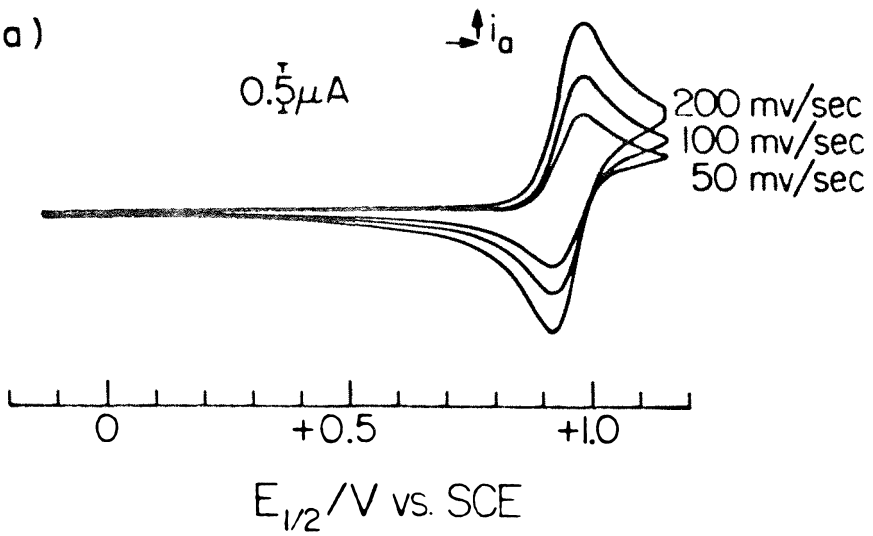

(b)

$(Bu_4N)_2 M_6 X_{14}$ M, X	$E_{1/2}(M_6 X_{14}^{-/2-})$ in CH_3CN	$E_{1/2}(M_6 X_{14}^{-/2-})$ in CH_2Cl_2
Mo, Cl	+1.56	+1.33
Mo, Br	+1.34	+1.17
W, Cl	+1.12	+0.94
W, Br	+0.97	+0.77
W, I	+0.71	+0.58

redox chemistry at potentials more positive than their reversible oxidation couples. These cyclic voltammetric waves are irreversible and their anodic currents are much greater than the currents of the single-electron oxidation waves suggesting either multielectron reactivity or adsorption of oxidized species on the electrode. In the case of $W_6I_{14}^{2-}$, the anodic wave appears at 1.00 V *vs.* SCE, only 290 mV more positive than the $W_6I_{14}^{-/2-}$ couple. This wave prevented the formation of $W_6I_{14}^{-}$ by controlled potential coulometry. The five cluster ions examined, also, exhibit cathodic waves at potentials more negative than -1.5 V *vs.* SCE; in the case of $Mo_6Cl_{14}^{2-}$, a quasi-reversible one-electron wave at -1.53 V *vs.* SCE may be attributed to the $Mo_6Cl_{14}^{2-/3-}$ couple. The wave is extremely sensitive to oxygen and water and their rigorous exclusion was required for a well-defined reduction wave. Thus, $Mo_6Cl_{14}^{2-}$ undergoes single one-electron oxidation and reduction reactions to produce the powerful oxidant, $Mo_6Cl_{14}^{-}$, and powerful reductant, $Mo_6Cl_{14}^{3-}$, respectively. The ability to cleanly electrogenerate $Mo_6Cl_{14}^{-}$ and $Mo_6Cl_{14}^{3-}$ in conjunction with the photophysical properties of $Mo_6Cl_{14}^{2-}$ suggested a study of the electrogenerated chemiluminescence (ECL) of this compound.

ECL of $(Bu_4N)_2Mo_6Cl_{14}$. A typical cyclic voltammogram of $(Bu_4N)_2Mo_6Cl_{14}$ (1.5 mM) in acetonitrile (0.1 M TBAP; 25°C) is illustrated in Figure 8. Intense red ECL is observed upon pulsing the potential applied to a Pt working electrode with a square wave potential program of 1.80 V

Figure 8. Cyclic voltammogram of $(Bu_4N)_2Mo_6Cl_{14}$ in CH_3CN (0.1 M TBAP, 22°C).

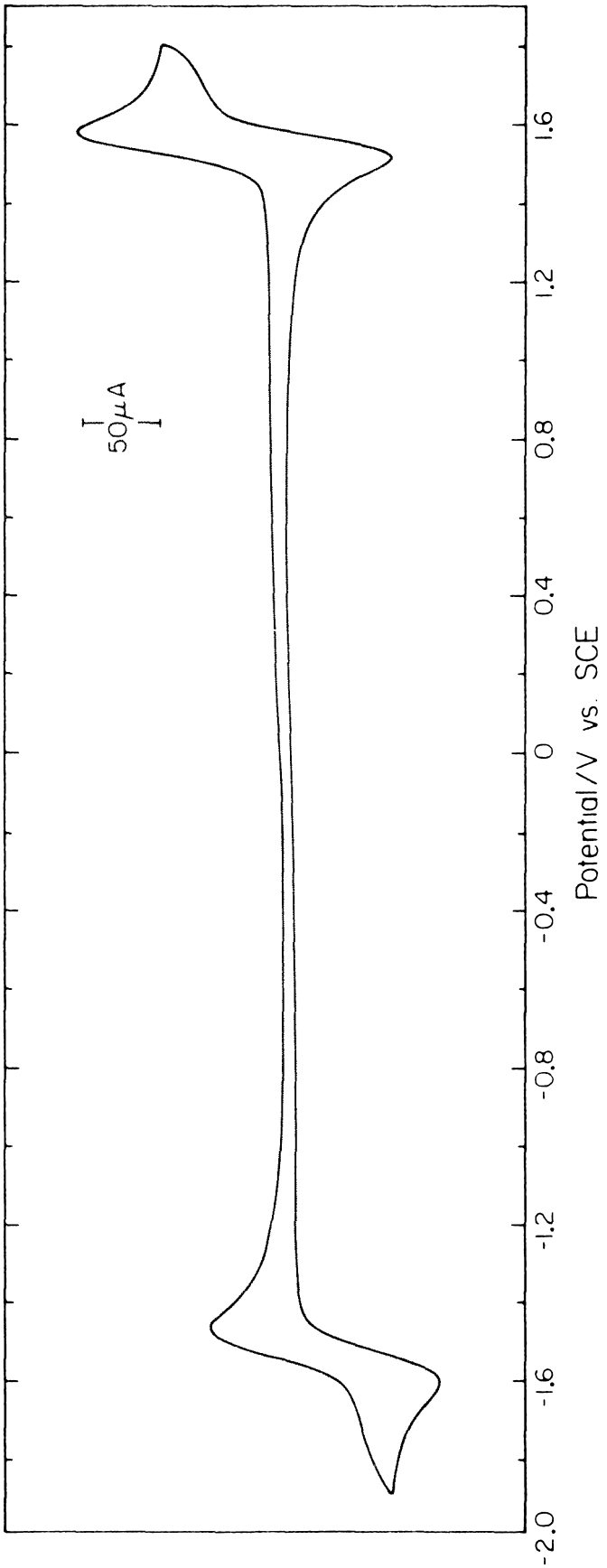
50μA
1.6
1.2
0.8
0.4
0
-0.4
-0.8
-1.2
-1.6
-2.0
Potential/V vs. SCE

and -1.80 V *vs.* SCE. The uncorrected ECL spectrum of a constantly stirring $Mo_6Cl_{14}^{2-}$ acetonitrile solution (100 Hz pulse train) is illustrated in Figure 9 and is identical to the uncorrected emission spectrum of $Mo_6Cl_{14}^{2-}$ produced by steady state ultraviolet irradiation (designated by the dark circles in Figure 9). The probable mechanism for ECL is diagrammed in Figure 10; the electrogenerated $Mo_6Cl_{14}^{3-}$ and $Mo_6Cl_{14}^{-}$ species react to produce one ground state $Mo_6Cl_{14}^{2-}$ molecule and $Mo_6Cl_{14}^{2-*}$, the creation of which is heralded by its red luminescence.

The thermodynamic parameters of the pertinent reaction pathways in the ECL mechanism are displayed on the modified Latimer diagram in Figure 10.[19] The e.m.f. change for the ground state reaction,

$$Mo_6Cl_{14}^{-} + Mo_6Cl_{14}^{3-} \longrightarrow 2Mo_6Cl_{14}^{2-} \qquad (1)$$

is 3.1 eV. This energy is sufficient to permit the ECL reaction to proceed by either (i) population of the singlet state which intersystem crosses (isc) to the emissive triplet state,

$$Mo_6Cl_{14}^{-} + Mo_6Cl_{14}^{3-} \longrightarrow {}^1Mo_6Cl_{14}^{2-*} + Mo_6Cl_{14}^{2-} \qquad (2)$$

$${}^1Mo_6Cl_{14}^{2-*} \xrightarrow{isc} {}^3Mo_6Cl_{14}^{2-*} \qquad (3)$$

Figure 9. ECL spectrum of $(Bu_4N)_2Mo_6Cl_{14}$ in CH_3CN at 22°C using a cyclic square wave at 100 Hz between 1.80 V and -1.80 V *vs.* SCE. Circles illustrate luminescence spectrum of $(Bu_4N)_2Mo_6Cl_{14}$ in CH_3CN with 436 nm excitation. Spectra are not corrected for photomultiplier or monochromator response.

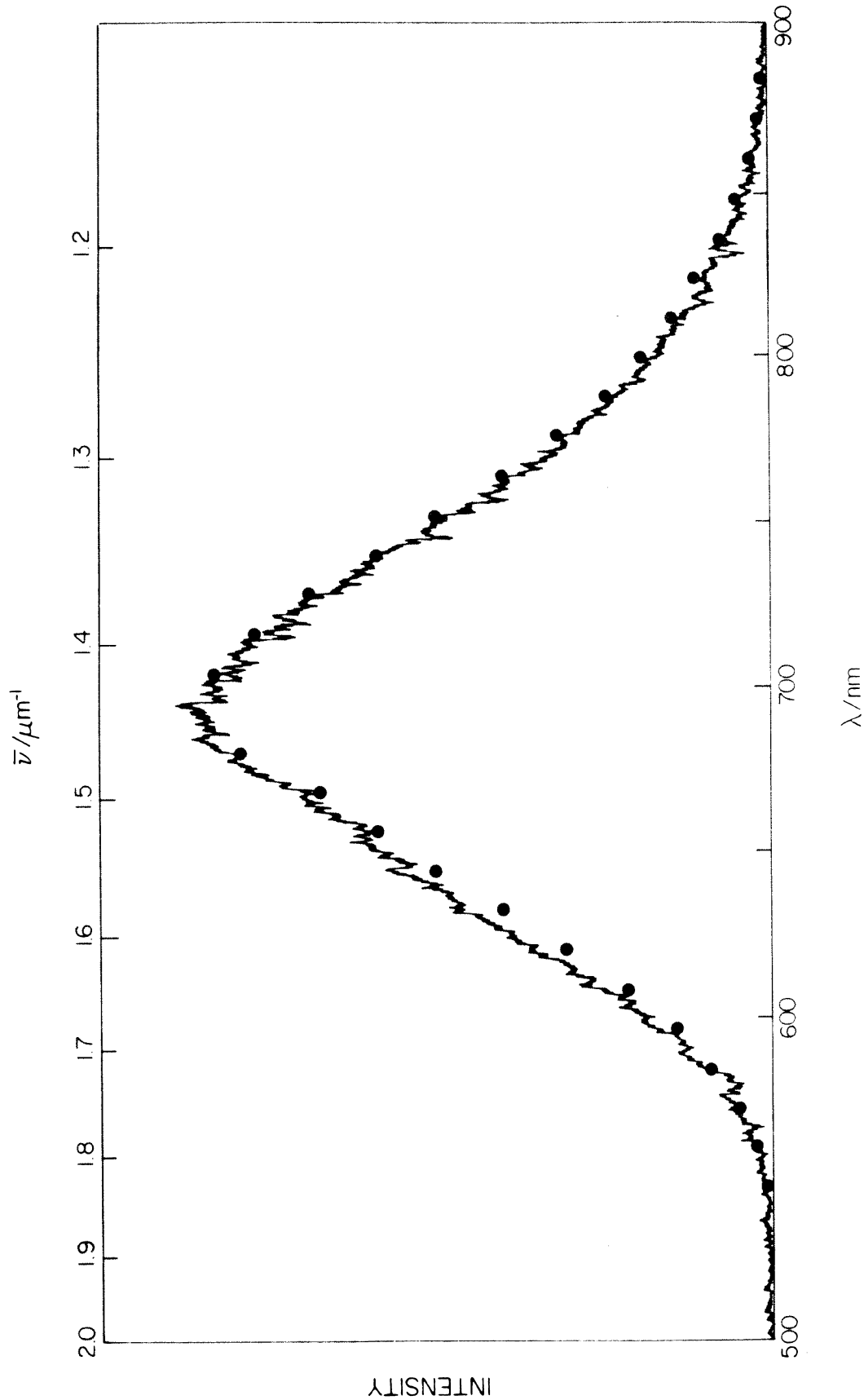
INTENSITY
$\bar{\nu}/\mu m^{-1}$
2.0
1.9
1.8
1.7
1.6
1.5
1.4
1.3
1.2
500
600
700
800
900
λ/nm

Figure 10. (a) Modified Latimer diagram for $(Bu_4N)_2Mo_6Cl_{14}$ in CH_3CN at room temperature (electrode potentials/V *vs.* SCE; excited state energy in eV). (b) Probable mechanism for ECL reaction.

(a)

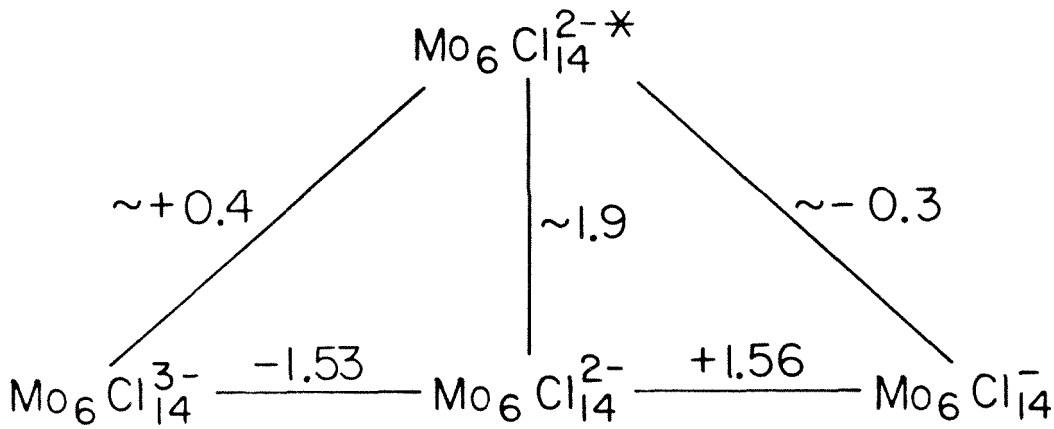

(b)

$$Mo_6Cl_{14}^{-} + Mo_6Cl_{14}^{3-} \longrightarrow Mo_6Cl_{14}^{2-} + Mo_6Cl_{14}^{2-*}$$

or (ii) direct population of the triplet state,

$$Mo_6Cl_{14}^{3-} + Mo_6Cl_{14}^{-} \longrightarrow {}^3Mo_6Cl_{14}^{2-*} + Mo_6Cl_{14}^{2-} \qquad (4)$$

which is determined, from an estimate of the location of the electronic origin in the luminescence spectrum, to lie 1.9 eV above the ground state. That the rate of **2** or **4** is great enough to effectively compete with that of **1** is a striking result in view of the much larger driving force for the ground state reaction (3.1 eV for **1**; <<1.2 eV for **2**; 1.2 eV for **4**) and may be evidence for the Marcus "inverted" region.[20] Indeed, it was Marcus who first proposed that ECL activity may be a manifestation of the "inverted" regime.[21] The ability to study the highly exergonic reactions involving the electrogenerated species, $Mo_6Cl_{14}^{3-}$ and $M_6X_{14}^{-}$ (M=Mo,W; X=Cl,Br,I), provides additional opportunity to evaluate the predictions of Marcus theory.

Observation of ECL from the $Mo_6Cl_{14}^{2-}$ ion is especially interesting in view of the fact that, to date, ECL from inorganic species has been a perquisite of mononuclear metal complexes with chelating aromatic ligands; these include Ru(II) chelates incorporating π-acid ligands (e.g. 2,2'-bipyridine);[22] Re(I)[23] and Os(II)[22f] diimine complexes; and Pt(II) and Pd(II) metalloporphyrins.[24] Electrogenerated chemiluminescence from organic aromatic compounds has long been an active field of research.[25] The

$Mo_6Cl_{14}^{2-}$ ion, however, represents the first example of pure inorganic ECL reactivity. Nevertheless, without pursuing the pedantry of the ECL observation, the $M_6X_{14}^{2-}$ complexes represent an exciting new class of polynuclear complexes which considerably expand the horizons of electron transfer reactions of electronically excited transition metal complexes.

E. REFERENCES

1. Graff, J. L.; Wrighton, M. S. J. Am. Chem. Soc. 1981, 103, 2225.
2. (a) Maverick, A. W. Ph.D. Dissertation, California Institute of Technology, 1982. (b) Maverick, A. W.; Najdzionek, J. S.; MacKenzie, D.; Nocera, D. G.; Gray, H. B. J. Am. Chem. Soc. 1983, 105, 1878. (c) Maverick, A. W.; Gray, H. B. J. Am. Chem. Soc. 1981, 103, 1298.
3. Sheldon, J. C. J. Chem. Soc. 1962, 410.
4. (a) Cotton, F. A.; Stanley, G. G. Chem. Phys. Lett. 1978, 58, 450. (b) Guggenberger, L. J.; Sleight, A. W. Inorg. Chem. 1969, 8, 2041. (c) Cotton, F. A.; Haas, T. E. Inorg. Chem. 1964, 3, 10. (d) Crossman, L. D.; Olsen, D. P.; Duffey, G. H. J. Chem. Phys. 1963, 38, 73. (e) Briat, B.; Rivoal, J. C.; Kahn, O.; Moreau, S. Proc. Int. Conf. Coord. Chem. 16th 1974, 2.25a.
5. Dorman, W. C.; McCarley, R. E. Inorg. Chem. 1974, 13, 491.
6. Hogue, R. D.; McCarley, R. E. Inorg. Chem. 1970, 9, 1354.
7. For $[Ru(bpy)_3]Cl_2$ in degassed H_2O (ϕ_e (436 nm) = 0.042 ±0.002: van Houten, J.; Watts, R. J. J. Am. Chem. Soc. 1976, 98, 4853.
8. Demas, J. N.; Crosby, G. A. J. Phys. Chem. 1971, 75, 991.

9. Drushel, H. V.; Sommers, A. L.; Cox, R. C. Anal. Chem. **1963**, 35, 2166.

10. $Fc^{+/0}$ couple *vs.* SCE: 0.310 V (CH_3CN, 0.2 M $LiClO_4$), (Kuwana, T.; Bublitz, D. E.; Hoh, G. J. Am. Chem. Soc. **1960**, 82, 5811); 0.315 V (CH_3CN, 0.2 M $LiClO_4$), (Little, W. F.; Reilley, C. N.; Johnson, J. D.; Lynn, K. N.; Sanders, A. P. J. Am. Chem. Soc. **1964**, 86, 1367); 0.310 V (CH_3CN, 0.1 M $NaClO_4$), (Hennig, H.; Gürtler, O. J. Organometal. Chem. **1968**, 11, 307).

11. Seifert, G.; Grossmann, G.; Müller, H. J. Mol. Struct. **1980**, 64, 93.

12. Hughbanks, T.; Hoffmann, R. J. Am. Chem. Soc. **1983**, 105, 1150.

13. Hartley, D.; Ware, M. J. J. Chem. Soc., Chem. Comm. **1967**, 912.

14. The spin-orbit splittings of the ^3E_g state could be greatly reduced as a result of the Ham effect (Ham, F. S. Phys. Rev. A. **1965**, 138, 1727). See also, Wilson, R. B.; Solomon, E. I. J. Am. Chem. Soc. **1980**, 102, 4085.

15. Freed, K. F.; Jortner, J. J. Chem. Phys. **1970**, 52, 6272.

16. Englman, R.; Jortner, J. Mol. Phys. **1970**, 18, 145.

17. The small quantities of $(Bu_4N)_2Mo_6I_{14}$ did not permit detailed electrochemical studies.

18. Bard, A. J.; Faulkner, L. R. "Electrochemical Methods", Chapter 6, Wiley: New York, **1980**.

19. Entropic contribution to the excited state energy is expected to be minor and has been ignored. See, Faulkner, L. R.; Tachikawa, H.; Bard, A. J. J. Am. Chem. Soc. 1972, 94, 691.

20. (a) Marcus, R. A. Discuss. Faraday, Soc. 1960, 29, 21. (b) Marcus, R. A. J. Chem. Phys. 1965, 43, 679.

21. Marcus, R. A. J. Chem. Phys. 1965, 43, 2654.

22. $Ru(bpy)_3^{2+}$ (bpy = 2,2'-bipyridine), (a) Tokel, N. E.; Bard, A. J. J. Am. Chem. Soc. 1972, 94, 2862; (b) Wallace, W. L.; Bard, A. J. J. Phys. Chem. 1979, 83, 1350; (c) Rubinstein, I.; Bard, A. J. J. Am. Chem. Soc. 1981, 103, 512; (d) Luttmer, J. D.; Bard, A. J. J. Phys. Chem. 1981, 85, 1155; (e) Glass, R. S.; Faulkner, L. R. J. Phys. Chem. 1981, 85, 1159, and RuL_3^{2+} (L = 1,10-phenanthroline; 2,2',2''-terpyridine), (f) Tokel-Takvoryan, N. E.; Hemingway, R. E.; Bard, A. J. J. Am. Chem. Soc. 1973, 95, 6582, and $Ru(bpz)_3^{2+}$ (bpz = 2,2'-bipyrazine), (g) Gonzales-Velasco, J.; Rubinstein, I.; Crutchley, R. J.; Lever, A. B. P.; Bard, A. J. Inorg. Chem. 1983, 22, 822.

23. Luong, J. C.; Nadjo, L.; Wrighton, M. S. J. Am. Chem. Soc. 1978, 100, 5790.

24. Tokel-Takvoryan, N. E.; Bard, A. J. Chem. Phys. Lett. 1974, 25, 235.

25. See, for example, Faulkner, L. R. MTP Int. Rev. Sci., Phys. Chem., Ser. Two 1976, 9, 213.

CHAPTER IV

FINAL REMARKS

At first glance, similarities between $Re_2Cl_8^{2-}$ and $M_6X_{14}^{2-}$ clusters are not apparent, however, closer scrutiny reveals that the structural and electronic properties of the two systems are closely related. Both species are constructed from the same basic MX_4 structural unit with halide ions at the base of a slightly distorted square pyramid and a d^4 metal atom at the apex. Two MX_4 units are juxtaposed by a metal-metal quadruple bond in $Re_2Cl_8^{2-}$ and in the $M_6X_{14}^{2-}$ clusters, the MX_4 unit is preserved in the $[M_6X_8]$ cluster core by single bonds to four other metal atoms.[1] These structural parallels are complemented by similarities in the electronic properties of $Re_2Cl_8^{2-}$ and $M_6X_{14}^{2-}$ ions as manifested in their diamagnetic ground states and the metal localized lowest energy excited states of the two systems. Both cluster systems exhibit red or near-infrared luminescence and the emission lifetimes for the all-inorganic $Re_2Cl_8^{2-}$ and $M_6X_{14}^{2-}$ clusters are among the longest known for transition metal singlet and triplet excited states, respectively.

The resemblance between the two metal halide systems extends into their oxidation chemistry. As demonstrated in Chapter II, oxidation of $Re_2Cl_8^{2-}$ in the presence of Cl^- leads to production of the confacial bioctahedron; halides occupy edge bridging positions between two rhenium centers in order to stabilize the higher oxidation state metal. Similar reactivity has been documented for at least one $M_6X_{14}^{2-}$ cluster. Oxidation of $[W_6Cl_8]Cl_6^{2-}$ by

Cl_2 under relatively mild conditions (100°C) yields $[W_6Cl_{12}]Cl_6$.[2] The cluster consists of an octahedral core of W(III) atoms with 12 edge bridging halides and six axial halides. Conversion of the $[M_6X_8]X_4$ core (where we have the basic M_6X_8 core with the 4 axial halides of an equatorial plane) into $[M_6X_{12}]$ can simply occur by rotating the halide coordination sphere 45° relative to the M_6 octahedron. As in the rhenium halide confacial bioctahedral system, the $[W_6Cl_{12}]$ cluster core has adopted a geometry which places halide ions in edge bridging positions to stabilize the higher oxidation state metals; in the $[W_6Cl_8]^{4+}$ core there is one chloride ion shared among three W(II) atoms and in $[W_6Cl_{12}]^{6+}$ there is one chloride ion shared among two W(III) metal centers. Thus, upon oxidation, both the $Re_2Cl_8^{2-}$ and $W_6Cl_{14}^{2-}$ clusters undergo relatively minor geometric rearrangements to place halides in coordination sites which more effectively stabilize the higher positive charge of the cluster metal core.

In view of the extensive structural and electronic correlation between the two cluster systems, the photochemistry of $Re_2Cl_8^{2-}$ may portend photoinduced multielectron reactivity of the $M_6X_{14}^{2-}$ polynuclear complexes. The results presented in Chapter II on $Re_2Cl_8^{2-}$ demonstrate that photooxidation of the rhenium core by one electron promotes halide rearrangement to edge bridging positions, thereby inducing the system to yield a second electron. This same reactivity pattern may be exploited in the $M_6X_{14}^{2-}$ systems.

Oxidation of electronically excited $M_6X_{14}^{2-}$ to generate a mixed valence M(II)/M(III) metal core may promote halide migration to edge bridging positions which would in turn further drive the oxidation of the cluster to produce a $[M_6X_{12}]^{6+}$ core, a reaction which entails a six-electron transformation. The multielectron electrochemical results of $M_6X_{14}^{2-}$ ions suggest that an initial quenching step involving the oxidation of two metal centers will be necessary to bias the system toward the $[M_6X_{12}]^{6+}$ final product. A system which neatly illustrates the potential multielectron chemistry of $M_6X_{14}^{2-}$ ions and employs the above concepts is illustrated by the modified Latimer diagram in Figure 1. The goal here is to quench the $[W_6Cl_8]^{4+}$ excited state in strongly acidic solutions to yield a metal hydride species. This photogenerated hydride may then react with a proton to make one mole of hydrogen and a mixed valence cluster intermediate which could further react with four moles of hydrohalic acid to yield the $[W_6Cl_{12}]^{6+}$ core and an additional two moles of hydrogen. Admittedly, this reaction pathway is purely speculative, however, the $Re_2Cl_8^{2-}$ photo-oxidation chemistry does offer encouragement for such a hydrogen producing scheme.

The results presented herein demonstrate polynuclear metal complexes to possess properties important to the design of photochemical multielectron reactions in homogeneous solution. The all-inorganic $Re_2Cl_8^{2-}$ and $M_6X_{14}^{2-}$ ions maintain the structural integrity of the metal cluster core

Figure 1. Potential multielectron photochemistry of $[W_6Cl_8]^{4+}$ in hydrohalic acid solution.

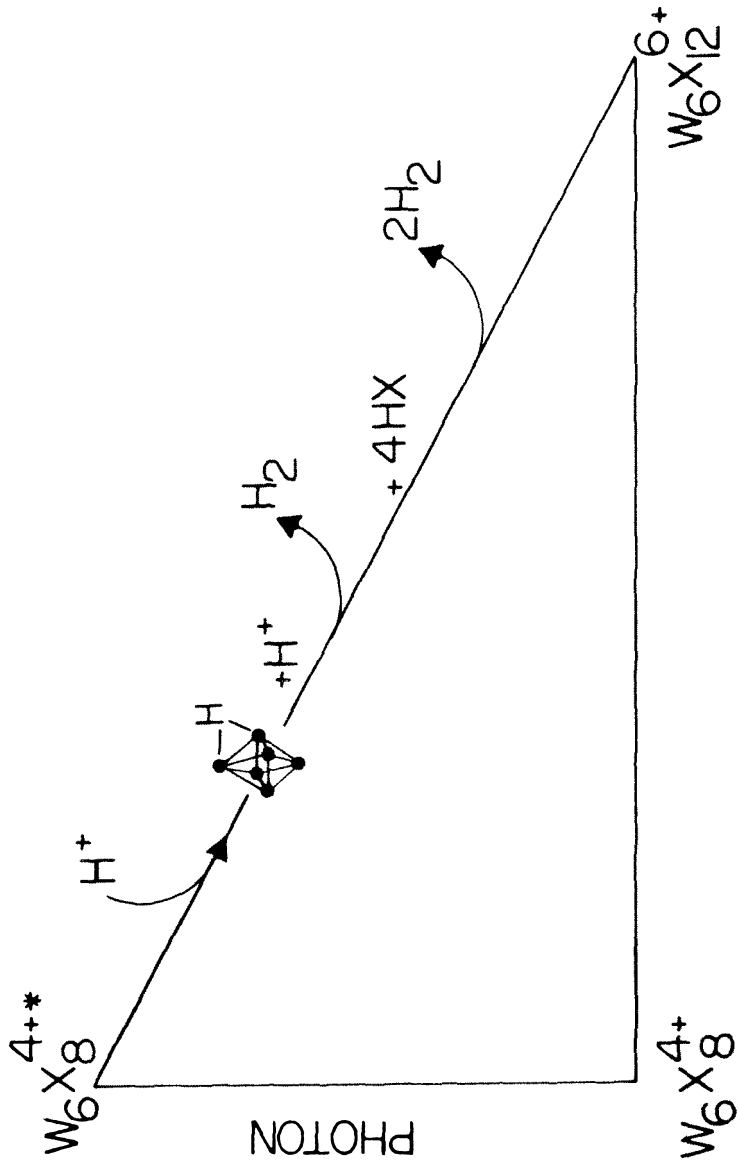

$$W_6X_8^{4+} + 2H^+ + 4HX \xrightarrow{\text{solar}} W_6X_{12}^{6+} + 3H_2$$

in a variety of oxidation states. In addition, the long-lived excited states of these systems permit bimolecular photoreactivity of the electronically excited cluster ions. The d^4 polynuclear metal complexes may well be harbingers of an exciting new era of multielectron reactivity in inorganic photochemistry.

REFERENCES

1. Cotton, F. A.; Wilkinson, G. "Advanced Inorganic Chemistry"; 4th ed., Wiley: New York, **1980.**

2. Siepmann, R.; v. Schnering, H.-G.; Schäfer, H. Angew. Chem., Int. Ed. Engl. **1967**, 6, 637.